



MINISTRY OF SUPPLY

AERONAUTICAL RESEARCH COUNCIL
REPORTS AND MEMORANDA

Tests in the Royal Aircraft Establish- ment 10-ft x 7-ft High-Speed Tunnel on 50-deg Swept-back Wings

Part I

Three of 7.5 per cent Thickness

Part II

One of 7.5 per cent Thickness with Stall Fences
and Leading-Edge Chord Extension

By

A. B. HAINES, B.Sc., and C. W. RHODES, B.Sc., D.AE.

Crown Copyright Reserved.

LONDON: HER MAJESTY'S STATIONERY OFFICE

1957

PRICE £1 10s. 0d. NET

Tests in the Royal Aircraft Establishment 10-ft x 7-ft High-Speed Tunnel on Three Wings with 50-deg Sweepback and 7.5 per cent Thick Sections

Part I

By

A. B. HAINES, B.Sc.,
and

C. W. RHODES, B.Sc., D.AE.

COMMUNICATED BY THE DIRECTOR-GENERAL OF SCIENTIFIC RESEARCH (AIR),
MINISTRY OF SUPPLY

*Reports and Memoranda No. 3043**

September, 1954

Summary.—Tests have been made in the Royal Aircraft Establishment 10-ft x 7-ft High-Speed Tunnel on three half-wings having a sweepback of about 50 deg on the quarter-chord line and 7.5 per cent thick sections. Two of the wings had sections of the RAE 101 shape (maximum thickness at 0.31c) and differed principally in aspect ratio (3.1 and 3.5). The third wing had an aspect ratio of about 3.1 but a different section shape with its maximum thickness further aft at 0.4c and, as shown by the results of the tests, an effectively sharper nose than for the RAE 101 shape.

Lift, drag, pitching moment and root bending moment were measured on all three wings over a range of Mach numbers from 0.50 to about 0.95 at a Reynolds number of about 2×10^6 , and also for the two wings of smaller aspect ratio for three Reynolds numbers up to about 6×10^6 at a Mach number near 0.2. The flow patterns at low Mach number were investigated at $R = 2.6 \times 10^6$ and in one case, at $R = 6 \times 10^6$ also, by an oil-film technique. A description of the technique and of how the flow patterns were interpreted is included. Two of the wings were also tested with surface tufts at various Mach numbers up to $M = 0.94$.

It is found that for all three wings, there is a serious reduction in longitudinal stability at both low and high Mach numbers at some value of C_L that is well below $C_{L \max}$. At the test Reynolds numbers, at low Mach number, a laminar separation bubble appears to form near the leading edge near the tip and to extend inward and rearward with increasing incidence. A part-span vortex sheet originates from near the inner end of this region and so, also moves in with increasing incidence until, near $C_{L \max}$, it originates from near the wing-root leading edge.

The values of C_L at which a significant separation first occurs on any section increase appreciably with Reynolds number up to about 4×10^6 for the RAE 101 section and to 5.5×10^6 for the other section at low Mach number. It seems likely, however, that there is little variation at higher Reynolds numbers and so the main features of the results obtained at $M = 0.2$, $R = 6 \times 10^6$ should then apply:

- (a) The flow over the outer sections first starts to separate at about $C_L = 0.7$ to 0.75
- (b) a serious reduction in longitudinal stability occurs above about $C_L = 0.85$, becoming more severe near $C_L = 0.95$
- (c) the actual value of $C_{L \max}$ is near 1.05 to 1.10 and is greater than for wings with the same thickness/chord ratio but smaller angles of sweep.

The basic nature of the stall appears to remain the same at Mach numbers up to about $M = 0.85$ but even in these tests at $R = 2 \times 10^6$, the separation on the outer sections occurs at lower values of C_L as the Mach number is increased. At higher Reynolds numbers, this deterioration might be more pronounced (*i.e.*, less scale effect at the higher Mach numbers).

Above about $M = 0.90$, the basic cause of the flow separation over the outer sections at high C_L is different from that at lower Mach numbers. The reduction in stability, which occurs near $C_L = 0.6$ at $M = 0.9$ or $C_L = 0.5$ at

* Part I. R.A.E. Report Aero. 2522, received 1st March, 1955.

Part II. R.A.E. Report Aero. 2521, received 25th March, 1955.

$M = 0.95$ is related mainly to a shock-induced separation over the outer sections and to a forward movement with incidence of this upper-surface shock wave. The results at $R = 2 \times 10^6$ for these Mach numbers are probably a reasonable guide to the full-scale behaviour.

In general, the RAE 101 section shape appears slightly superior; in particular, it gives a smaller reduction in stability with increasing C_L between $C_L = 0.5$ and 0.8 at high Mach numbers.

The increase in aspect ratio from 3.1 to 3.5 increases the severity of the reductions in stability at high C_L but does not result in any reduction in the values of C_L at which they occur.

The steep drag rise with Mach number, for all values of C_L , occurs at Mach numbers about 0.03 lower for the wing with its maximum thickness at $0.4c$ than for the RAE 101 wing. This confirms (and to a more marked degree) the superiority of the RAE 101 section for moderately tapered swept wings, already found for 10 per cent thick wings of 40 deg sweep.

1. *Introduction.*—The results of tests in the R.A.E. 10-ft \times 7-ft. High-Speed Tunnel on a series of swept-back wings, all having a sweep of 40 deg on the quarter-chord line and a thickness/chord ratio of 10 per cent have been reported in Ref. 1. The programme has since been extended to include both thinner wings and also wings of greater sweep. First, the effect of thickness/chord ratio for a given angle of sweep (40 deg) and a given section shape (RAE 101) has been investigated with wings of 10 per cent, 8.5 per cent and 6 per cent thickness/chord. (These tests are reported in Ref. 2.) Secondly, three wings of about 50-deg sweep and a thickness/chord ratio of 7.5 per cent have been tested and the results for these wings are discussed in the present report.

In the earlier tests on the thicker, less swept, wings¹, most interest centred on the performance at high subsonic speeds and low values of C_L , e.g., the results were compared to find which section of those tested was the most effective in delaying the steep increase of drag to a high Mach number. With the 7.5 per cent thick, 50-deg swept wings, however, this question cannot be explored fully in the test Mach-number range which is limited to 0.95 for the best of the wings, the steep drag rise for $C_L = 0$ is only just starting at $M = 0.95$. Instead, the chief interest has now shifted to the pitching-moment characteristics, particularly at high values of C_L , for it will be seen that for all the 50-deg swept wings tested, a serious loss of longitudinal stability occurs at the Reynolds number of the tests, for values of C_L , well below $C_{L\max}$. If this behaviour is also reproduced in flight, the available C_L both for take-off and landing and also for manoeuvring at moderate and high subsonic speeds will be restricted.

For various reasons, precise estimates of the usable C_L to be expected in flight cannot be quoted on the basis of these results. In the first place, the tests over the full Mach-number range up to 0.95 were made at a Reynolds number of only about 2×10^6 ; at low Mach number (0.2), additional tests were made for Reynolds numbers up to about 6×10^6 . These values of Reynolds number are not sufficient to avoid the likelihood that further changes in the value of C_L , at which the loss of stability occurs, would result from a further increase in Reynolds number (except, probably for Mach numbers greater than about 0.9). Secondly, the tests described here were made by the half-model technique on half-wings with no tailplane. In general, the addition of a tailplane would tend to aggravate the problem, if it were set above the extended wing-chord plane or might alleviate it somewhat if it were below. Finally, the usable C_L in flight may be determined by buffeting or wing-dropping rather than by a reduction in longitudinal stability.

In view of these reservations, it is clearly important to understand the flow phenomena underlying the changes in stability and so this report contains a fairly detailed analysis of the overall lift and moment results on the three wings, with the aid of photographs of the flow over the wing surface at low Mach number, as obtained by an oil-film technique, and of the behaviour of surface tufts over the full Mach-number range. It is naturally not possible to gain a full understanding of the various flow phenomena from merely the overall results supplemented by these flow patterns and so a detailed pressure-plotting survey is to be made over the surface of one of these wings in the R.A.E. 10-ft \times 7-ft High-Speed Tunnel and also on a model to the same design in the large high-speed (8m) tunnel at Modane (the latter test will give a Reynolds number of about 14×10^6 at a Mach number of 0.9).

The tests described in this report were made at various dates between March, 1952 and February, 1953.

For a quick, first reading, section 6 may be omitted.

2. *Design of the Wings.*—The plan-forms of the wings tested are shown in Figs. 1 and 2; leading dimensions are given in these figures and in Table 1.

All the wings have symmetrical sections with a thickness/chord ratio of 7.5 per cent; each wing has the same section throughout the span.

Wings A and B have RAE 101 sections and the sweep of their quarter-chord line is 50 deg. The major difference between these two wings is in aspect ratio: 3.1 for A and 3.5 for B. Since wing A was actually obtained from wing B by cropping and reshaping the tip, there is also a small difference between the taper ratios of the wings. Both wings have a curved leading edge near the tip; this extends inwards for a distance equal to a third of the basic tip chord (see Fig. 1). These wings were tested in the presence of a half-fuselage mounted on the floor of the tunnel. The fuselage cross-section opposite the wings is elliptic with the major axis lying in the spanwise direction. The wing-body angle is zero and wings A and B have no dihedral.

Fig. 2 shows that wing C has almost the same plan-form as wing A except that the sweepback of the quarter-chord line is slightly less, being 48.8 deg. The main difference between wings A and C, therefore, is in their section shapes (These are compared in Fig. 4 and ordinates are given in Table 2). The section of wing C has its maximum thickness further aft at 0.38c and although its actual leading-edge radius is very large for a section with this maximum-thickness position, the slope of the section decreases rapidly just aft of the nose. As a result, at high incidence and low Mach number, a large peak-suction value is obtained just behind the nose (see Fig. 34). With a sharp leading edge, the same characteristic would appear, only nearer the leading edge and so it seems fair to describe this section as having an 'effectively' sharper nose than say, the RAE 101 section of wings A and B.

Wing C has certain peculiar features that are probably not of great consequence as regards the longitudinal-stability characteristics, e.g., at the tip, not only is the leading edge curved but also the trailing edge curves forward. The wing has a dihedral of -1 deg and there is a wing-body angle of 1.5 deg. The body cross-section opposite the wing root is almost circular, rather than elliptic as for wings A and B.

Summarizing:

- (a) A comparison of the results for wings A and C shows, principally, the effects of the change in section shape with a small effect due to the slight reduction in sweep
- (b) A comparison between A and B shows the effects of the change in aspect ratio with a small effect due to the change in taper ratio.

3. *Experimental Details.*—3.1. *Manufacture and Mounting of the Wings.*—The wings were made of compressed wood ('Hydulignum') and the bodies were of teak. The surfaces had a finish of black 'Phenoglaze'.

Originally, in each case, the body and wing were mounted separately, i.e., the body was attached to the tunnel floor and the wing passed through the body and the floor to be mounted on the six-component mechanical balance, situated below the tunnel working-section. There was a gap, about 0.1 in. wide, between the wing and body. Airflow between the working-section and the surrounding 'dead space' through this gap were prevented, as usual, by means of a mercury seal. With this method, the forces and moments are measured on the net wing alone and it was hoped that any spurious effects due to the boundary layer on the floor of the tunnel were being avoided. The flow pictures obtained by the oil-film technique suggested, however, that it was doubtful whether the arrangement was satisfactory in the present case. There was evidently a considerable airflow over the wing stub above the mercury seal with the effect that

the spanwise component of flow in the boundary layer was increased over the rear part of the chord. This can be seen from Fig. 3a which gives photographs of the flow over wing A at $\alpha = 12$ deg both when the gap at the wing root is open as for the balance tests and when it is sealed. With the gap open, the oil flow (and presumably, the flow in the boundary layer) is roughly along the wing, even near the root; when the gap is sealed, however, the direction of flow over the inner half of the wing is only diverted from the free-stream direction by about half this amount.

It was feared that the increased spanwise drift of the boundary layer over the inner sections with the gap open might influence the development of the stall and so to provide a check on this, the tests on wing C were repeated with the half-body attached to the wing, *i.e.*, with the small gap now being between the floor and the base of the body. Fig. 3b, giving photographs of the oil flow for $\alpha = 14$ deg, confirms that this change has the desired effect of preventing the strong outward flow in the boundary layer near the wing root. With body attached, it can be seen that the flow over the innermost part of the wing, inboard of where it is affected by the part-span vortex sheet, is in a direction only slightly different from that of the free stream. It is reassuring to note, however, that the nature of the flow over the outer parts of the wing and for example, the position of the part-span vortex sheet has not been greatly affected by attaching the body, suggesting that the doubts expressed above may have been exaggerated*.

With the body attached, the forces and moments are measured on the gross wing-body combination but the values obtained for the position of the aerodynamic centre and to a lesser extent, the lift-curve slope are likely to be affected slightly by the fact that much of the body is in the boundary layer on the tunnel floor. These effects are discussed in section 9.

3.2. Range of Tests.—Lift, drag, pitching moment and root bending moment were measured in all the balance tests. All three wings were tested over a range of Mach numbers from 0.50 to 0.95 at a Reynolds number of between $R = 1.7 \times 10^6$ and 1.8×10^6 , based on the mean chord of the net wing. Additional tests were made with wings A and C at several Reynolds numbers at low Mach number, *viz.*, wing A was tested at $10^{-6} R = 1.8, 4.3$ and 6.1 at $M = 0.18$ and wing C at $10^{-6} R = 1.9, 3.8$ and 5.4 at $M = 0.20$. In the latter tests, wing C was tested at both positive and negative incidences. Because of its dihedral and wing-body angle, results in the two directions should not necessarily agree but the stalling characteristics should not be markedly affected. Hence, since the required data at the higher Reynolds numbers could not be obtained by a test in the positive direction (owing to a balance limitation), it was considered justifiable to fill in this gap by the results at negative incidence.

All three wings were tested with surface tufts at several Mach numbers between $M = 0.50$ and 0.95, at $R = 1.7 \times 10^6$. Flow visualisation tests were also made with wings A and C† at low Mach number by the technique described below and in Appendix I. For wing A, these tests were only made at $R = 2.6 \times 10^6$, $M = 0.27$ but for wing C, tests were made both for this condition and for four incidences at $R \simeq 6 \times 10^6$, $M = 0.20$.

3.3. Flow Visualisation Technique.—The technique used for visualising the flow at low Mach number consists of coating the wing surface with a suspension in oil of a finely divided powder. When the wind is turned on, the oil flows over the wing surface. Eventually the oil dries off or is blown off but its previous motion is shown and preserved by the deposition on the wing surface of the powder that had been suspended in the oil. The pattern can then be studied at leisure. In principle, therefore, the technique is the same as that described, for example, in Ref. 3 but here titanium oxide has been used instead of lampblack. A detailed description of the experience that has been gained in how the mixture should be prepared and applied to the wing is given in Appendix I.

* The criticisms of the net-wing technique do not apply to the same extent to the tests in Ref. 1.

† With and without body attached.

Photographs of the flow patterns were taken not merely after the titanium oxide was quite dry and all movement of the oil had ceased, but also at earlier times. In general, the final pictures are of most interest but the others are also useful in giving a qualitative idea of the relative magnitude of the local velocities over different parts of the wing. For example, the earlier photographs may be used in establishing the presence of a part-span vortex sheet or in showing where the flow has completely separated from the surface.

The flow patterns should be analysed with care and restraint because the density and viscosity of the oil are different from those of air and so, the path of an oil particle may differ from that of the air. The oil is in fact in equilibrium under the action of both inertial and viscous forces and the balance between these depends not only on the properties of the oil but also on the characteristics of the airflow over the wing under the test condition. In general, when there is no region of complete full-chord separation, it is thought that the oil pattern gives a good qualitative picture of the flow in the boundary layer and experiments elsewhere have suggested that even the quantitative differences between the oil flow and air flow are small for a swept-back wing at moderate incidences when there is no serious boundary-layer separation or complex vortex patterns in the flow. Under other conditions, and particularly in the region of a serious separation, the oil may respond rather to the pressure gradients over the wing and may even possibly move against the flow, seeking the peak-suction position. It may be necessary to interpret the validity of the oil pattern differently for even different parts of a given wing at a given incidence. To argue about the general validity of the technique or even to attempt to understand every feature shown in the oil patterns would be futile. Rather, each particular example must be judged on its own merits and in general, in each case, it will be possible to accept the evidence of some features in the oil pattern quite unequivocally (*see* section 6.12) and use these in helping to understand the overall force and moment data. The technique should be regarded as one link in a chain that also includes the evidence obtained from the overall data, a knowledge of aerofoil stalling characteristics, experiments by other techniques such as a water tunnel, pressure-plotting tests and so forth.

Whatever its limitations, it may be noted that the oil-film technique, as described gives a more refined picture and one that should be closer to the actual behaviour of the air than can be obtained by the use of surface tufts. This is because, first, with tufts, it is not possible to obtain a 'continuous' picture over the wing surface and further, the evidence of an individual tuft is integrated over its length and so is dependent on the magnitude and direction of the velocity and on the depth of the boundary layer at each point along its length. Second, it has been found experimentally that the overall force and moment data even near the stall are not sensibly affected by the thin coating of titanium oxide but are often markedly influenced by the presence of surface tufts. Incidentally, these remarks concerning the validity of evidence from tufting tests are again reasons, not for ignoring such evidence but merely for being careful in its interpretation.

4. *Correction and Reduction of Results.*—Corrections were applied to the observed Mach number and to the dynamic pressure to allow for the blockage effect of the models. These corrections were calculated by the method of Ref. 4 and typical values of the Mach number increment, ΔM , are given in the following table:

Corrected Mach number Incidence (deg)	0.50	0.80	0.90	0.94
0	0	0.002	0.007	0.015
8	0.001	0.004	0.011	0.022
14	0.001	0.007	0.020	—

Corrections were also applied to the results for the effects of tunnel constraint.

In the 'net'-wing tests, the coefficients are based on the net wing area and the mean chord of the netwing and the pitching moments are related to the mean quarter-chord point of the netwing. Similarly, the dimensions of the gross wing are used in reducing the results of the tests on wing C with body attached, *e.g.*, the pitching moments in this case are referred to the mean quarter-chord point of the gross wing.

In all cases, the spanwise centre of load C_l/C_L is related to the aircraft centre-line (*i.e.*, the floor of the tunnel) and is never related to the root of the net wing.

5. *Presentation of Data and Discussion.*—The order in which the results of these tests are discussed and illustrated in the figures is determined by two considerations: First, the fact that, as stated in the introduction, most interest centres on the stalling characteristics and in particular, on the pitching moments at high values of C_L and second, the fact that the variation of these characteristics with both Mach number and Reynolds number is understood better after correlating the results obtained at low Mach number with the observed flow patterns.

Accordingly, a description is first given of how the major features of these flow patterns at low Mach number are interpreted (section 6.1). The development of the patterns with increasing incidence is then described (section 6.2) and it is convenient to combine this with a discussion of how these characteristics are affected by Reynolds number. In the next section (section 6.3), the main trends in the force and moment data are correlated with the changes in the flow patterns. This discussion is helped by the fact that, as far as possible, an appropriate selection of flow patterns is shown for each wing opposite the corresponding C_L vs. α and C_m vs. C_L curves in the figures (*e.g.*, Figs. 5, 6, 8, 9, 11 and 12).

For various reasons that will appear from the subsequent discussion, the results for wing C are the most suitable basis for this detailed discussion in sections 6.1 to 6.3. Many of the points raised also apply of course to the results for wing A and the two wings are compared in section 6.4. The main characteristics of the two wings at high Reynolds numbers are summarised in section 7 and so, for quick reading, this section should be read before section 6.

The variation of the characteristics at high C_L with increasing Mach number is considered in section 8 where it is shown that the basic nature of the characteristics, as described for low Mach number, continue to apply up to near $M = 0.85$ but that at higher Mach numbers, the problem is dominated by the effects of shock-induced separations. The discussion in section 8 is therefore sub-divided into these two Mach number ranges.

Finally, the data for low values of C_L are discussed in section 9; here, most interest centres on the effect of the change in section shape between wings A and C on the variation of C_D with Mach number.

6. *Detailed Discussion of Stalling Characteristics at Low Mach Number.*—6.1. *Interpretation of Basic Features Shown in Oil-flow Patterns.*—Some description of the main features of the oil-flow patterns at high incidence and of how they are interpreted is essential for the subsequent discussion.

The basic ideas suggested by the flow patterns are that, for the wings being considered here, at low Mach numbers, as the incidence is increased, the laminar boundary layer separates from near the leading edge of the outer sections; that, as the incidence is increased further, the area of wing affected by this separation extends rearward and inward; that, as suggested in Ref. 5, a part-span vortex sheet is formed, originating from near the wing-root leading edge at the inboard end of the separation and that this vortex sheet trails across the wing, standing up from the wing surface and bent outward at an angle which, when measured in the plane of the wing, is often about 20 deg, relative to the free-stream direction. The words 'part-span' are here used in the sense that the vortex sheet originates from some point that is part of the way out along the wing from root to tip.

These features can be deduced most clearly from the photographs for $\alpha = 12$ deg, 14 deg for wing C at $R = 2.5 \times 10^6$ (Fig. 9). The most distinctive feature in these flow patterns is the 'herring-bone' effect starting from near the wing-root leading edge. The flow close to the surface on either side of the back-bone (A—Fig. 9) of this pattern is evidently influenced by the velocities induced by a part-span vortex sheet. It is considered that the approximate position of the projection of this vortex sheet in the wing surface is given by the locus (B) joining the points where the flow lines ahead of (A) reach their maximum deflection from the free stream. Hence, ahead and outboard of (A), the outward flow is under the vortex sheet while just inboard and behind (A), where the flow lines turn markedly towards the free-stream direction, flow from over the top of the vortex sheet has evidently come down to the wing surface and there is again attached, streamwise flow. The line of demarcation (C) separates this flow from over the top of the sheet and the flow over the innermost part of the wing, which, as remarked earlier, has an appreciable spanwise component because of the flow out through the gap between the wing and body.

It may be noted that the idea of a 'part-span vortex sheet' trailing across the wing is a simplified mathematical concept from what is probably a diffuse region of concentrated vorticity. The above interpretation of the 'herring-bone' pattern can be substantiated, for example, by a study of the photograph for $\alpha = 12$ deg, taken soon after starting the tunnel (*see* Fig. 9). This shows that the oil flow on both sides of (A) is more rapid than elsewhere on the wing and thus, in particular, that the outward flow on the outer side of the 'dividing' line (A) is due to an increase in the spanwise velocity component (resulting from the presence of the vortex sheet) rather than a decrease in the chordwise velocity component which would be the case if all this area were a 'dead-air' region close to the surface.

Outboard of the vortex sheet (B), the flow lines turn back towards the trailing edge, *i.e.*, towards the free-stream direction and finally merge into one line (E) which marks the rearward limit of a region where the titanium oxide appears mottled, with no clearly defined direction of flow. In the final pictures, this mottled region is confined to between lines (D) and (E) while the diagonal flow lines, slightly more swept than the leading edge, ahead of (D) represent a slow movement of oil, largely spanwise, from the lower surface round the leading edge. In the earlier stages, soon after starting the tunnel, the whole region ahead of (E) appears mottled. This evidence is interpreted as indicating that the cause of the appearance of the part-span vortex sheet is that the laminar boundary layer has separated from near the leading edge throughout the span outboard of the origin of the vortex sheet and that the whole area ahead of (E) is substantially a 'dead-air' region close to the surface. The high peak suction, close to the leading edge would collapse as a result of the separation, thus permitting the drift of oil (and possibly air) round the leading edge from the lower surface*.

Such terms as 'separation', 'dead-air region' and 'reattachment' have so far been used somewhat loosely and it is important to understand the sense in which they have been used and to emphasize how the three-dimensional characteristics may differ from those familiar in two-dimensional flow. In two-dimensional flow, a separation of the laminar boundary layer near the leading edge of a wing may take one of three forms⁵: a short bubble with almost immediate reattachment, a long bubble with reattachment further aft along the chord and a 'burst' short bubble in which there is no reattachment. It would not be easy to detect the first of these with certainty from the flow patterns being considered here and also it would not be expected that a significant vortex sheet would separate a region where there was a short bubble from one where there was no separation. Hence, it may be concluded that, though a short bubble may be present on these wings at low and moderate incidences and also inboard of the vortex sheet when present, the separation outboard of the vortex sheet is of one of the other two types.

It is not possible to decide definitely from the observed flow patterns between these two alternatives but it seems more likely that the separation at this Reynolds number, is of the 'long bubble' type. The absence of any tendency for the oil to flow forward (as found to a

* The oil flow would be expected to be closely parallel to the leading edge for the region near the stagnation point on the lower surface.

marked extent on certain other swept-back wings) suggests that the chordwise pressure gradient in this region is small (*i.e.*, as with a 'long' bubble in two-dimensional flow) rather than appreciable and adverse as behind the point of separation of a 'burst short' bubble in two-dimensional flow. The evidence is not conclusive because the behaviour of the oil in the region of the separation is probably also affected by other considerations, *e.g.*:

- (a) The sweep of the leading edge which affects the magnitude of the spanwise flow from the lower surface
- (b) Whether the plane of the part-span vortex sheet intersects the wing trailing edge inboard or outboard of the tip and of the section under consideration. This depends on the shape of the vortex sheet and of the geometry of the wing. Clearly, the possibility of reverse flow is greater when the vortex sheet has moved further inboard.

If it is correct to conclude that the separation is of the 'long' bubble type, then it is possible for the boundary layer to reattach ahead of where the vortex sheet crosses the section being considered, *e.g.*, in the vicinity of (E). This is not thought to be likely but it is important to note the possibility because it serves to emphasize that, though it is being assumed that the vortex sheet has its origin at the inboard end of the separation, this does not necessarily mean that the boundary layer has separated over all the wing outboard of the part-span vortex sheet as it subsequently trails back across the wing.

It has already been seen that streamwise flow with an attached boundary layer is apparently established behind the vortex sheet (near A) and this indicates one of the most important differences between the two-dimensional and three-dimensional problems. If a laminar boundary layer separates from a section in two-dimensional flow, then the only normal means at low Mach number whereby the boundary layer can reattach further aft along the chord is for transition to turbulence to occur in the separated layer⁵. In the three-dimensional case of a swept-back wing, it appears that reattachment is also possible through the medium of a part-span vortex sheet that has originated further inboard. It follows that for the sections of at least the present wing, irrespective of whether the original separation is of the 'long' or 'burst short' bubble types, the sectional force and moment characteristics should more resemble those obtained with a 'long' bubble in two-dimensional flow, *e.g.*, the local $C_{L\max}$ should be appreciably greater than the value of C_L at which a separation first occurs on the section. The distinction between a 'long' or a 'burst short' bubble may still be of significance in determining the shape of the outer edge of the separated boundary layer ahead of the vortex sheet and hence, the chordwise pressure distribution over the wing surface in this region.

A final general point is that, although attached, streamwise flow only appears aft of (A) (Fig. 9), an increase in lift and hence in the local values of $-C_p$ on the upper surface should occur inboard of the vortex sheet (B) on the simplified potential-flow approach and there is clearly a component of flow close to the surface and not merely a dead-air region aft of (D), thus implying a possible increase in $-C_p$ between (D) and (B) also. If the position of the vortex sheet were to remain the same over some range of incidence (as would happen when the sheet originates from just outboard of the wing root*), the rear end of the dead-air region would not move rearward with increasing incidence. This situation can be described crudely but graphically in the terms that 'the presence of the vortex sheet is limiting the rearward extension of the area affected by the separation'. Such a remark can strictly be criticized but it conveys the right impression of how the vortex sheet can influence the flow over the wing. From the reasoning developed above, it will be realized that it is not a self-evident fact implied by the definition of the vortex sheet.

The spanwise extent of the separation and position of the part-span vortex sheet vary with both incidence and Reynolds numbers and there are in addition several other features in the foregoing general description of the flow characteristics that vary with these variables:

* Or similarly, a stall fence.

(i) *Shape of the part-span vortex sheet.*—As stated in Ref. 5, the vortex sheet cannot sustain any side force and so it takes up the characteristic shape, bent outward, relative to the chord.

For all Reynolds numbers, when the vortex sheet originates from somewhere on the inner half of the wing, it lies at about 20 deg to the chordwise direction over most of the chord and only bends back near the trailing edge.

At $R = 2.5 \times 10^6$, at the lower incidences, when the origin of the vortex sheet is further out along the wing, the initial shape of the sheet is more curved and for some distance back from the leading edge, the projection of the sheet appears to be only slightly more swept than the wing leading edge. This experimental fact is at present only imperfectly understood. The characteristic does not appear to the same extent at $R = 6 \times 10^6$, provided it is assumed that some uncertainty regarding the origin of the vortex sheets (see section 6.2) is dismissed as the oil behaviour being unrepresentative of the airflow.

(ii) *Rearward extension of dead-air region with incidence.*—No data regarding the characteristics of this particular section in two-dimensional flow are available and so it is not possible to draw any general conclusion regarding whether the rearward extension of the dead-air region is greater or less than that of the long bubble to be expected on this section in two-dimensional flow. With more certainty, however, it can be suggested that the growth of the dead-air region for the sections say, from $\eta^1 = 0.1$ to 0.4 will be retarded over some incidence range beyond $\alpha = 14$ deg at $R = 2.5 \times 10^6$ because the part-span vortex sheet will continue to originate from near the same point as at $\alpha = 14$ deg.

(iii) *Displacement of vortex sheet from wing surface.*—At $R = 2.5 \times 10^6$, the flow patterns suggest that the bottom of the sheet remains close to the wing upper surface back to about $0.75c$ but that behind this, at least the strength of the vorticity close to the surface becomes less. This can be interpreted in various ways:

- (A) That there is an actual displacement of the vortex sheet from the edge of the boundary layer*
- (B) That, as the vorticity tends to be concentrated near the top of the sheet, proportionately less of the vorticity is near the wing surface where the sheet is higher
- (C) That the effect is apparent and results from a marked thickening of the boundary layer under the sheet.

At $R = 6 \times 10^6$ and at the higher incidences (e.g., above $\alpha = 15$ deg) it appears that the vortex sheet effectively or literally leaves the surface further forward along the chord. Using as a crude criterion, the extent of the region near the trailing edge in which the usual spanwise flow in the boundary layer can be observed throughout the wing span, it seems that the displacement of the sheet from the surface moves forward from about $0.75c$ at $\alpha = 15$ deg to about $0.6c$ by $\alpha = 18$ deg. As this effect proceeds, the spanwise extent over which the 'presence of the vortex sheet can limit the rearward extent of the dead-air region decreases', thus allowing the latter to extend over the whole chord except immediately outboard of the origin of the sheet.

(iv) *Presence of a turbulent separation.*—The flow patterns for $R = 6 \times 10^6$ (Fig. 12) suggest that above $\alpha = 15$ deg, a region of turbulent separation appears to form near the trailing edge near the tip and to extend forward and inward with increasing incidence until by $\alpha = 18$ deg; it extends from about mid-semi-span to the tip and the furthest forward point of the separation appears to occur at about $0.85c$. The flow photographs cannot be used as conclusive evidence that turbulent separation is occurring but merely that it is probable. Flow photographs for these incidences at the lower Reynolds number are not available but it is likely that then the laminar separation from near the leading edge would have extended to the trailing edge before the turbulent separation could occur.

* If this is the case, the inclination of the surface to the free-stream direction is a major parameter (see section 7).

6.2. *Variation of Spanwise Extent of Separation with Incidence and Reynolds Number (Wing C).*—Since the wing has the same section at all positions along the span, the spanwise extent of the separation should be determined by four factors:

- (a) The spanwise loading
- (b) The change in shape of the chordwise loading with position along the span
- (c) The increase in Reynolds number from tip to root and possibly
- (d) The spanwise drift of the boundary layer.

The spanwise lift distribution for the wing at $M = 0$ has been calculated by the method of Ref. 10 and is shown in Fig. 32. The peak value of C_L/α occurs between about 0.6 and 0.7 of the net semi-span but, outboard of this, C_L/α does not decrease rapidly until beyond $\eta^1 = 0.85^*$ which is at about the inner end of the curved tip. The change in shape of the chordwise loading is such that, near the tip, the peak-suction value for a given C_L , is larger and occurs nearer the leading edge than for sections further inboard. Combining these two results, therefore, it would be expected that any separation of the laminar boundary layer near the leading edge would occur first at the outer end of the region where (C_L/α) is relatively high, *i.e.*, at about $\eta^1 = 0.85$. This is confirmed by the flow patterns.

For example, for $R = 2.5 \times 10^6$, the presence of a part-span vortex sheet is first observed in the photograph for $\alpha = 7$ deg (not included in Fig. 9) when it is lying very close to the tip, appearing to originate from near the leading edge at about the inner end of the curved portion ($\eta^1 = 0.85$). At $\alpha = 8$ deg (Fig. 9), it has moved in slightly and springs from near $\eta^1 = 0.78$. Its subsequent inward movement at $R = 2.5 \times 10^6$ with increasing incidence is correlated in the following table with the estimated local C_L at the appropriate spanwise position and the Reynolds number based on the local chord.

Incidence (deg)	Distance along net semi-span of origin of vortex sheet as proportion of net semi-span (<i>i.e.</i> , η^1)	Estimated local C_L at this position	Local Reynolds number (R_l) $\times 10^{-6}$
7	0.85	0.41	1.77
8	0.78	0.50	1.92
9	0.68	0.57	2.12
10	0.44	0.61	2.62
12	0.23	0.68	3.08
14	0.10	0.75	3.34

Several provisos have to be made regarding these estimated values of local C_L . In their estimation, all non-linear effects have been ignored. Prior to the formation of a part-span vortex sheet, the overall lift curve is closely linear and it would be expected that any serious non-linearity in the local lift curves would be confined to a relatively small region near the tip. The part-span vortex sheet, when present, however, would increase the values of local C_L inboard of it and so the values quoted above would certainly not be representative of the values that would apply if a vortex sheet has formed near to the spanwise position being considered and would even be somewhat in error if a vortex sheet is present anywhere on the wing, outboard of this position.

Despite these reservations, the quoted values of C_L should be a reasonable guide to when the laminar boundary layer separates on any given section. It should be particularly noted that any errors are in the sense that the values of C_L , applicable for the inner sections are underestimated and hence that the variation with position along the span in the value of C_L for separation is at least as great and probably rather more than that shown in the table.

* η^1 based on net wing, outboard of body.

The spanwise lift distribution does not therefore provide the complete answer to the development of the stall. As already suggested, the change in shape of the chordwise loading from root to tip is probably responsible for the separation bubble first forming outboard of the point for maximum C_L (*i.e.*, for it forming for $C_L \approx 0.4$ at $\eta^1 = 0.85$, compared with $C_L \approx 0.5$ for $\eta^1 = 0.78$, despite the small difference in Reynolds number) and it also probably results in the onset of the separation being delayed near the root. In fact, very close to the root, the chordwise pressure gradient near the leading edge may never be sufficient to induce a laminar separation. On the other hand, over much of the central part of the semi-span, the changes in shape of the chordwise loading should be relatively slight and so, the steady increase in the value of the 'critical' C_L between $\alpha = 8$ deg and 14 deg from near 0.5 to near 0.75 is probably largely due to the increase in local Reynolds number from about $R_l = 2 \times 10^6$ to about $R_l = 3.3 \times 10^6$.

This view is supported by the comparison of the results obtained from the tests at mean Reynolds numbers of $R = 2.5 \times 10^6$ and $R = 6 \times 10^6$. Before showing this, it may be noted that the oil flow patterns obtained at $R = 6 \times 10^6$ (Fig. 12) are not so clear as those for $R = 2.5 \times 10^6$ in suggesting that the vortex sheet originates from the most inboard point on the wing at which the laminar boundary layer has separated. It is true that as before, if the projection of the vortex sheet over most of the chord is extrapolated forward to the leading edge as a straight line, it appears to intersect the leading edge just inboard of where the dead-air region becomes evident on the photograph. On the other hand, the locus drawn through the points where the oil flow lines reach their maximum deflection from the free stream appears to originate further inboard and at a point about $0.1c$ back from the leading edge. This characteristic is not at present understood and it is possible that it is a function merely of the behaviour of the oil*. It therefore seems reasonable to consider just the positions corresponding to the inward extent of the dead-air region, as observed from the photographs. The following table gives the correlation between these positions for incidences of 14 deg, 15 deg, 16 deg and 18 deg with the estimated local values of C_L (subject to the same provisos as before) and the local Reynolds numbers:

Incidence (deg)	Position as proportion of net semi-span	Estimated local C_L	Local Reynolds number (R_l) $\times 10^{-6}$
14	0.83	0.84	4.3
15	0.76	0.93	4.7
16	0.59	1.01	5.6
18	0.25	1.03	7.3

These values of local C_L are plotted against the local Reynolds number in Fig. 33, together with the values deduced earlier from the flow patterns for $R = 2.5 \times 10^6$. It can be seen that the values from the two series of tests lie remarkably close to a single mean curve and the scatter, in view of the various approximations in the analysis, is certainly sufficiently small to justify the contention that the increase in the value of the 'critical' C_L with inward spread of the separation, particularly at the lower Reynolds numbers, is a function mainly of the local Reynolds number.

* The different oil behaviour may be related to the fact that at the higher Reynolds number, the vortex sheet is lying well out on the wing at a relatively higher incidence and hence when there is a more pronounced spanwise drift of the boundary layer inboard of the sheet. This is shown by the fact that the oil flow lines on the inner wing lie close to the free-stream direction near the leading edge where the boundary layer is relatively thin and where the local velocity outside the boundary layer is high but then they soon turn markedly outward. Consequently, soon after starting the tunnel, a large amount of the titanium oxide suspension collects inboard of the vortex sheet in the region that appears particularly black in the final photograph. Subsequently this disperses, some flowing towards the trailing edge and some turning towards the leading edge. It is not clear, therefore, whether the oil pattern in this region is formed merely because the accumulation of oil tends to flow towards the peak-suction region just inboard of the separation.

Fig. 33 shows that the scale effect on the 'critical' C_L is appreciable up to about $R_i = 5.5 \times 10^6$ but then becomes insignificant in the test range. The fact that the variation is of this form strongly suggests that, using the terms as for the characteristics in two-dimensional flow, the separation is of the 'long' bubble type for $R_i < 5.5 \times 10^6$ but of the 'burst short bubble' type except near the tip for $R_i > 5.5 \times 10^6$. As already pointed out, even when the separation is of the 'burst short bubble' type, reattachment may still occur further aft along the chord of a section on a swept wing such as this, *i.e.*, aft of a part-span vortex sheet that crosses the section, having originated from a point further inward. Leading features of the results that are associated with the existence of this scale effect are:

- (i) With increasing Reynolds number, the first appearance of the part-span vortex sheet is delayed—from about $\alpha = 7$ deg ($C_L \simeq 0.35$) at $R = 2.5 \times 10^6$ to $\alpha = 10$ deg ($C_L \simeq 0.57$) at $R = 6 \times 10^6$
- (ii) At the higher Reynolds number ($R = 6 \times 10^6$), the part-span vortex sheet remains located far out (near the inboard end of the curved leading edge at the tip) for an appreciable range of incidence ($\alpha = 10$ deg to 13 deg) but then moves in more rapidly than at lower Reynolds numbers
- (iii) At Reynolds numbers higher than those covered in these tests, the first appearance of the vortex sheet should be further delayed but the patterns for $\alpha = 16$ deg and above are likely to be similar to those at $R = 6 \times 10^6$ —at least, as regards the extent of the outer dead-air region and the position of the part-span vortex sheet.

6.3. *Correlation between Flow Patterns and Overall Balance Results (Wing C).*—The overall results for wing C at low Mach number in Figs. 8, 10, 13, 14 and 15 can be interpreted in terms of the flow characteristics discussed above. In the following discussion, the values of C_L that are quoted are a mean between those for the net wing and for the gross wing-body combination which differ by almost 10 per cent in their measured lift-curve slopes for reasons discussed later in section 9.1.

At incidences below that at which a significant separation or part-span vortex sheet first becomes evident in the flow patterns, the C_L vs. α and C_m vs. C_L curves are reasonably linear while the increase in the effective profile drag with C_L can be accounted for largely by an observed forward movement of the transition position on the upper surface from about $0.7c$ at $C_L = 0$, $R = 2.5 \times 10^6$ to near the leading edge by $\alpha = 4$ deg.

Good agreement is found between the incidence at which a separation first appears in the flow patterns and that above which $C_D - C_L^2/\pi A$ starts to increase appreciably with C_L . In the absence of any flow patterns, the drag data would give the clearest idea of when a separation had first occurred ($C_L \simeq 0.35$ at $R = 2 \times 10^6$; $C_L \simeq 0.57$ at $R = 6 \times 10^6$).

6.3.1. *Effects at $R = 2 \times 10^6$ following appearance of separation and vortex sheet.*—It is convenient to divide the range between $C_L = 0.35$ and $C_{L_{\max}} \simeq 1.05$ into two at about $C_L \simeq 0.7$. In the lower range, the origin of the part-span vortex sheet moves in from about $\eta^1 = 0.85$ to $\eta^1 = 0.23$ but the dead-air region does not extend back even to mid-chord except near the extreme tip. Hence a rough distinction between the two incidence ranges is that the lower is characterised more by the effects of the vortex sheet and of its inward movement than by the direct effect of the separation outboard of it while in the higher range, the results are mostly dependent on the growth of outer dead-air region and on the fact that the increase in lift inboard of the vortex is now largely occurring near the wing root and ahead of the wing aerodynamic centre.

In the first range ($C_L = 0.35$ to 0.7), the principal effects are as follows:

- (a) *Drag* (Figs. 10 and 15).—As would be expected, the increase of $(C_D - C_L^2/\pi A)$ with C_L occurs gradually rather than suddenly. A very crude analysis suggests however that the increase is more than could be accounted for entirely by the growth of the dead-air

region, considered as a long bubble (by comparison with the results⁵ for the NACA 64A006 section in two-dimensional flow). Part of the increase in drag is presumably a result of the changes in chordwise and spanwise loading induced by the vortex sheet. Near $C_L = 0.65$, the rate of increase of C_D with C_L tends to decrease slightly, perhaps because the rate of inward extension of the region of separation with increasing C_L is also then beginning to decrease. If $C_D \equiv C_{D0} + (\kappa/\pi A) C_L^2$, κ increases from a value of the order of 1.1 at low C_L to about 1.9 for $C_L \approx 0.7$ (N.B. $R = 2 \times 10^6$).

(b) *Lift* (Figs. 8 and 14).—The lift-curve shape for values of C_L between 0.35 and 0.7 is higher than at low C_L . This shows that the increase of lift inboard of the vortex sheet has a greater effect than the reduction in lift-curve slope on the outer sections. The increase in overall lift-curve slope is particularly marked in the early stages between about $C_L = 0.35$ and 0.5 and then tends to die out. In this connection, it should be noted that the increase in lift, resulting from the vortex sheet, should reach a maximum at some value of C_L . For an untapered wing, the increase in lift produced by a vortex sheet of a given height would be greatest when the sheet was at the tip because then, the full end-plate effect would be obtained. In the present case, however, the maximum effect should be reached when the vortex sheet is part of the way in along the span because, in the first place, the height of the sheet would increase as it moves inboard (owing to the increase in incidence) and secondly, its strength should be roughly proportional to the 'critical' C_L which has been seen to increase appreciably from root to tip.

(c) *Longitudinal stability* (Figs. 8 and 14).—In the initial stages, after the formation of the vortex sheet, between about $C_L = 0.35$ and 0.5, there is a gradual increase in $(-\partial C_m / \partial C_L)_M$ which, by $C_L = 0.7$, amounts to about 0.09. These overall results are an integration of various opposing effects, *viz.*:

- (i) Outboard of the vortex sheet and mostly aft of the c.g. there is a slight loss in lift because of the reduced value of $(\partial C_L / \partial \alpha)_M$ for the sections with effectively a 'long bubble'. This gives, at least in this incidence-range, a nose-up contribution to the overall C_m .
- (ii) Outboard of the vortex sheet, the local aerodynamic centre would move rearward as a result of the change in shape of the chordwise loading—a nose-down contribution.
- (iii) Inboard of the vortex sheet and particularly close to it, there is an increase in lift. Initially, this gives a nose-down contribution as with an end-plate but as the vortex sheet moves inward, the effect on the overall C_m decreases and if sufficient of that part of the sheet that lies close to the wing surface moves ahead of the c.g., this contribution to C_m could become nose-up. The tendency for this to happen is of course reduced by the characteristic shape, *i.e.*, the bending outward of the vortex sheet.
- (iv) The local aerodynamic centres of the sections cut by the vortex sheet is moved rearward by the effects of the vortex sheet—another nose-down contribution.

Clearly, the overall effect on C_m could not be predicted easily and it evidently depends intimately on the particular wing plan-form. Qualitatively, for the present wing, it seems that initially (iii) is slightly the more important effect, particularly with reference to the quarter-chord point of the gross wing and that the gradual loss of stability between $C_L = 0.5$ and 0.7 is to some extent, due to the disappearance of the nose-down contribution introduced by (iii) between $C_L = 0.35$ and 0.5, coupled with a steady increase in effect (i). The changes in stability are gradual in sympathy with the gradual changes in the flow pattern.

(d) *Spanwise centre of load* (Figs. 10 and 15).—There is no systematic variation in the spanwise position of the centre of load until it starts to move inward at about $C_L = 0.6$ or $\alpha = 10$ deg. These results can also be explained qualitatively. At lower incidences, the part-span vortex sheet is lying outboard of the centre of load which,

for the net wing, is at about $\eta = 0.47$ and so, in terms of the root bending moment, an approximate balance is obtained between the effects of the increase in lift due to the vortex and the smaller decrease in lift outboard of it. As the vortex sheet moves further in, however, the second factor grows in importance and also, when the mean arm of the increased lift due to the vortex is smaller than the distance to the centre of load, the two factors then act in the same sense in producing an inward shift of the centre of load.

In the upper range (above $\alpha = 12$ deg or $C_L = 0.7$), the overall C_D increase more rapidly with C_L . There is a significant reduction in $(\partial C_L / \partial \alpha)_M$ and there is a greater forward movement of the wing aerodynamic centre position, *e.g.*, for $C_L = 0.8$, the reduction in $(-\partial C_m / \partial C_L)_M$ for the gross wing, compared with the value at low C_L , is about 0.16 (and rather more, locally, near $C_L = 0.7$). All three effects are consistent with the explanation that maximum lift has been attained on the sections near the tip and that, as the incidence is increased, this happens over progressively more of the semi-span. (The considerable extension of the dead-air region between $\alpha = 12$ deg and $\alpha = 14$ deg at $R = 2.5 \times 10^6$ can be noted in Fig. 9.) The overall results suggest that, the outer sections attain their local values of $C_{L \max}$ before the dead-air region has extended fully along the chord, *e.g.*, when it has extended to about $0.3c$ to $0.5c$. No precise estimate of the actual values of the local $C_{L \max}$ can be given but, for the sections near $\eta^1 = 0.8$, $C_{L \max}$ appears to be rather less than 0.7. This value is appreciably less than what might be expected for this section in two-dimensional flow but probably better than $\cos \phi \times$ the two-dimensional value.

As with the values of $C_{L \text{crit}}$, there should be a considerable spanwise variation in the value of the local sectional $C_{L \max}$. This is indeed shown by the fact that although the reduction in $(\partial C_L / \partial \alpha)_M$ and probably the attainment of $C_{L \max}$ on the sections near the tip, starts at about $\alpha = 12$ deg, the $C_{L \max}$ for the wing as a whole is not reached until near $\alpha = 24$ deg (Fig. 14). During this range of incidence:

- (A) the inward movement of the centre of load becomes less above about $C_L = 0.85$ ($\alpha = 16$ deg). At higher incidences, the centre of load is about 0.04 to $0.05 \times$ semi-span further inboard than at low values of C_L
- (B) the reduction in longitudinal stability becomes somewhat less severe above about $C_L = 0.95$.

Both these effects, and in this order, could be predicted qualitatively.

The value of $C_{L \max}$ achieved by the wing should be noted particularly. The measured value for the gross wing-body combination is about 1.0 and so the corrected value (*see* section 9.1) is probably near 1.05. This swept-back wing, therefore, gives a higher value of $C_{L \max}$ than would be expected from this section in two-dimensional flow, for which the value should be near 0.9. From a comparison of the results of tests on various other swept-back wings, it appears that this conclusion applies generally if the angle of sweep is more than about 45 deg. The relatively high value for the overall $C_{L \max}$ implies that the sectional values of $C_{L \max}$ for the inner wing sections are high for it has been seen above that for the sections out near the tip, the local $C_{L \max}$ is only about 0.7 at this Reynolds number. The effect must therefore be related to the effect of the part-span vortex sheet which, at high incidences, originates from near the wing-root leading edge and as already discussed, limits the rearward extension of the substantially dead-air region on those sections immediately outboard of the origin of the sheet. These sections would achieve a higher local $C_{L \max}$ than if the vortex sheet were not present because the region where the values of $-C_p$ are relatively low and constant along the chord is limited to only the forward part of the sections.

Various series of tests have shown that these relatively high values of overall $C_{L \max}$ are only achieved with wings of say, 50-deg to 60-deg sweep and this is presumably because:

- (a) With a smaller angle of sweep, the distortion in the shape of the chordwise loading near the root of the wing may not be sufficient to prevent a separation-bubble forming

close to the wing-root leading edge. If this did form right into the wing-body junction, the part-span vortex sheet would probably be eliminated

- (b) Since experimental observation on various wings of different plan-forms shows that the angle at which the vortex sheet is deflected outward from the free-stream direction is always about 20 deg, the angle of sweep of the sheet, relative to the wing leading edge is less for the highly swept wing. Hence less of the wing lies outboard and ahead of the vortex sheet and the dead-air region is more closely limited.

In the present case, the actual value of $C_{L\max}$ is only of academic interest because of the large reduction in longitudinal stability that occurs at lower values of C_L but it does illustrate the possible useable C_L that might be achieved if the stalling of the outer sections was delayed sufficiently by some means such as a drooped leading edge or a fence⁶. Since the relatively high value of $C_{L\max}$ appears to depend on the presence of a vortex sheet across the inner sections of the wing, the correct choice of tail position is clearly very important.

6.3.2. *Effects at $R \approx 6 \times 10^6$.*—The effects at $R \approx 6 \times 10^6$ are similar qualitatively to those just described. The differences that exist are due first and foremost to the delayed appearance of a part-span vortex sheet and area of separation; then, to the fact that the separation is limited to a small region near the tip over a larger range of incidence than at $R = 2 \times 10^6$ and finally to the fact that the subsequent inward movement of the vortex sheet is more rapid than before.

As already noted, the first effect is responsible for the results that the appreciable increase of $(C_D - C_L^2/\pi A)$ with C_L and the non-linearities in the lift and pitching moment results do not appear until beyond $\alpha = 10$ deg ($C_L = 0.57$) at $R = 6 \times 10^6$, compared with $\alpha = 7$ deg ($C_L = 0.35$) at $R = 2 \times 10^6$.

The results at $R = 6 \times 10^6$ between $\alpha = 10$ deg and 13 deg ($C_L = 0.73$) are consistent with the part-span vortex sheet remaining located far out near the tip for this incidence range (see the flow pattern for $\alpha = 14$ deg, Fig. 12). In this range, the increase of $(C_D - C_L^2/\pi A)$ with C_L is relatively slow and there is a pronounced nose-down change in C_m , amounting to an increase in $(-\partial C_m/\partial C_L)_M$ of about 0.06. At a higher Reynolds number, when the boundary layer would be thinner, this nose-down change might be more marked*. In itself, this nose-down trend may appear innocuous but it follows that the subsequent reduction in stability as the trend is eliminated and reversed with the inward movement of the vortex sheet is also more pronounced. This can be seen more clearly in the results for wing A (Fig. 5) but even for wing C, the useable C_L (defined by the value of C_L above which $(-\partial C_m/\partial C_L)_M$ is more than 0.1 less than at low C_L) only increases from 0.7 to about 0.82 with the increase in Reynolds number from $R = 2 \times 10^6$ to $R = 6 \times 10^6$ whereas the corresponding increase in the value of overall $C_{L\max}$ at which it is thought that the outermost sections attain their local $C_{L\max}$ is from 0.7 to about 0.9 ($\alpha = 16$ deg). Hence, the full potential gain of the increase in the local $C_{L\max}$ of these outer sections is not being realized. This serves to emphasize a general point regarding how the stall should develop for good stability characteristics: the separation on the outer wing sections should clearly be delayed to as high an incidence as possible but when it occurs, it should be allowed to spread rapidly in along the leading edge to near mid-semi-span rather than remaining for a time localized near the wing tip.

The suggestion made above that the outermost sections attain their local values of $C_{L\max}$ near $\alpha = 16$ deg ($C_L \approx 0.9$) is again based on determining the incidence above which there is a marked reduction in $(\partial C_L/\partial \alpha)_M$, a steeper increase of $(C_D - C_L^2/\pi A)$ with C_L and a more severe loss of longitudinal stability. In confirmation, the extent of the dead-air region at $\alpha = 16$ deg, $R = 6 \times 10^6$ is similar to that at $\alpha = 12$ deg, $R = 2.5 \times 10^6$. A crude estimate of the value of the local $C_{L\max}$ of these outer sections suggests that it increases from about 0.7 at $R = 2 \times 10^6$ to about 0.9 at $R = 6 \times 10^6$. This improvement is not as great as the increase in the 'critical'

* As shown more clearly by the results for wing A, it is probable that in this incidence range, the relatively thick boundary layer over the rear of the outer sections gives an increase in C_m which partly offsets the nose-down change which is a result of the effects discussed in section 6.3.1.

value of C_L (*i.e.*, that at which a separation first occurs on the section) and so the difference ($C_{L\max} - C_{L\text{crit}}$) decreases with Reynolds number. This supports the idea previously put forward that at the lower Reynolds number, the laminar separation is of the long bubble type. It is reasonable to suggest that this is so below $R_l = 5.5 \times 10^6$ but that when $R_l > 5.5 \times 10^6$ and $C_{L\text{crit}}$ is near 1.0 and roughly independent of R_l , the separation is of the 'burst short' bubble type (the influence of the vortex sheet would still give $(C_{L\max} - C_{L\text{crit}}) \neq 0$).

Despite the improvement with increasing Reynolds number in the local values of $C_{L\max}$ for the outer sections, the overall $C_{L\max}$ appears to be almost independent of Reynolds number. There are at least three possible contributory reasons for this:

- (a) The values of C_L on the outer sections at high incidence, when they are no longer affected by the part-span vortex sheet may be appreciably less than the values of $C_{L\max}$ on these sections and the influence of Reynolds number be less marked
- (b) The probable occurrence of a turbulent separation over part of the wing (*see* section 6.1, para. 4)
- (c) The reduction in the spanwise extent of the wing affected by the part of the part-span vortex sheet, lying close to the wing surface (*see* section 6.1, para. 3).

The principal features of the overall results for wing C at $R = 6 \times 10^6$, together with those for wing A are summarized in section 7 where some comment is also made on whether these results are likely to apply at higher Reynolds numbers.

6.4. Comparison of Results for Wings C and A.—6.4.1. Flow patterns and overall results for $R = 2$ to 2.5×10^6 (Figs. 5 to 7).—Both the flow patterns and drag data suggest that for $R = 2$ to 2.5×10^6 , the laminar boundary layer first separates on wing A at between α 8 deg and 9 deg ($C \simeq 0.5$) compared with $\alpha = 6.5$ deg ($C_L = 0.35$) for wing C. The flow pattern for wing A at $\alpha = 8$ deg (Fig. 6) shows, for example, that there is a small region near the tip where the flow lines are diverted outward and it is thought that this indicates the presence of a part-span vortex sheet near the tip. Further supporting evidence is provided by the pitching moments where a nose-down trend is evident above $C_L = 0.45$.

The subsequent position on wing A of the origin of the vortex sheet or the inward extent of the outer 'dead-air' region at $\alpha = 12$ deg, 14 deg and 16 deg can be determined* from the flow pattern in Fig. 6 and in the following table, are correlated with the estimated local C_L 's and local Reynolds number:

α (deg)	Position of origin of vortex sheet (expressed as fraction of net semi-span)	Estimated local C_L (('critical' C_L))	Local Reynolds Number (R_l) $\times 10^{-6}$
12	0.68	0.76	2.17
14	0.52	0.85	2.48
16	0.19	0.89	3.12

* In analysing these photographs, it should be noted that the chordwise line and white rectangles near $0.5 \times$ net semi-span indicate the position and points of attachment of the stall fences that were tested on this wing. They are therefore irrelevant features except in so far that the condition of the wing leading edge was not perfect close to where the fence was fitted. The position of the vortex sheet for $\alpha = 12$ deg can be seen clearly but for $\alpha = 14$ deg and 16 deg, the picture is confused by the fact that apparently a series of vortex sheets spring from near the leading edge at various points. However, at $\alpha = 14$ deg, the photographs taken soon after starting the tunnel shows that the outermost sheet originating from about $0.52 \times$ semi-span is evidently the main vortex sheet, since the two further inboard appear much weaker. Observation of the model has shown that the manufacture of the inboard half of the leading edge is not perfect and so faults, such as a depression in the leading edge near $\eta^1 = 0.35$ may be sufficient to induce a premature separation of the boundary layer and an associated vortex sheet. At $\alpha = 16$ deg, the early photograph proves that the main vortex sheet has moved much of the way in towards the root and now, the depression in the leading edge and the imperfection where the fence fits are modifying somewhat the flow outboard of the main vortex sheet.

These estimated critical values of C_L , which are again subject to the provisos noted in section 6.2, are plotted against R_l in Fig. 33 for comparison with the values derived previously for wing C. It follows from this comparison that the result, which can be seen clearly in the flow photographs, that the vortex sheet reaches a given spanwise position at a higher incidence on wing A than on wing C, can be expressed more logically as follows: In the range of Reynolds number from about $R = 2 \times 10^6$ to $R = 3 \times 10^6$, the change in section to the RAE 101 shape results in an improvement of about 0.21 in the value of C_L at which a laminar separation forms near the leading edge. The relative position of the three points derived for wing A (Fig. 33) suggests strongly that this improvement in $C_{L \text{ crit}}$ at a given Reynolds number is a consequence of a shift in the Reynolds number range in which R_l has a marked effect on $C_{L \text{ crit}}$. In other words, $C_{L \text{ crit}}$ is likely to attain a value, comparable with $C_{L \text{ max}}^*$, and roughly independent of R at a lower Reynolds number for wing A (RAE 101 section) than for wing C, the difference in R_l being possibly as much as 1.5×10^6 (*i.e.*, 4×10^6 rather than 5.5×10^6) (*see* also section 6.4.2. below).

These differences can be explained qualitatively in terms of the comparison between the pressure distributions near the leading edge on the two sections at incidence, as shown in Fig. 34. For $C_L = 0.6$, for example, the value of $(-C_p)_{\text{max}}$ for the RAE 101 shape is about 4.0, compared with 5.5 for the section of wing C. Hence, a separation, probably of the long bubble type, would be expected at a lower C_L on wing C and, as seen above, this is what actually happens. The reason for the high peak suctions on wing C is that the immediate leading-edge shape is more bluff than an ellipse. This leads to the same sort of result as if the leading edge radius had been greatly reduced except that, in the latter case, the peak suction would occur nearer the leading edge. Hence, it is possible to describe the section of wing C as having an 'effectively sharper' nose than that of the RAE 101 section of wing A. The change from wing C to wing A should therefore have a similar effect to that produced by an increase in thickness/chord ratio with no change in section shape. On this basis, the present results are quite consistent with other data. For example, it has been found² that for swept wings, with a thickness/chord ratio of 10 per cent, the values of $C_{L \text{ crit}}$ and $C_{L \text{ max}}$ for the outer sections are about equal to each other for even a test Reynolds number of $R = 2 \times 10^6$. This is in accord with an extrapolation of the trend from wing C to wing A.

The improvement due to the change to the RAE 101 shape is greater as regards the values of $C_{L \text{ crit}}$ for $\alpha = 12$ deg and above and hence for $\eta^1 <$ about 0.7 than for the values for the sections near the tip of the wing. For example, as already mentioned, the first appearance of a part-span vortex sheet occurs for about $\alpha = 8$ deg for wing A, compared with $\alpha = 6.5$ deg for wing C, whereas the position of the vortex sheet at $\alpha = 12$ deg on wing A is comparable with that on wing C at $\alpha = 9$ deg, *i.e.*, a delay of 3 deg rather than 1.5 deg. In other words, the vortex sheet remains located near the tip for a larger incidence range on wing A than on wing C and so the initial nose-down moment, following its appearance, is more pronounced for wing A. By the same reasoning as that used in section 6.3 above, the subsequent reduction in stability as the vortex sheet moves in is also greater. The reduction in $(\partial C_m / \partial C_L)_M$, for the net wing, compared with the value at low C_L , already amounts to about 0.24 above about $C_L = 0.7$ even though both the flow patterns and overall results suggest that $C_{L \text{ max}}$ is not reached over a significant proportion of the semi-span until about $\alpha = 15$ deg ($C_L = 0.87$). Compare, for example, the flow patterns which show that there is a considerable increase in the dead-air region ahead of the vortex sheet between $\alpha = 14$ deg and 16 deg. The reduction in $(-\partial C_m / \partial C_L)_M$ above about $C_L = 0.87$ increases to a mean value of about 0.35.

A crude estimate suggests that the value of the local $C_{L \text{ max}}$ of the outer sections of wing A is about 0.8 and so is intermediate between the value (0.7) for wing C at the same Reynolds number and that (0.9) for wing C at $R = 6 \times 10^6$. Hence, in this respect, as for $C_{L \text{ crit}}$, it seems that the difference between the wings at $R = 2$ to 3×10^6 arises from a shift in the Reynolds number range in which scale effect has a large influence on the results (*see* Fig. 33).

* Throughout this discussion, $C_{L \text{ max}}$ implies the local value for the section when it is no longer affected by a vortex sheet originating further inboard.

The overall $C_{L \max}$ (corrected to apply to the full wing-body combination) for wing A is about 1.08 and is possibly about 0.05 higher than for wing C. This may be a result of the better values, noted above, for the local $C_{L \max}$ for the outer sections. It shows at least that the arguments used earlier in explanation of the relatively high values of $C_{L \max}$ apply equally to both wings.

The flow photographs for wing A show that, once again, the projection of the vortex sheet in the wing surface is bent outward, relative to the free-stream direction at an angle of about 20 deg over most of the chord. The patterns observed for the two wings differ in one important respect, however, in that no flow from over the top of the vortex sheet can be seen in the patterns for wing A, *i.e.*, the rear part of the 'herring-bone' pattern is absent (This is why it was stated at the beginning of the discussion that the patterns for wing C give a clearer idea of the behaviour of the flow on these wings). A major factor in accounting for this difference is likely to be the larger incidence that is required with wing A for the vortex sheet to move in to a given position along the span. The larger incidence implies:

- (a) a vortex sheet of greater height and with less of its total vorticity, close to the wing surface
- (b) increased spanwise drift of the boundary layer inboard of the vortex sheet and hence, the difference in the oil patterns may be simply due to a difference in boundary-layer thickness on the two wings, aft of the vortex sheet.

6.4.2. *Effect of increasing Reynolds number to $R = 6 \times 10^6$.*—No flow patterns are observed on wing A at $R = 6 \times 10^6$ but, following the detailed analysis of section 6, the overall results, together with some photographs of tuft behaviour are sufficient to give a fair appreciation of the flow characteristics.

It has already been suggested that the differences between the results for wings A and C at about $R = 2 \times 10^6$ arise largely because the change in section shape gives a shift in the Reynolds-number range in which there is a marked scale effect on the values of $C_{L \text{crit}}$ and $C_{L \max}$ with the RAE 101 section of wing A, this range is shifted to lower values of R . The comparative results obtained at $R = 6 \times 10^6$ prove to be quite consistent with this hypothesis. For example:

- (a) The effects of increasing the test Reynolds number from $R = 2 \times 10^6$ to $R = 6 \times 10^6$ are less marked for wing A, than for wing C, as would be expected in view of the higher values of $C_{L \text{crit}}$ already obtained for wing A at $R = 2 \times 10^6$
- (b) Wing A retains its superiority over wing C even at $R = 6 \times 10^6$ in respect of the value of overall C_L at which a boundary-layer separation and part-span vortex sheet first have a significant effect, as would be expected since it has been suggested (Fig. 33) that a Reynolds number of $R = 6 \times 10^6$, based on the mean chord, is sufficient to eliminate the scale effect for virtually all the outer sections of wing A but not those of wing C
- (c) At higher incidences, however, the results for wings A and C are closely similar as would be expected since, then, the characteristics are related principally to the values of $C_{L \text{crit}}$ on the inner sections, the values of $C_{L \max}$ for the sections outboard of the vortex sheet and on the shape of the vortex sheet. All these factors should be less subject to scale effect near $R = 6 \times 10^6$ and also, as already suggested, appear to be less dependent on the change in section shape between the two wings.

A final point about the results for wing A at $R = 6 \times 10^6$ is that between about $C_L = 0.5$ and 0.7 a reduction in $(-\partial C_m / \partial C_L)_M$ of about 0.07 occurs (accompanied by a reduction in $(\partial C_L / \partial \alpha)_M$). This seems to occur prior to the first appearance of a separation near the leading edge or of a part-span vortex sheet and on the basis of subsequent tests with stall fences fitted (Part II), would appear to be caused by the effective camber of the thick boundary layer over the upper surface of the outer sections and should be less pronounced at higher Reynolds numbers. For wing C, the effect is probably present but masked by the effects of the vortex sheet which has already formed by these values of C_L .

7. *Summary of Characteristics of Wings A and C at High C_L , Low Mach Number and High Reynolds Number.*—It has been seen that the results for these wings are subject to considerable scale effect at low Mach number between $R = 2 \times 10^6$ and $R = 6 \times 10^6$ and that this is largely associated with a variation, as shown in Fig. 33, in the value of $C_{L \text{ crit}}$ with R_l where $C_{L \text{ crit}}$ is the value of C_L at which the laminar boundary layer first separates near the leading edge of the section and R_l is the local Reynolds number (the curves in Fig. 33 apply to the central part of the semi-span rather than to the immediate vicinity of the root and tip).

Above about $R_l = 5.5 \times 10^6$ for wing C and, it is thought, $R_l =$ about 4×10^6 for wing A, this variation of $C_{L \text{ crit}}$ with R_l appears to die out, as might be expected, since $C_{L \text{ crit}}$ is then of the order of 1.0 and hence should be about the same as the ultimate values of the sectional C_L (though higher values of C_L would probably be attained in the incidence range immediately beyond the incidence for $C_{L \text{ crit}}$ when the section would be cut by a part-span vortex originating from a point further inboard). It seems therefore that once all the sections of the wings are operating above these values of R_l , scale effect of the type encountered between $R = 2 \times 10^6$ and $R = 6 \times 10^6$ should not occur. More generally, further scale effect is unlikely provided the stall is still basically caused by a laminar separation from near the leading edge. Even, if at a higher Reynolds number, transition occurred ahead of the point where the laminar layer would normally separate, no marked change in the overall results would necessarily result since the turbulent boundary layer might continue to separate near the leading edge rather than from near the trailing edge.

At a Reynolds number of $R = 6 \times 10^6$, based on the mean chord, the above condition is satisfied for wing A but not for wing C. However, even in the latter case, on the above suppositions, further scale effect would be confined to a further increase in the value of C_L at which a separation first occurred near the tip but the results for $\alpha > 16$ deg, including the value of C_L corresponding to the first reduction in longitudinal stability, should not be seriously affected. These suggestions are supported by the fact that tests elsewhere at low Mach number on a configuration closely similar to the wing-body combination of wing C have shown a similar scale effect up to $R = 6.8 \times 10^6$ to that shown by the present results but little further scale effect between $R = 6.8 \times 10^6$ and $R = 11 \times 10^6$, except possibly in a small range of incidence near that at which the vortex sheet first appears.

It seems likely therefore that the more important features of the overall results obtained at $R = 6 \times 10^6$ should apply in flight. The principal results are as follows—values quoted are for wing A with those for wing C in parentheses:

- (a) The boundary layer separates near the leading edge near the inboard end of the curved tip and a part-span vortex sheet forms at about $\alpha = 13$ deg (10 deg) or $C_L \approx 0.72$ (0.58)*. An increase in $(C_D - C_L^2/\pi A)$ with C_L immediately follows and while the vortex sheet is close to the tip, there is an increase in $(\partial C_L/\partial \alpha)_M$ and a rearward movement of the aerodynamic centre. The nose-down moment is more marked for wing A but at higher Reynolds numbers, wing C might reproduce this effect.
- (b) The first serious reduction in longitudinal stability, associated mainly with the inward movement of the vortex sheet occurs near $C_L = 0.85$ (0.82). This is rather more marked for wing A because of the previous larger nose-down trend and the reduction in $(-\partial C_m/\partial C_L)_M$, compared with the value at low C_L is about 0.20 for the net wing A.
- (c) The dead-air region outboard of the vortex sheet extends considerably near $C_L = 0.92$ (0.92) [$C_{L \text{ gross}} = 0.94$ or $C_{L \text{ net}} = 0.90$], giving a more severe reduction in longitudinal stability, a decrease in lift-curve shape and a steeper increase in $(C_D - C_L^2/\pi A)$ with C_L . The reduction in $(-\partial C_m/\partial C_L)_M$ is at least 0.25 and in some cases is as much as 0.5.

* At higher Reynolds numbers than $R = 6 \times 10^6$, there may be an improvement for wing C from $C_L = 0.58$ to near $C_L = 0.7$.

- (d) These serious effects occur, therefore, at values of C_L well below the actual $C_{L\max}$ which for the wing as a whole is about 1.1 (1.05). These values of $C_{L\max}$ are higher than would be expected for the section in two-dimensional flow and are thought to result from the action of a part-span vortex sheet continuing to originate from just outboard of the wing-root leading edge and limiting the rearward extension of the dead-air region on the sections just outboard of its origin (The basic reason is, therefore, the effect of the change in shape of the chordwise loading near the wing-root itself, which tends to prevent the separation of the laminar boundary layer near the leading edge there).

Other effects noted are:

- (e) The reduction in stability becomes rather less severe above $C_L = 1.0$.
- (f) The centre of load moves inwards above about $C_L = 0.8$, and near $C_{L\max}$ is about $0.06 (0.05) \times$ semi-span further in than at low C_L .
- (g) With wing A, a gradual reduction in stability occurs between about $C_L = 0.5$ and 0.7 , amounting to a decrease in $(\partial C_m / \partial C_L)_M$ of about 0.07 . This seems to occur prior to the first appearance of a separation near the leading edge and is thought to be caused by the effective camber of the thick boundary layer over the upper surface of the outer sections. The effect may appear on wing C also at rather higher Reynolds numbers and ultimately would in general be expected to decrease with Reynolds number.

Precise values of the maximum usable C_L cannot be quoted, partly because the results of these tests are for a configuration without a tailplane. It can be concluded, however, that the flow over the outer wing sections (including probably the aileron) may become disturbed near $C_L = 0.7$ to 0.75 , a serious reduction in longitudinal stability may be expected above about $C_L = 0.85$, culminating in a more severe loss near $C_L = 0.92$. Hence the usable C_L seems certain to be appreciably less than the actual $C_{L\max}$ which is between 1.05 and 1.1 and instability prior to or at the stall should occur for untwisted wings having 50 deg of sweep, 7.5 per cent thick symmetrical sections for aspect ratios greater than some value less than 3.1. The need exists, therefore, for the development of some device such as a fence (see Part II) or a drooped nose to improve these characteristics. The RAE 101 section of wing A is slightly superior to the section of wing C (Fig. 4) in these qualities, as would be expected from the comparison in Fig. 34.

8. *Effect of Mach Number on Pitching-Moment Characteristics at High C_L .*—A detailed discussion is given first in section 8.1 for the results on wing A (RAE 101 section, $A = 3.1$) since these form the basis for the comparisons for the effects of aspect ratio (section 8.2) and section shape (section 8.3). The quoted values of C_L are 5 per cent less than those measured for the net wings and should be reasonably representative for both the net wing and gross wing-body combination.

8.1. *Wing A (RAE 101 Section).*—8.1.1. *Principal results.*— C_m vs. C_L curves for wing A for various Mach numbers from 0.50 to 0.95 at $R = 2 \times 10^6$ are given in Fig. 16 and the corresponding lift carpet in Fig. 22.

For all Mach numbers from 0.50 to 0.95, a reduction in longitudinal stability with increasing C_L occurs at a C_L value (the 'break' C_L) of between 0.45 and 0.6, compared with $C_L = 0.7$ at the same Reynolds number at $M = 0.2$.

The initial severity of this reduction in stability becomes rather less with increasing Mach number up to about $M = 0.88$, e.g., for $M = 0.88$, $(-\partial C_m / \partial C_L)_M$ decreases above about $C_L = 0.45$ but for the net wing about the net mean quarter-chord point*, it does not become negative until about $C_L = 0.65$ and a severe reduction does not occur until locally above $C_L = 0.8$, when $(\partial C_m / \partial \alpha)_M$ has also fallen to a low value and possibly $C_{L\max}$ has almost been

* This gives $(-\partial C_m / \partial C_L)_M \approx 0$ at low C_L and low Mach number.

attained. It follows that if the usable C_L is determined by this reduction in stability, then its value at Mach numbers such as 0.88 will clearly depend closely on both the choice of c.g. position and also on the effectiveness of the tail under these conditions and so cannot be quoted precisely. If a limit is set by buffetting, then the usable C_L may in fact be only $C_L = 0.45$ or even less.

Between $M = 0.88$ and 0.91 , the value of the 'break' C_L increases from about 0.45 to 0.55 but above $M = 0.91$, it shows a tendency to decrease again to near 0.5. Because there is a considerable increase with Mach number in the value of $(-\partial C_m/\partial C_L)_M$ at low C_L , $(-\partial C_m/\partial C_L)_M$ at high C_L and high Mach number is about the same as at low C_L and low Mach number. Again, therefore, it is not immediately clear whether the reduction in stability in itself represents a usable C_L limitation.

8.1.2. *Analysis of results.*—In the absence of any pressure-plotting data, it is not possible to make a detailed quantitative analysis of the results but, with the aid of the photographs of the behaviour of tufts on the wing surface, a qualitative discussion is possible. It appears that the Mach-number range can be conveniently divided in three, *viz.*, up to about $M = 0.85$, in which the basic nature of the stalling characteristics seems to remain similar to that at low Mach number; a transitional range between about $M = 0.85$ and $M = 0.91$; and finally, the range above $M = 0.91$, in which the flow either adheres over the nose of the outer sections or else, any laminar separation there, remains closely limited in chordwise extent at all values of C_L , but there is a severe shock-induced separation further aft.

8.1.2.1. *Up to about $M = 0.85$.*—In this range, the basic nature of the stalling characteristics appears to remain the same but there is a tendency for the various effects at even the test Reynolds number of $R = 2 \times 10^6$ to occur at lower values of C_L as the Mach number is increased. This applies particularly to the value of $C_{L \text{ crit}}$ at which separation first occurs on the outer wing sections.

The first appreciable increase in $(C_D - C_L^2/\pi A)$ with C_L and the initial nose-down moment change occur above about $C_L = 0.4$ at $M = 0.5$ and $C_L = 0.3$ at $M = 0.85$, compared with $C_L = 0.5$ at $M = 0.2$. The subsequent reduction in stability occurs at about $C_L = 0.55$ at $M = 0.5$ and $C_L = 0.5$ at $M = 0.85$, rather than $C_L = 0.7$ as at $M = 0.2$. The loss in stability becomes more severe near $C_L = 0.65$ to 0.7 for $M = 0.5$ to 0.85 rather than near $C_L = 0.9$ as at $M = 0.2$.

Analysis of these results and of the approximate positions of the part-span vortex sheets, as shown by the tuft photographs, suggests that:

- (a) the value of C_L at which a laminar separation first occurs on any section is reduced by about 0.1 between $M = 0.2$ and 0.5 . As a result, for example, the part-span vortex sheet is close to the inboard end of the curved tip at about $\alpha = 6.5$ deg at $M = 0.5$, compared with $\alpha = 8$ deg at $M = 0.2$ and later, for $\alpha = 14$ deg, it originates from nearer the root than $\eta^1 = 0.2$ instead of from near mid-semi-span (Fig. 6)
- (b) $C_{L \text{ max}}$ for the outer sections at $M = 0.5$ is probably about 0.6, compared with 0.8 at $M = 0.2$
- (c) between $M = 0.5$ and 0.85 , the value of C_L at which a separation bubble forms on the tip sections continues to decrease with Mach number but near mid-semi-span, there is little further change in this respect. This suggestion is supported by the evidence from the tufts (Fig. 17a). An inward extension with Mach number can be noted for the region affected by the separation at $C_L \approx 0.53$ whereas, for $C_L \approx 0.73$, when the separation extends further inboard, little change with Mach number can be detected in this Mach-number range.

The variation in $C_{L \text{ crit}}$ and $C_{L \text{ max}}$ between $M = 0.2$ and 0.5 is similar to what has been observed in various aerofoil tests in two-dimensional flow and hence is presumably not caused

by any characteristic, peculiar to a swept wing. The further deterioration near the tip between $M = 0.5$ and 0.85 should be principally ascribed, however, to the change in shape of the chordwise loading on the outer sections. At high Mach number, the wing is effectively more swept and so there is a greater relative increase between mid-semi-span and the tip in the value of $(-C_p)_{\max}$ for a given C_L .

The basic idea that the character of the stall does not vary up to about $M = 0.85$ implies that a separation bubble may still form near the leading edge even after the local Mach number (M_1), perpendicular to the isobars has exceeded 1.0 and also that the difference, close to the surface, between the values of $(-C_p)$ in the regions where the bubble has and has not formed is still sufficient to induce a part-span vortex sheet of significant strength.

In connection with the first of these conclusions, an analogy may be drawn with some results in two-dimensional flow. For example, in the tests⁷ at the National Physical Laboratory on a 10 per cent thick, RAE 104 section, it was found that a laminar separation bubble occurred near the leading edge at about $\alpha = 8$ deg at low Mach number and that for this incidence, a local Mach number of 1.0 was exceeded ahead of the separation at about $M = 0.47$. A limiting local Mach number of 1.35 to 1.4 was attained by about $M = 0.59$. Nevertheless, a laminar separation, close to the leading edge, persisted up to some Mach number between 0.64 and 0.69 . Under these conditions, there was a λ -shock system with the separation lying between the two limbs of the shock system. The separation must then be a consequence of the shock-wave-boundary-layer interaction, since no separation would occur at low Mach number for a comparable value of $(-C_p)_{\max}$.

In the present case, the tuft photographs suggest that for the sections near mid-semi-span, a significant separation first occurs near $C_L = 0.6$ and so, an estimate has been made, assuming subcritical flow, of the variation with Mach number of the values of $(-C_p)_{\max}$ corresponding to $C_L = 0.55$ and 0.65 . This is shown in Fig. 35, together with the estimated variation of the values* of $(-C_p)$, corresponding to $M_1 = 1.0$ and 1.4 . Even if it is assumed, as in two-dimensional flow, that $(-C_p)_{\max}$ can increase until $M_1 = 1.4$, the value of $(-C_p)_{\max}$ for a given C_L decreases appreciably, *e.g.*, for $C_L = 0.65$, from about 4.5 at $M = 0$ to about 3.1 at $M = 0.5$ ($M_1 = 1.4$) should be attained by about $M = 0.6$ but the similarity of the two sets of curves is such that C_L would not have to be reduced appreciably or the estimates to be much in error for this value of M to be considerably higher. The persistence of the separation near the leading edge, though induced, as above, for different reasons, would therefore have been predicted to at least $M = 0.6$ and probably to appreciably higher Mach numbers. The first of the conclusions above cannot therefore be counted as unexpected.

The apparent continued existence up to $M = 0.85$ of the part-span vortex sheet, is more surprising because the values of $(-C_p)$ inboard of the region of separation are likely to be limited to about 1.3 and so are probably only slightly in excess of the values that might be expected for the dead-air region. It should be noted, however, that the presence of the vortex sheet is suggested both by the overall results (*e.g.*, the increase in $(\partial C_L / \partial \alpha)_M$ near $C_L = 0.5$ at $M = 0.85$ (Fig. 22)) and also by the behaviour of the tufts (Fig. 17a). This point is a good illustration of the need for pressure-plotting data at high Mach number and high C_L on such a wing as this.

8.1.2.2. $M = 0.85$ to 0.91 .—In the two-dimensional tests⁷ referred to above, it was found that above a certain Mach number (*e.g.*, between $M = 0.64$ and 0.69 for $\alpha = 8$ deg), the laminar boundary layer adhered over the leading edge and higher local Mach numbers were attained in the supersonic expansion round the nose (Values of 1.6 to 1.7 were achieved in this particular case and values up to 2.0 in other tests on aerofoils with smaller leading-edge radii). One of the effects of this change in the flow characteristics was that C_D decreased with Mach number for a range of about 0.05 in M . Subsequently the main shock wave, at a given incidence, tended to move back and the turbulent separation from near its foot to become more severe, giving a renewed increase of C_D with Mach number.

* These values are only approximate.

It appears that a similar fundamental change in the behaviour of the boundary layer round the nose occurs on the present swept wing between $M = 0.85$ and 0.91 . For example, Fig. 27 shows that C_D at constant C_L decreases with Mach number in this range for those values of C_L such as 0.5 in which a separation from close to the leading edge occurred at lower Mach numbers. Comparison of the tuft photographs for $C_L \sim 0.53$ in Fig. 17a shows that the drag results cannot be explained by a decrease in the spanwise extent of wing affected by the separation because actually, more of the wing is affected at $M = 0.88$ than at $M = 0.5$ for this C_L . Hence, the observed decrease in the overall C_D implies that the local C_D for some sections on the wing has decreased, as in the two-dimensional test quoted. The tuft photographs also appear to confirm that by $M \sim 0.91$, the boundary layer over the nose either remains attached or else, the separation is very limited in chordwise extent for it will be seen (Fig. 17a) that for both $C_L = 0.56$ and 0.76 , such tufts as are still present near the leading edge after their severe buffeting at previous conditions of test are mostly aligned in the streamwise direction.

It would be expected that for some Mach numbers in this transitional range, as the incidence is increased, both types of boundary-layer behaviour over the nose may be obtained on any section of the wing. In other words, at moderate incidences, there should be no separation near the leading edge and the local values of M_1 should not be greater than about 1.4 . Then, as the incidence is increased, a laminar separation occurs near the nose as at lower Mach numbers but with a further increase in incidence, the boundary layer adheres again over the nose and higher local Mach numbers are attained there. It is thought that this is, qualitatively, what happens on the wing near $M = 0.88$. Hence, on the one hand, the trends with increasing Mach number up to 0.85 are continued in the sense that the C_L values for the initial nose-down moment change and the succeeding reduction in stability are smaller than for all lower Mach numbers but, on the other hand, the actual reduction in stability is less severe (at least, below $C_L = 0.8$), because of the partial recovery in $(\partial C_L / \partial \alpha)_M$ on the outer sections when the separation near the nose has been eliminated.

8.1.2.3. $M = 0.91$ and above.—By $M = 0.91$, it seems that the long-bubble separation near the nose of the outer sections does not occur at any incidence and so this is the explanation why, for example, the value of C_L , corresponding to the reduction in stability, increases from about $C_L = 0.45$ at $M = 0.88$ to over $C_L = 0.55$ at $M = 0.91$ (The attainment of higher local Mach numbers over the nose enables the tip sections to achieve higher values of C_L).

In this Mach-number range, the changes of stability with increasing C_L should be intimately related to the development on the upper wing surface of a strong shock wave, the changes in shock-wave position with incidence and the severity of the turbulent separation behind it. No quantitative analysis is possible without pressure-plotting data but it is helpful in this discussion to correlate the overall results for $M = 0.93$ with the tuft photographs for this Mach number, given in Fig. 17b. The main features of this correlation are:

- (a) $(-\partial C_m / \partial C_L)_M$ increases appreciably above about $C_L = 0.25$ and remains at the higher value up to about $C_L = 0.55$. This nose-down moment change is not now associated as at lower Mach numbers with the appearance of a part-span vortex sheet near the tip but is a consequence of the development of a local supersonic* region on the wing. This conclusion is based on the evidence of both the drag data (Fig. 27) and the tuft photographs. The steep increase of C_D with M that follows the formation of a shock wave is shown, for example, to be only just starting near $M = 0.93$ at $C_L = 0.2$, whereas for higher values of C_L , it has begun at lower Mach numbers. Also, the tuft photographs for $C_L < 0.25$ (not given in Fig. 17a) shows no sign of any disturbed flow whereas a few tufts near the tip are disturbed at $C_L = 0.33$ and this is more pronounced at $C_L = 0.51$. The latter photograph is particularly interesting because the flow appears undisturbed for about three 'tuft lengths' back from the leading edge (*cf.* the pictures for similar values of C_L at lower Mach numbers in Fig. 17a). Most

* Perpendicular to the local isobars.

signs of disturbance are evident along a line stretching in from the tip at about $0.4c$ and it is thought that this corresponds to the probable shock position. In this C_L range up to 0.55 , therefore, the shock is near the maximum-thickness position or slightly behind it.

- (b) A large reduction in stability (amounting to a decrease in $(-\partial C_m/\partial C_L)_M$ of about 0.10) occurs near $C_L = 0.55$ and reference to the lift carpet in Fig. 22 shows that this is evidently associated with a large reduction in lift—presumably on the outer wing sections. The tuft photographs show that as the incidence is increased, the flow behind the shock waves becomes more disturbed and, in agreement with the overall results, the largest difference is found near $\alpha = 7$ deg ($C_L = 0.59$). It is important to note that the position of the shock appears to move forward from about $0.4c$ at $C_L = 0.51$ to near $0.2c$ by $C_L = 0.65$ and at higher values of C_L , the flow again becomes disturbed even near the leading edge. It is significant that in the two-dimensional tests reported in Ref. 9, such a forward movement of the position of the shock wave with incidence was observed and in that case, a rapid thickening of the turbulent boundary layer occurred near the foot of the shock wave at about the same or a slightly higher incidence. It thus seems that the behaviour of the outer sections of the present swept wing at $M = 0.93$ near $C_L = 0.55$ is similar to this, *i.e.*, there is a forward movement of the shock and a separation occurs from near its foot. At higher incidences, the separation would become more severe, and the suction over the rear part of the upper surface would increase, giving a pronounced rearward movement of the local aerodynamic centre. This would tend to alleviate the reduction in $(-\partial C_m/\partial C_L)_M$ for the wing as a whole and could explain the increase in $(-\partial C_m/\partial C_L)_M$ above $C_L = 0.62$ at $M = 0.94$. The tuft photographs show that even at $C_L = 0.73$ at $M = 0.92$, the separation does not appear to extend further inboard than about mid-semi-span.
- (c) Near $C_L = 0.8$ at $M = 0.91, 0.92$, a more severe reduction in stability occurs; the tuft photographs suggest that this is due to a part-span vortex sheet forming, as at lower Mach numbers, from near the wing-root leading-edge and hence to the increase in lift inboard of the vortex sheet and ahead of the c.g. This suggests that even at these Mach numbers a laminar separation still occurs near the leading edge on most of the inner part of the wing. If the effect occurs at Mach numbers above $M = 0.92$, it is beyond the incidence-range of these tests.

The principal effect of an increase in Mach number from 0.91 to 0.95 is that there is a decrease in both the value of C_L for the initial nose-down moment change (because the upper-surface shock forms at a lower C_L as the Mach number is increased) and also in the value of C_L at which the first reduction in stability occurs (from about $C_L = 0.55$ to 0.5). At some Mach number higher than 0.95 , it is expected that the forward movement of the shock wave with incidence would cease to occur, that the local supersonic region would extend over more of the chord and thus, that the area of wing affected by the turbulent separation would be reduced. The reduction in stability near $C_L = 0.5$ would then tend to disappear.

Another significant difference between the flow characteristics in this Mach-number range and those at lower Mach numbers, as shown by the tufts, is that at high Mach number, there is no longer a sudden change at some point along the span from largely streamwise flow to outward flow under a vortex sheet. Instead, the flow direction changes gradually with spanwise position. Because of the relative loss in lift near the tip at high incidence, vorticity must still be shed somewhere along the span but this is probably diffused over a significant proportion of the span.

8.1.3. *General discussion including a note on scale effect.*—It follows from the above description that, in various important respects, the flow characteristics leading to the reduction in stability at $C_L = 0.5$ to 0.6 for Mach numbers of 0.9 and above are very different from those at low Mach number and hence that the measures that may be required to delay or eliminate the loss in stability may well be different. At low Mach number, the essential problem is to find a means of

preventing the development of high suction peaks very close to the leading edge but at high Mach number, a method must be found to suppress or reduce the turbulent separation aft of the shock for a given shock strength or to decrease the latter and if possible, to prevent the shock from moving forward to near the leading edge at high incidence.

The change of flow characteristics with Mach number also has a bearing on the possibility of serious scale effect. A correlation of experience in flight and tunnel on less swept aircraft suggests that the values for C_L for instability at high Mach number are not so likely to be subject to a large variation with Reynolds number. For Mach numbers from 0.5 to 0.85, an increase in Reynolds number should improve the C_L value for instability, as found for $M = 0.2$ but the magnitude of this improvement is uncertain. Even at a higher Reynolds number, it is likely that this C_L value would decrease with Mach number in this range and by $M = 0.88$, the instability would probably not be delayed beyond about $C_L = 0.6$. These conclusions regarding scale effect at high Mach number are somewhat tentative and for this reason, a model to the same design as wing A is to be pressure plotted in the O.N.E.R.A. tunnel at Modane to provide data at a higher Reynolds number (about $R = 14 \times 10^6$ for $M = 0.9$). For comparison, pressure-plotting data are also to be obtained on another model to this design in the RAE 10-ft \times 7-ft High-Speed Tunnel. For the present, it may be noted that, fortunately, the most important conditions in flight are those at low Mach number (discussed earlier) and at high Mach numbers of the order of 0.9 to 0.95, whereas most uncertainty surrounds the applicability of the results between $M = 0.5$ and about 0.85. It seems fair to conclude that the available C_L for manoeuvring at Mach numbers near 0.9 to 0.95 is unlikely to be appreciably greater than $C_L = 0.5$ to 0.55*.

8.2. *Results for Wing B: Effects of Aspect Ratio (Figs. 18 and 23).*—The outer sections of wing B, with the higher aspect ratio of 3.5, are further behind the wing mean quarter-chord point and so the reduction in longitudinal stability above the 'break' C_L is greater than for wing A; e.g., at $M = 0.5$, the reduction in $(-\partial C_m/\partial C_L)_M$ is 0.34 rather than 0.24 while at $M = 0.92$, it is about 0.17 rather than 0.10. As a result, even although the basic value of $(-\partial C_m/\partial C_L)_M$ for wing B about the mean quarter-chord point of the net wing is about 0.05, $(-\partial C_m/\partial C_L)_M$ becomes negative at a C_L value, only slightly above the break C_L , whatever the Mach number. Hence it appears that for wing B, there is less doubt that the limiting usable C_L will be equal to or possibly less than the 'break' C_L at all Mach numbers, whatever the c.g. position or tail effectiveness at high C_L .

The actual values of the 'break' C_L are, in general, about the same for wings A and B, as would be expected, since the change in aspect ratio from 3.1 to 3.5 should have no large effect on the spanwise or chordwise loadings.

8.3. *Results for Wing C: Effect of Section Shape.*—The general picture presented by the C_m vs. C_L curves for wing C in Figs. 19 and 21 is similar to that for wing A and indeed, from $M = 0.5$ to 0.85, there is good agreement in the main features in even a quantitative sense, e.g., for $M = 0.85$, the nose-down moment change occurs above about $C_L = 0.3$ and the reduction in stability above about $C_L = 0.5$ for both wings. Hence it is only at low Mach number in this 'subcritical' range of Mach numbers that wing C is notably poorer (at $R = 2 \times 10^6$) than wing A. The key to the relative behaviour of the two wings is to be found in Fig. 35. The value of $(-C_p)_{\max}$ for a given C_L at subcritical speeds is only markedly different for the two wings at low Mach numbers. As the Mach number increases, $(-C_p)_{\max}$ for a given C_L decreases more rapidly with wing C, thus narrowing the difference between the two wings.

The tuft photographs again confirm that at least up to about $M = 0.85$, the basic nature of the stall remains the same as at low Mach number. The patterns shown in the photographs

* As noted earlier, since the value of $(-\partial C_m/\partial C_L)_M$ at high Mach number and high C_L is about the same as at low C_L and low Mach number, an assessment of whether the reduction in stability in itself will limit the usable C_L must depend on the actual choice of c.g. position, tail effectiveness, etc.

for $M = 0.5$, $C_L = 0.66$ and $M = 0.8$, $C_L = 0.69$, given at the top of Fig. 20, are comparable with those obtained for $M = 0.2$ by the oil-film technique (Fig. 9).

Judging by the drag results, it appears that for values of C_L near 0.5, at least, the flow adheres over the leading edge of the tip sections at rather lower Mach numbers for wing C than for wing A because it will be seen from Fig. 30 that the subsequent steep increase of C_D with Mach number for, say, $C_L = 0.5$ occurs at a Mach number about 0.03 lower on wing C. This suggestion that the flow regime near the leading edge changes at a lower Mach number for wing C is again what might be expected if it is concluded, as earlier, that the section of wing C has effectively a smaller leading-edge radius than for the RAE 101 section of the same thickness/chord ratio.

In the high Mach number range from about $M = 0.90$ to 0.95, the value of the 'break' C_L , above which the reduction in stability occurs is about the same for wings A and C but the two wings differ greatly in respect of the magnitude of this reduction in stability. This is much more severe in the case of wing C, *e.g.*, for the 'net' wings, the decrease in $(-\partial C_m/\partial C_L)_M$ above the 'break' C_L is about 0.2 for wing C, compared with only about 0.1 for wing A. Similarly, a comparison of the lift carpets for the two wings in Figs. 22 and 24 shows that the reduction in $(\partial C_L/\partial \alpha)_M$ between, say, $C_L = 0.6$ and 0.8 at high Mach number, is also much greater for wing C.

There appear to be two major reasons for the more severe reduction in stability at high Mach number with wing C:

- (a) A more severe reduction in $(\partial C_L/\partial \alpha)_M$ for the outer sections, owing to the shock-induced separation having a more serious effect on the section with the further aft position for the maximum thickness. Such a comparative effect has been observed in the results of tests at the N.P.L. on the RAE 102 and RAE 104 sections in two-dimensional flow. It is also suggested by a comparison of the tuft photographs for wings A and C in Figs. 17 and 20. The tuft photographs for wing C at $M = 0.93$ (Fig. 20) show that:
 - (i) for values of C_L below the 'break' C_L , the main shock wave is apparently located at about $0.55c$ on the outer wing sections. This is about $0.15c$ further back than for wing A but in both cases it means that the shock wave is near or just behind the estimated peak-suction position at zero lift for the mid-semi-span region of the wing
 - (ii) between $C_L = 0.47$ and 0.60 (and similarly at other Mach numbers above 0.9 for values of C_L on either side of the 'break' C_L), there is a large change in the behaviour of the tufts over the outer sections. The shock wave has evidently moved forward to close to the leading edge (rather than to near $0.2c$ as for wing A) and the boundary layer evidently separates from near its foot. Hence the forward movement of the upper-surface shock wave with increasing C_L is much greater than for wing A. The behaviour of the tufts also suggests that the separation aft of the shock wave is more violent for wing C.
- (b) The second reason is that for wing C, a separation near the leading edge of the inner sections and a part-span vortex sheet originating from near the wing-root leading edge appear to form at about the same C_L as for the serious shock-induced separation on the outer sections, whereas for wing A, these two effects occurred at different values. For example, for wing A, at $M \simeq 0.91$, the first of these effects does not occur until near $C_L = 0.8$, compared with $C_L = 0.6$ for the shock-induced separation on the outer sections, whereas for wing C at this Mach number, both effects occur near $C_L = 0.6$. The tuft photographs for wing C suggest that the effect on the inboard part of the wing occurs in the range of C_L up to $C_L = 0.7$ up to a Mach number of about $M = 0.93$ (the presence of a part-span vortex sheet from near the root has been observed at $M = 0.92$ but not at $M = 0.94$).

Even although the effects on the inner part of the wing may possibly be alleviated by an increase in Reynolds number, it appears likely that wing C would continue to be poorer than

wing A at flight Reynolds numbers in respect of this more severe reduction in stability at $C_L = 0.5$ to 0.6 at high Mach number. Hence for wing C, unless buffeting in flight sets an even lower limit, the 'break' C_L should represent a limiting usable C_L at Mach numbers of 0.9 to 0.95 for any likely choice of c.g. position and even if the tailplane retained its full effectiveness under these conditions.

9. *Discussion of Results at Low C_L .*—9.1. *Lift-curve Slope.*—The lift carpets for the three wings are given in Figs. 22 to 25 and the variation of $(\partial C_L / \partial \alpha)_M$ at low C_L with Mach number is plotted in Fig. 26. Owing to the non-linear nature of some of the C_L vs. α curves, it is difficult to obtain a consistent set of values of $(\partial C_L / \partial \alpha)_M$. Those presented in Fig. 26 are mean values over a range of C_L from 0 to 0.2 and by this means, it is hoped that some of the random errors that would be present if the slopes at merely $C_L = 0$ had been read off, have been eliminated.

It will be noted that there is a large difference between the values of $(\partial C_L / \partial \alpha)_M$ obtained for the net exposed wing C in the presence of the half-fuselage and for the gross wing-body combination. This difference is present to about the same extent at all Mach numbers and so it is sufficient to compare the measured values of $(\partial C_L / \partial \alpha)_M$ obtained in the tests at $M = 0.18$ at high Reynolds number with the estimated values derived from the calculated spanwise lift distributions given in Fig. 32. It is found that:

measured value of $(\partial C_L / \partial \alpha)_M$ for net wing*	= 3.40
estimated value of $(\partial C_L / \partial \alpha)_M$ for net wing*	= 3.30
measured value of $(\partial C_L / \partial \alpha)_M$ for gross wing	= 2.95
estimated value of $(\partial C_L / \partial \alpha)_M$ for gross wing	= 3.10.

It appears therefore that the difference between the results for the gross and net wings is considerably greater than would be estimated because the measured values of $(\partial C_L / \partial \alpha)_M$ are apparently about 3 per cent too high for the net wing and 5 per cent too low for the gross wing.

It is possible to account for both these discrepancies, at least partly, by weaknesses in the experimental technique:

- (a) In the 'net' wing test, the true aerofoil section is retained on the wing stub for some distance below the wing-body junction and the passage between the wing is almost straight. The flow photographs have shown that there is evidently some airflow over the stub and hence the part, having an aerofoil shape, probably develops some lift, thereby increasing the overall value of $(\partial C_L / \partial \alpha)_M$, when based on merely the net wing area. Also, the local values of $(\partial C_L / \partial \alpha)_M$ on the wing-root sections may be increased somewhat by the effect on the boundary layer of the outward flow through the gap and over the rear of these sections.
- (b) In the 'gross' wing tests, the half-fuselage was almost entirely in the tunnel-floor boundary layer and so would not develop its full lift.

The values of $(\partial C_L / \partial \alpha)_M$ for the 'net' wings A and B should also be about 3 per cent too high in the same way as for wing C. The difference between the values for A and B is almost exactly the same as would be predicted for the change in aspect ratio from 3.1 to 3.5 and similarly, the difference between the values for A and C can be almost accounted for by the change in plan-form, *i.e.*, the change in section shape appears to have little effect below the Mach number for lift divergence.

The peak values of $(\partial C_L / \partial \alpha)_M$ for all three wings are reached at about $M = 0.92$.

9.2. *Aerodynamic-Centre Position.*—The variation of $(-\partial C_m / \partial C_L)_M$ with Mach number is shown in Fig. 26. This figure is only intended to present the broad comparison because the

* In presence of fuselage.

values of $(-\partial C_m/\partial C_L)_M$ are mean values for the range of C_L from 0 to 0.3. Particularly at high Mach number, there is a significant increase in $(-\partial C_m/\partial C_L)_M$ with C_L even in this limited range and so the values at any given C_L may differ from those shown in Fig. 26.

In the 'subcritical' range up to $M \approx 0.88$, the aerodynamic centre moves back by about $0.03\bar{c}$. At higher Mach numbers, as a shock wave forms first at the higher incidences, a more rapid rearward movement occurs and by $M = 0.94$, averaging the results for the wings, it is about $0.075\bar{c}$ further aft than at low Mach number.

It may be noted that comparisons for other models have shown that the measured aerodynamic centre positions for the gross wing-body combination may be about $0.03\bar{c}$ further back than the true position as obtained in a complete model test. The variation with Mach number should not, however, be in error.

9.3. *Drag*.—Curves of C_D vs. Mach number at constant C_L for the three wings are given in Figs. 27 to 30.

The differences in C_D between wings A and B can be largely accounted for by the effect of the change in aspect ratio on the induced drag. There is no significant change in the induced drag factor κ , where $C_D = C_{D0} + (\kappa/\pi A)C_L^2$ or on the drag-divergence Mach number at any value of C_L .

The more interesting comparison is between the results for wings A and C (*see* Fig. 31) which shows the effect of the change in section shape. It is found that:

- (a) at low and moderate Mach numbers, wing C gives the larger increase of C_D with C_L . This is caused first by the larger forward movement of transition position on the upper surface with C_L and second, because at $R = 2 \times 10^6$, the separation over the outer sections occurs at a lower C_L with wing C. The differences in C_D at low Mach numbers between the two wings should not be so marked at higher Reynolds numbers. At high Mach numbers, however, scale effect should have less influence. Because of these two conclusions, the results at high Mach number should be judged by a comparison of the Mach numbers at which a given value of C_D is attained rather than of the Mach numbers for a given ΔC_D above the value at low Mach number.
- (b) the steep drag rise for any value of C_L from 0.2 upwards occurs at a Mach number about 0.03 higher for the wing A with the RAE 101 section than for the other wing with its maximum thickness further aft at 0.38c. The test Mach number range did not extend to high enough values to give a quantitative comparison near $C_L = 0$ but the gain with the RAE 101 section is then probably about the same as at higher values of C_L .

This result is similar to what was found previously¹ with the 10 per cent thick, moderately tapered wings with 40 deg sweep but the advantage for the RAE 101 section is greater in the present case (0.03 rather than 0.02 in Mach number). A detailed analysis of the reasons for the better performance with the maximum thickness forward near 0.3c can be found in Ref. 7. Briefly, the effects of the higher values of $(-C_p)$ with such a section are more than offset by the effects of the greater sweep of the isobars near where the main wave shock forms and over the forward part of the sections on the inner half of the wing. The net effect is that the drag rise with Mach number on both the inner sections and those near mid-semi-span is considerably delayed.

It thus seems that for a wing of the present type of plan-form, the drag and pitching-moment results both favour the use of the RAE 101 shape rather than a section with its maximum thickness further back.

10. *Principal Conclusions*.—The most important feature of these results is that for all three wings, throughout the Mach number range of the tests, there is a serious reduction of longitudinal

stability at values of C_L well below the actual $C_{L \max}$. At low Mach number, there is a reduction in $(-\partial C_m / \partial C_L)_M$ of 0.25 or more above about $C_L = 0.85$, whereas the value of $C_{L \max}$ is between 1.05 and 1.1; at high subsonic Mach numbers (*e.g.*, 0.9 to 0.95), the reduction in stability occurs near $C_L = 0.5$ to 0.55.

The flow patterns at high C_L and low Mach number have been studied in detail and are discussed in sections 6.1 and 6.2. Briefly, at some incidence, the laminar boundary layer separates from near the leading edge near the inboard end of the curved tip ($\eta^1 = 0.85$) and with a further increase in incidence, the area affected by this separation extends inward and rearward. A part-span vortex sheet originates from near the leading edge at the inboard end of this region of separation and trails back across the wing, the projection of the sheet in the wing surface being bent outward, in general at an angle of about 20 deg to the free-stream direction.

The results at low Mach number are subject to considerable scale effect between $R = 2 \times 10^6$ and $R = 6 \times 10^6$ and this appears to be largely associated with a variation with R_l , the Reynolds number based on the local chord, of the value of $C_{L \text{ crit}}$, the local C_L at which the boundary layer first separates on the section being considered. The results suggest, however, that $C_{L \text{ crit}}$ is near 1.0 and becomes virtually independent of R_l for $R_l > 5.5 \times 10^6$ for the section of wing C and possibly $R_l > 4.0 \times 10^6$ for wing A with the 7.5 per cent thick, RAE 101 section. Consequently, it is thought that the results at low Mach number obtained at a mean Reynolds number of $R = 6 \times 10^6$ should, with certain reservations as detailed in the test, be applicable to full-scale conditions. The principal results are:

- (a) the boundary layer first separates and a part-span vortex sheet forms at about $C_L = 0.7$ giving an increase in $(C_D - \partial C_L^2 / \partial \alpha)$ with C_L and initially, while the vortex sheet lies close to the tip, a nose-down change in C_m .
- (b) the first serious reduction in stability occurs near $C_L = 0.85$ and is largely associated with the inward movement of the vortex sheet
- (c) this reduction in stability becomes accentuated and there is also a steeper increase of $(C_D - \partial C_L^2 / \partial \alpha)$ and a marked decrease in $(\partial C_L / \partial \alpha)_M$ above about $C_L = 0.95$. These effects are associated with the increase in the dead-air region near the tip; the reduction in $(-\partial C_m / \partial C_L)_M$ is between 0.25 and 0.5
- (d) the value of $C_{L \max}$ is between 1.05 and 1.1 and is higher than for these sections in two-dimensional flow. The relatively high values are thought to be associated with the continued influence of a part-span vortex sheet originating from near the wing-root leading edge
- (e) the spanwise centre of load moves inboard above about $C_L = 0.8$ and near $C_{L \max}$ is about $0.05 \times$ semi-span further in than at low C_L
- (f) in most of these respects, the RAE 101 section appears slightly superior to the section of wing C.

The basic nature of the stall appears to remain unaltered up to about $M = 0.85$ but even in the tests at $R = 2 \times 10^6$, the various effects, particularly the initial separation near the tips tend to occur at lower values of C_L as the Mach number is increased. This tendency would probably be more marked at a higher Reynolds number. At $R = 2 \times 10^6$, $M = 0.85$, the separation near the tips occurs above about $C_L = 0.3$ and a reduction in stability occurs near $C_L = 0.45$, though the reduction in stability is much milder than at low Mach number.

Above $M = 0.85$, the flow characteristics over the outer sections change and by $M = 0.91$, the flow appears to adhere round the leading edge of the outer sections at all values of C_L . The reduction in stability, which now occurs near $C_L = 0.5$ appears to be mainly associated with a shock-induced separation over the upper surface of the outer sections, coupled with a forward movement of this shock wave. The reduction in $(-\partial C_m / \partial C_L)_M$ for wing A with the 7.5 per cent thick, RAE 101 section is about 0.10 but for wing C, it is about 0.20.

Two contributory reasons can be suggested for the poorer characteristics with wing C at high C_L and high Mach number:

- (i) The separation over the outer sections would be expected to give a more serious reduction in $(\partial C_L / \partial \alpha)_M$ for sections with their maximum thickness near $0.4c$ than for those like RAE 101 with a position near $0.3c$
- (ii) A separation near the leading edge of the inner sections and a part-span vortex sheet from near the wing-root leading edge also occur near $C_L = 0.6$ with wing C up to about $M = 0.93$ whereas, with wing A, this does not occur below about $C_L = 0.8$.

The increase in aspect ratio from 3.1 to 3.5 has little effect on the values of C_L at which reductions in longitudinal stability occur but considerably augments the magnitude of these reductions.

The steep drag rise with Mach number occurs at Mach numbers about 0.03 higher with the RAE 101 section than with the section of wing C, thus confirming that a maximum thickness position near $0.3c$ is preferable for a moderately tapered, swept wing, such as those considered here (in agreement with the results of earlier tests with 10 per cent thick wings of 40 deg sweep).

APPENDIX TO PART I

Detailed Description of Flow-Visualization Technique

In the present tests, the wing was coated with a thin film of titanium oxide suspended in light diesel oil (Dieselene). The choice of oil depends on the wind speed of the tests which was here about 300 ft/sec. For lower speeds, paraffin would be preferable while for higher speeds, a heavier oil would have to be used. Titanium oxide was used rather than lampblack for several reasons, *e.g.*, the wings were painted black for photographic purposes and so a white powder was required; it is a clean powder, in good supply and is one of the least hygroscopic powders available. Other reasonably good alternatives are zinc oxide and Kaolin. Oleic acid was added to the suspension to act as an agent for dispersing the moisture round the titanium-oxide granules, thus helping to prevent coagulation. The relative amounts of the different constituents should be approximately 100g of titanium oxide to 135 c.c. of Dieselene with about 2 c.c. of oleic acid.

It is important that the titanium oxide and Dieselene should be carefully mixed. A thick paste was first formed and a smooth mixture obtained by means of a spatula. The oleic acid was then added and then finally, a little more Dieselene.

The wing surface was moistened with Dieselene, using a silk or Rayon cloth, and a thin film of the mixture brushed on to the wing. This was then wiped with a lightly oiled cloth to give an even, relatively dry, finish that should not affect the position of transition. If the film was left too wet, transverse wavelets of paint appeared when the tunnel was run up to speed, or else it was found that the oil did not flow evenly but formed a number of discrete 'rivers'. If, on the other hand, the film was applied satisfactorily, a fine indication was obtained of the whole flow field over the wing surface and not merely of those regions where large changes in flow velocity or direction occurred.

The film remained unaltered indefinitely, prior to starting the tunnel, *i.e.*, the oil showed no tendency to trickle down the wing under gravity or to dry off. Hence, it was possible to carry out tests not merely at atmospheric pressure, when the tunnel could be started almost immediately after coating the wing, but also when the tunnel was pumped up to give a higher Reynolds number at low Mach number, when there was a delay of possibly over an hour before the tunnel was started. For example, in the present tests, the technique was applied successfully to obtain flow patterns over wing C at $R \simeq 6 \times 10^6$ for four incidences.

The main difficulty in using this technique under conditions of increased or reduced pressure in the RAE 10-ft \times 7-ft High-Speed Tunnel is the time factor in making the experiments. The model has to be set at the required incidence before starting the tunnel and it was not found possible to investigate more than one incidence at a time. This is the reason why more tests were not made at high Reynolds numbers and why the technique has not yet been developed for use at high Mach numbers. Some development is needed for the latter case but the problem should be soluble in the case of the RAE 10-ft \times 7-ft High-Speed Tunnel by the use of a heavier oil.

The flow patterns were photographed both during the test while the oil was still flowing and at the end when the pattern had dried out.

Part II

Tests in the Royal Aircraft Establishment 10-ft x 7-ft High-Speed Tunnel on a 7.5 per cent Thick, 50-deg Swept Wing Fitted with Stall Fences and a Leading-Edge Chord Extension

Summary.—Various alternative devices have been fitted to a 50-deg swept-back wing with 7.5 per cent thick, RAE 101 sections in attempts to improve the longitudinal stability characteristics of the wing at high values of C_L at both low and high Mach number, as shown by tests in the RAE 10-ft x 7-ft High-Speed Tunnel. This report discusses the results obtained in turn with various stall fences (with a total height from top to bottom equal to 1.2 and 2.4 x the local wing thickness), placed at 0.56 x semi-span and with a leading-edge chord extension from 0.56 to 0.88₅ x semi-span.

Measurements of lift, drag, pitching moment and root bending moment were made for all configurations at various Mach numbers from 0.5 to 0.95 at $R = 2 \times 10^6$ and for the three basic cases: plain wing, wing with full large fence and wing with leading-edge chord extension at $M = 0.2$ for three Reynolds numbers between 2×10^6 and about 6×10^6 . Flow visualization tests were made by an oil-flow technique at $R = 2.5 \times 10^6$ and $M = 0.2$ for the same three basic cases and by means of surface tufts over the full Mach-number range for the plain-wing and for the wing with chord extension.

The full large fence increased the value of C_L for the serious reduction in stability by 0.15 to 0.2 for all Mach numbers up to about 0.9 but at $M = 0.94$, it was quite ineffective. Similar results were obtained when the fence round the lower surface aft of 0.05c was removed and the drag increment at low C_L was then about $\Delta C_D = 0.001$ for all Mach numbers up to $M = 0.94$. It is suggested that a multiple fence arrangement (with additional fences further inboard) might produce somewhat better results at high values of C_L .

The major reason for the effectiveness of the fence for $M \leq 0.9$ is that it prevents the separation of the laminar boundary layer near the leading edge of the sections immediately outboard of the fence and so the part-span vortex which occurs at high C_L is located near the fence. This vortex sheet lies across the outer wing sections and effectively limits the rearward extent of the dead-air region on the sections outboard of its origin.

With the chord extension, the reduction in stability at low Mach number and at a Reynolds number of 5.6×10^6 occurs at a lower value of C_L than for the plain wing but is smaller in magnitude. A large gain in stability, due to the extension, is apparent at $R = 2 \times 10^6$ for Mach numbers up to 0.9 but in view of the results at low Mach numbers, this may not be realized at higher Reynolds numbers; at $R = 2 \times 10^6$, the chord extension is ineffective at $M = 0.94$.

Despite these results, the analysis shows that the concept of a leading-edge chord extension over the outer sections has notable advantages and provided that the leading-edge shape of the extended section is modified to give peak-suctions for a given C_L no higher than for the original section and provided that the outer end of the extension is not located just inboard of the tip, useful gains might well be recorded. Correctly applied, a leading-edge extension should give better results than a fence.

1. *Introduction.*—Tests have been made (see Part I) in the R.A.E. 10-ft x 7-ft High-Speed Tunnel on three half-wings having their quarter-chord line swept back at 50 deg, a thickness/chord ratio of 7.5 per cent, and aspect ratios of 3.1 and 3.5. The most outstanding results from these tests is that for all the wings, at both low and high subsonic Mach numbers, a serious reduction in longitudinal stability occurs for values of C_L that are considerably below $C_{L \max}$.

Basically, the reductions in stability at high C_L are related to the fact that the first serious separation of flow occurs far out on the wing near the tips. This is largely a consequence of the shapes of the spanwise and chordwise loadings over the wing and is a function of both the wing-plan geometry and, as shown in Refs. 10 and 11, of the wing suction shape. In general, the effects at low Mach number are aggravated for sections having either a small leading-edge radius or a rapid change in slope close to the leading edge while at high Mach numbers, the reduction in stability is more severe if the sections on the outer part of the wing have a far-back position for the maximum thickness.

It thus appears that the stability characteristics at high C_L for these wings are undesirable in themselves and also may set too low a limit to the values of C_L that may be used either for

landing or for manoeuvring at high Mach number. The most effective method at least, at low Mach number, for improving the characteristics at high C_L should be to adopt a suitable combination of twist and camber, varying with position along the span. It is of considerable practical interest, however, to investigate whether worth-while improvements can be obtained by a less radical change, *i.e.*, by making some modification to the original design with symmetrical sections and no twist. A series of tests has been planned, therefore, to find the effects of various stall-fence arrangements, of a forward extension of the leading edge on the outer part of the wing, of various forms of drooped nose with and without some local thickening of the leading edge and with and without appreciable forward extension of the leading edge, and of different types of vortex generators. Of the tests so far made, the most successful has been with a drooped and thickened leading edge on the outer half of the wing but the present report is concerned with the tests made earlier with the different stall fences and with the simple leading-edge chord extension. The remaining tests will be discussed in later reports.

The discussion of the overall results at low Mach number is facilitated by reference to the photographs of the flow over the wing surface, as observed by an oil-flow technique, using titanium oxide as an indicating agent. These photographs were obtained for three representative cases: the plain wing with no device fitted, the wing with the largest of the stall fences tested and the wing with chord extension. Also, tests with surface tufts were made for various Mach numbers for the plain wing and for the wing with chord extension. Some of the photographs obtained in these flow-visualization tests are included in this report.

The tests discussed here were made at various times between May and December, 1952.

2. *Design of Wing, Fences and Chord Extension.*—The plan-form of the wing used for these tests is shown in Fig. 36. The main features are that the sweepback of the quarter-chord line is 50 deg, the gross aspect ratio (for the wing with the tip squared off) is 3.1 and the taper ratio (obtained on the same basis) is 0.36. Near the tip, the leading edge is curved according to the 'Kuchemann-type' fairing shape, extending in from the tip for a distance equal to one third of the basic tip chord (*see* Fig. 36). The wing sections are 7.5 per cent thick and of the RAE 101 shape throughout the span. The half-wing was tested in the presence of a half-fuselage which, opposite the wing, was of elliptic cross-section with no special shaping of the wing-body junction. Leading dimensions of the wing and body are given in Table 3 and the ordinates of the wing section in Table 4.

All the fences were mounted in turn at the same spanwise position, *viz.*, 0.56 of the gross semi-span. There is no aerodynamic significance in the choice of this location, which was determined by practical considerations for a particular type of aircraft with a similar design of wing. On the other hand, this choice of position was found to be aerodynamically very sound.

Five fences were tested and these are shown in Fig. 37. Two basic heights of fence were compared, *i.e.*, for a complete fence extending round both the upper and lower surfaces, the two heights were 1.2 and 2.4 \times the local wing thickness. Alternatively, if h is the total height of the complete fence and s is the total wing span (*i.e.*, 2 \times model span), the values of the ratio h/s are 0.029 and 0.058₅. Details of the fences are given in the following table:

Fence (<i>see</i> Fig. 37)	Height of corresponding complete fence	Description of fence
A	1.2 t (t = local wing max. thickness)	Upper surface only. Extending aft from maximum thickness position (0.31 c) to 0.02 c behind trailing edge
B	1.2 t	As fence A, but on both surfaces instead of upper surface only.

Fence (see Fig. 37)	Height of corresponding complete fence	Description of fence
C	$1.2t$	Both surfaces. Extending from $0.1c$ ahead of leading edge to $0.02c$ aft of trailing edge
D	$2.4t$	Similar to fence C but of double the height. Subsequently referred to as the 'full-large' fence
E	$2.4t$	Upper surface as for D. Lower-surface fence $0.3t$ deep and only ahead of the section (see Fig. 37)

The leading-edge chord extension is applied over that part of the wing, outboard of $\eta = 0.56$ that has a straight leading edge, *i.e.*, it extends from $\eta = 0.56$ to $\eta = 0.88_5$, or between sections AA and BB in Fig. 36. The amount of the forward extension is $0.1 \times$ local chord and details of the extended shape are shown in Fig. 38 and the ordinates are given in Table 4. The new shape is, basically elliptic and blends into the original section at $0.2c$ behind the original leading edge. The leading-edge radius of the extended section is only $0.0028c$ compared with $0.0043c$ for the original section and so can be considered as typical of a wing with a thickness/chord ratio of 6 per cent.

3. *Details of Tests.*—3.1. *Manufacture and Mounting of Model* (see also Part I).—The half-wing and body were made of compressed wood (Hydulignum) and the fences were made of sheet brass, about 0.10 in. thick.

The wing and body were mounted separately, the wing passing through the body and the floor of the tunnel and being mounted on the balance-plate of the six-component mechanical balance under the working-section. The body was attached to the floor of the tunnel. The balance, therefore, only measured the forces and moments on the exposed net wing outside the body.

3.2. *Range of Tests.*—Measurements of lift, drag, pitching moment and root bending moment were made for all the configurations over a range of Mach numbers from 0.50 to 0.95 at a Reynolds number, based on the gross mean chord, of 2×10^6 . Measurements were also made at low Mach number ($M = 0.18$) for three Reynolds numbers between $R = 2 \times 10^6$ and $R \simeq 6 \times 10^6$ for three configurations: plain wing, wing with large stall fence D and with the chord extension.

For the latter three basic configurations, flow-visualization tests were made at $R \simeq 2.5 \times 10^6$, $M = 0.2$. This technique has not yet been developed for use in this tunnel at high Mach numbers and so in two cases, the plain wing and the wing with chord extension, tests were also made with surface tufts up to Mach numbers of 0.95 and 0.92 respectively. The plain wing was also tested with tufts at low Mach number and high Reynolds number (e.g., $R = 6 \times 10^6$).

3.3. *Reduction and Correction of Results.*—The values of C_L , C_D and C_m are based on the area and mean chord of the net plain wing*, *i.e.*, no difference was made in the case of the wing with chord extension even though this involved a 3.3 per cent increase in the net wing area. The values of C_m are related to the mean quarter-chord point of the net plain wing. The root bending moments have been used to find the spanwise position of the centre of load of the net wing and when plotted, this is related to the aircraft centre-line.

Corrections were applied for the effects of blockage and tunnel constraint. The corrections for blockage were calculated by the method of Ref. 4. None of the changes in configuration

* Erroneously, the values used refer to a wing with square tip but this should have a negligible effect on the results as discussed later.

materially affected the blockage and the same corrections were used for each test. Typical values of ΔM are given in the following table:

M_c	0.50	0.80	0.90	0.94
α				
0°	0	0.002	0.006	0.014
8°	0	0.003	0.010	0.021
14°	0.001	0.007	0.018	—

4. *Results for Plain Wing.*—The stalling characteristics of the plain wing are discussed in detail, together with a full analysis of the flow patterns, in Part I. Results for the plain wing are included in Figs. 40 to 44 and Figs. 47 to 49.

5. *Effectiveness of Full Large Stall Fence (D. Fig. 37).*—5.1. *Effectiveness at Low Mach Number (Figs. 40 to 45).*—5.1.1. *Effects on overall results.*—Before giving a detailed account of how the addition of the fence affects the flow characteristics at high C_L , it is useful to state what are the major effects on the overall results. These are as follows:

- (a) The addition of the fence completely eliminates the reduction in stability (and slight decrease in $(\partial C_L / \partial \alpha)_M$) that occur for the plain wing at the higher test Reynolds numbers between $C_L = 0.5$ and 0.7 , prior to the occurrence of any separation near the leading edge. Since, as already suggested, this particular change in stability may not be present to the same extent for the plain wing at flight Reynolds numbers, this effect may not be of great significance in practice.
- (b) The initial nose-down change in C_m and increase of $(C_D - C_L^2 / \pi A)$ and $(\partial C_L / \partial \alpha)_M$ with C_L , that correspond with the first appearance of a separation near the leading edge and of a part-span vortex sheet occur at about the same C_L (e.g., $C_L = 0.72$ for $R = 6 \times 10^6$) with the fence fitted as for the plain wing and the results continue to be closely similar for an increase in C_L of about 0.1 above this value.
- (c) At higher values of C_L , C_D is reduced significantly and also the reduction in stability is both delayed to a higher value of C_L and greatly reduced in magnitude as a result of fitting the fence. The value of C_L above which $(-\partial C_m / \partial C_L)_M$ is less than at low C_L is improved from about $C_L = 0.84$ for the plain wing to about $C_L = 0.91$ with the fence fitted. The subsequent reduction in $(-\partial C_m / \partial C_L)_M$ does not exceed about 0.12 in the C_L range up to about $C_L = 1.08$, i.e., up to almost $C_{L \max}$. Particularly as these results do not include the effect of a tailplane, it is not possible to assert categorically whether this reduction of stability would be acceptable or not but there is at least some hope that it would be so. Certainly the trim changes are not appreciable because the nose-up change in C_m above $C_L = 0.91$ is only about the same as the nose-down change between $C_L = 0.7$ and $C_L = 0.9$. Therefore, if the usable $C_{L \max}$ is determined for both configurations by these changes in stability, the addition of the fence should certainly improve it by 0.1 and there is some hope that the gain would be about 0.2 , i.e., from about $C_L = 0.85$ to about $C_L = 1.05$. The reduction in C_D owing to the fence at $C_L = 1.05$ amounts to 0.035 .
- (d) The tests for the wing with fence were not extended to a sufficiently high incidence to determine the effect of the fence on the value of $C_{L \max}$.
- (e) The inward movement of the spanwise centre of load at high C_L is delayed and considerably reduced by the addition of the fence, e.g., for $C_L = 1.05$, $R = 6 \times 10^6$, it is only about $0.02 \times$ net semi-span further in than at low C_L , rather than 0.06 as for the plain wing.

5.1.2. *Detailed analysis with aid of flow photographs.*—Basically, the chief effects of a fence are that it results in a modification of the spanwise and chordwise loadings on the wing and that it acts as a barrier to the spanwise drift of the boundary layer, thus in particular reducing the thickness of the boundary layer over the rear of the upper surface of the sections just outboard of the fence.

The latter has frequently been quoted as the chief reason for using a fence and this is probably true in the case of a swept wing of high aspect ratio or of a swept wing with a spanwise distribution of camber and twist such that the stalling of the outer wing sections is by a turbulent separation from the rear. In the present case, it appears to be the reason why the fence almost completely eliminates the reduction in stability which is found to occur for the plain wing between about $C_L = 0.5$ and 0.7 at the higher test Reynolds numbers. This suggestion is supported by the evidence of the flow patterns (Figs. 44 and 45) which show that the direction of the flow lines immediately outboard of the fence is much closer to that of the free stream than for either the sections inboard of the fence or for this part of the wing in the absence of the fence.

As seen above in section 5.1.1, however, the more important effects of the fence are those that occur above $C_L = 0.7$ and it will be shown below that these can be related to the changes in chordwise and spanwise loading owing to the fence rather than to its prevention of boundary-layer drift from the inner to the outer sections.

The effect of the fence on the spanwise lift distribution on the wing has been calculated by the method of Ref. 12 with the result shown in Fig. 39. The local lift is decreased outboard of the fence and increased inboard but the magnitude of these changes is fairly small because of the relatively low value of the ratio of the fence height to wing span ($h/b = 0.058$). For example, outboard of the fence, the peak value of (C_L/α) is reduced by only 2 per cent and even at a distance of only $0.02 \times$ net semi-span from the fence, its effect is only about 4 per cent.

The more important effect of the fence is the way in which it modifies the shape of the chordwise loading in its vicinity. Outboard of the fence, as at the wing root, the chordwise loading is flattened while inboard of it, the peak suction near the leading edge for a given C_L is increased as near the wing tip. Pressure-plotting tests on a wing with a similar size of fence (in relation to the wing chord) have shown that about 50 per cent of the full reflection effect is obtained close to such a fence. The effect is significant within about $0.05 \times$ net semi-span of the fence.

A close correlation can be established between these estimated effects of the fence on the loading over the wing and its effect on the extent of the regions of flow-separation at various incidences at $R = 2.5 \times 10^6$, as deduced from the flow photographs in Figs. 44 and 45. As before it can be assumed that the origin of a part-span vortex sheet near the wing leading edge corresponds to the inner end of the region where the boundary layer has separated. The positions of the origin of the vortex sheets at different incidences for the wing with and without the fence (at $0.5 \times$ net semi-span) are compared in the following table:

Incidence (deg)	Position of origin of vortex sheet as fraction of net semi-span ($R = 2.5 \times 10^6$)	
	Plain wing	Wing with fence
8	About 0.9	About 0.9
12	0.68	0.70
13	—	0.66
14	0.52	0.60 and 0.36
15	—	0.56 and 0.15
16	0.19	0.54 and 0.10

It follows from this comparison that:

- (a) The fence has no significant effect on the incidence at which separation first occurs near the tip and at which a part-span vortex sheet forms. This is consistent with the conclusion above that the fence has a negligible influence on the spanwise and chordwise loadings near the tip. It also explains why the initial nose-down change in C_m and increase in $(C_D - C_L^2/\pi A)$ with C_L occur at the same C_L and initially to the same extent when the fence is fitted as for the plain wing.
- (b) The subsequent inward movement of the vortex sheet is first gradually retarded as a result of the effect of the fence on the spanwise loading* and then virtually halted when the origin of the vortex sheet is located a little way out from the fence. This implies that the effect of the fence on the chordwise loading over the wing just outboard of it is sufficient to prevent the boundary layer separating near the leading edge there, at least, for incidences up to $\alpha = 16$ deg. This effect is similar to what has already been observed to occur at the root of the plain wing.
- (c) The importance of this last effect (b) is greatly enhanced by the fact that the vortex sheet, when it originates from just outboard of the fence, is effective in limiting the rearward extent of the dead-air region on the sections further outboard. This is because the vortex sheet is of the usual characteristic shape, being bent outward relative to the free-stream direction at an angle of about 20 deg and so, as shown in Fig. 45, when it originates from just outboard of the fence ($\eta = 0.5$), it crosses the wing trailing edge at about $\eta = 0.85$. It follows that though the fence has little influence on the incidence at which separation first occurs on the outer sections, it exercises a considerable influence, through the medium of the vortex sheet, outboard of it, on the rearward growth of this separation and that, as regards the overall effect of the fence, this is more important than its effect on the spanwise extent of the separation. The large total reduction in the area of separation at these incidences can be seen by comparing the photographs for $\alpha = 16$ deg in Figs. 44 and 45. These results are a good illustration of how, on a swept-back wing, the rearward extent of a dead-air region is not merely determined by the factors that apply in two-dimensional flow, such as a transition to turbulence in the separated layer.
- (d) Another important consequence of the vortex sheet being 'anchored' from a point just outboard of the fence is that the additional lift due to it occurs further out on the wing than if it had moved in as for the plain wing and occurs mostly behind the moment reference axis. It is thought that the height of the vortex sheet is considerably greater than that of the fence tested and so the additional lift induced inboard of it should be correspondingly greater.
- (e) It is likely that at some higher incidence, the area of separation outboard of the fence does finally extend considerably. From the overall results, it seems that this may happen near $C_L = 0.95$ at $R = 2 \times 10^6$ or $C_L = 1.08$ at $R = 6 \times 10^6$ †. An extension of the area of separation may result in one of two ways: either the flow may separate near the leading edge of even the sections immediately outboard of the fence, thus leading to the disappearance of the vortex sheet outboard of the fence or it may result from simply a decrease at the higher incidences in the strength of the vorticity in the part of the sheet close to the wing surface.
- (f) Just inboard of the fence, the flow would be expected to separate at a lower incidence when the fence is fitted because of both the increase in the local C_L there (Fig. 39) and the increase in the value of $(-C_D)_{\max}$ for a given C_L , owing to the partial 'tip-kink' effect. This is confirmed by the flow observations since signs of a separation just inboard of the fence are first evident (at $R = 2.5 \times 10^6$) near $\alpha = 10$ deg, compared with $\alpha = 14$ deg for this section in the absence of the fence. Hence, from $\alpha = 10$ deg

* The effect of the fence on the position of the origin of the vortex sheet at $\alpha = 14$ deg is equivalent to the change in local C_L (Fig. 39), *i.e.*, the separation is occurring at the same local C_L when the fence is present as when it is not.

† This effect certainly occurs in the test C_L range at Mach numbers of 0.5 and above when a final abrupt reduction in stability may be observed (*see* Fig. 51a and section 5.2).

to at least $\alpha = 16$ deg; two part-span vortex sheets are present in the flow about the wing with fence. For all incidences, as shown in the table in section 5.1.2, the vortex sheet on the inner half of the wing with fence is further in than the vortex sheet on the plain wing. The reduction in $(\partial C_L / \partial \alpha)_M$ and increase in C_D for the inner sections for incidences up to $\alpha = 16$ deg at $R = 2.5 \times 10^6$ should be greater as a result of fitting the fence and as regards C_D , this partly offset the improvement achieved further outboard. No adverse effect on C_m results, however, because the additional loss of lift occurs near or ahead of the wing aerodynamic centre.

It is clear from the above description that the spanwise position of the fence is an important factor in determining its effectiveness. The possible effect of a change in its position from that chosen for these tests is discussed later in section 6.2.

5.2. *Variation of Effectiveness with Mach Number (Figs 51 and 52).*—5.2.1. *Up to about $M = 0.88$.*—It appears from the C_m vs. C_L curves in Fig. 51a that the nature of the improvement due to the fence in the Mach-number range up to about $M = 0.88$ remains similar to that at low Mach number, as already discussed, e.g.:

- (a) The fence has little effect on the initial nose-down change in C_m and appreciable increase of $(C_D - C_L^2 / \pi A)$ with C_L which occur above about $C_L = 0.4$ at $M = 0.5$ or $C_L = 0.3$ near $M = 0.88$.
- (b) The value of C_L for $(-\partial C_m / \partial C_L)_M = 0$ as at low C_L and low Mach number is improved by the addition of the fence by an amount varying from about 0.05 at $M = 0.5$ (as at $M = 0.2$ for this Reynolds number) to 0.15 at $M = 0.8$ or about 0.2 at $M = 0.88$. In this respect, therefore, the effectiveness of the fence increases significantly with Mach number in this range until for $M = 0.88$, there is no reduction in $(-\partial C_m / \partial C_L)_M$ with increasing C_L up to about $C_L = 0.7$ at even the test Reynolds number of $R = 2 \times 10^6$.
- (c) The severe reduction in stability that would probably be unacceptable, is delayed by the fence from about $C_L = 0.65$ to about $C_L = 0.8$ (the actual value for the wing with fence decreases from about $C_L = 0.84$ at $M = 0.5$ to $C_L = 0.77$ at $M = 0.88$). As at low Mach number, these values should be improved somewhat by an increase in Reynolds number.

An interesting feature of the C_m against C_L curves for the wing with fence is that the final severe reduction in stability, when it occurs, is more abrupt than for the plain wing, particularly for $M = 0.8$ and above. As suggested under (e) in the previous section, the abrupt loss in stability probably corresponds with the disappearance (real or effective) of the vortex sheet lying across the wing sections outboard of the fence, which would permit a sudden increase in the area affected by the separation. This occurs either when the flow separates near the leading edge immediately outboard of the fence or merely when the vortex sheet effectively lifts off the surface.

The gain in usable C_L in this Mach-number range, owing to the fence, cannot be quoted precisely but it seems likely that, as at low Mach number, the gain is probably at least 0.1 and may be as great as 0.2.

5.2.2. *Above $M = 0.88$.*—Above about $M = 0.88$, the improvement due to the fence progressively disappears until by $M = 0.94$ (Fig. 51b), the reduction in stability actually occurs at a slightly lower value of C_L for the wing with fence than for the plain wing. This deterioration in effectiveness is also seen in the drag results (Fig. 52), whereas, for Mach numbers up to $M = 0.88$, the addition of the fence gives either a reduction in the drag at high values of C_L or at least, a smaller increment than at low C_L ; for Mach numbers above 0.88, the drag is increased considerably for values of C_L above $C_L = 0.5$. There is also a significant reduction, due to the fence, in the value of C_L for a given incidence at high Mach number and high incidence.

It thus seems that the addition of the fence is of no benefit for those Mach numbers when the reduction in stability at high C_L is largely caused by a shock-induced separation over the outer wing sections. In the absence of either pressure-plotting data or a test using tufts with fence present, a detailed analysis is not possible but several factors can be suggested which, when taken together, should account for the ineffectiveness of the fence under these conditions:

- (a) As shown in Part I, the observations with tufts on the plain wing suggest that at high Mach numbers, no single strong part-span vortex sheet forms over the outer sections, presumably because the changes in $(-C_p)$ with position along the span occur gradually rather than suddenly. Hence, at high Mach number, the fence is no longer able to influence the extent of the separation on the outermost sections (say, outward of $\eta = 0.65$ to 0.7) in the same way as at low Mach number (see section 5.1.2).
- (b) The only other means by which the fence could influence the flow over these outermost sections, *i.e.*, beyond the immediate vicinity of the fence is by its prevention of the spanwise drift of the boundary layer from the inner half of the wing. On the other hand, it can be argued that this is not likely to be of great significance while the shock wave and point of separation are well forward on the section. At higher Mach numbers than those reached in the present tests, when the shock wave, even at high C_L , is likely to be nearer the trailing edge, some benefit from fitting the fence may result in this way.
- (c) At high Mach number, it does not necessarily follow that the effect of the fence on even the flow over the sections immediately outside the fence is beneficial. The values of $(-C_p)_{\max}$ for a given C_L should here be reduced at sub-critical speeds by the addition of the fence, but the reflection effect implies a loss of effective sweep. Hence the shock strength (and local drag) for these sections at a given C_L at high Mach numbers may be increased by the fence.
- (d) The major reason why the fence actually increases the total drag at high C_L and high Mach number is, however, probably to be found in its effects on the flow over the sections inboard of it. All these effects act in the same sense of giving an earlier rise of drag with Mach numbers for these sections, *viz.*, there is the increase in local C_L and in $(-C_p)_{\max}$ for a given C_L at sub-critical speeds and the reduction in isobar sweep owing to the reflection effect similar to that at the tip of a swept-back wing. For the plain wing, the tuft photographs (Fig. 49) show that at high Mach numbers, for values of C_L just greater than that for the reduction in stability, the severe separation appears to be confined to those sections outboard of roughly where the fence was fitted. With fence present, this is probably not the case and so the poorer results then obtained can be crudely ascribed to the fence having increased the proportion of the span over which there is a serious separation of flow (*i.e.*, in direct contrast to the result at low Mach number).

The relative ineffectiveness of the fence at high Mach numbers, when the separation over the outer sections is shock-induced, is in accord with the results of most wind-tunnel tests with fences on swept wings of moderate aspect ratio. On the other hand, the use of fences on some aircraft in flight has given improvements in the usable C_L at high Mach number. This does not necessarily mean that there is a discrepancy between flight and tunnel in this respect but it may rather be related to the basic performance of the wing without fence. For example, in the present case, the value of C_L above which there is a reduction in stability has only decreased to about $C_L = 0.5$ at $M = 0.94$ but in at least one case in flight in which a fence proved effective, this limiting C_L for the aircraft without fence decreased from near $C_L = 0.6$ at $M = 0.88$ to about $C_L = 0.25$ at $M = 0.94$. Hence it seems possible that a fence is only really effective at high subsonic Mach numbers in applications where there is a very marked reduction with Mach number in the usable C_L for the aircraft without fence. The wing-section shape, as well as the plan-form, would play a large part in determining this.

5.3. *Drag Penalty at Low C_L (Fig. 52).*—The increase in C_D at low C_L from fitting the full large fence (D) is appreciable at all Mach numbers. Up to about $M = 0.85$, it amounts to

about $\Delta C_D = 0.002$, compared with $C_D \simeq 0.006$ for the plain wing at $C_L = 0$. Some of this increase in C_D is presumably caused by a forward movement of transition on the sections of the model wing, inboard of the fence, and so the measured values of ΔC_D may be rather greater than those to be expected in flight with transition near the leading edge for even the plain wing.

For $C_L = 0, 0.1$, the increase in C_D , owing to the fence, does not increase with Mach number up to $M = 0.94$ but for $C_L = 0.2$ and 0.3 , ΔC_D increases to about 0.0025 and 0.003 respectively by $M = 0.94$. This increase in ΔC_D with Mach number tends to occur just prior to the start of the steep drag rise for the plain wing at the same C_L and should result from the earlier appearance of a shock wave over the sections near the fence (particularly inboard of it). From the results for $C_L = 0.2, 0.3$, it seems that the reduction in the drag-divergence Mach number, owing to the addition of the fence is about 0.01 (a reduction of this order may also apply for $C_L = 0$ but this is beyond the test Mach-number range).

6. *Results for Other Fences Tested.*—The effect of removing most of the fence round the lower surface of the wing is shown by comparing the results for fences D and E (Fence E extends just round the nose back to about $0.05c$ on the lower surface, as shown in Fig. 37). Results at low Mach number and $R \simeq 6 \times 10^6$ are not available for fence E but on the basis of the C_m against C_L curves for $R = 2 \times 10^6$ in Fig. 51, it seems that removal of the lower fence has no significant effect on the pitching-moment characteristics at any Mach number tested except that the final loss of stability occurs more abruptly. There should certainly be little difference in the usable C_L range. This conclusion might have been expected since the reflection effect on the upper-surface pressure distributions in the vicinity of the fence should not be affected by removal of the fence and also estimates by the method of Ref. 12 predict that both fences should have about the same effect on the spanwise C_L distribution.

Fig. 52 shows that removal of the lower fence is well justified by the fact that generally, the drag increment with fence E is only about half that for the full fence D, *e.g.*, for $C_L = 0, 0.1$, the value of ΔC_D for fence E is only about 0.001 for all Mach numbers up to $M = 0.94$ and even for $C_L = 0.3, M = 0.94$, ΔC_D is only about 0.0015 .

Fence C is similar to the full large fence D except that it is of only half the height, with the result that the top of the fence is only $0.1t$ above the wing at its maximum-thickness position. Comparing the results for fence C and those for the plain wing (Figs. 51 and 52), it appears that:

- (a) the fence gives little improvement at any Mach number in the value of C_L above which there is some reduction of stability
- (b) at Mach numbers up to near $M = 0.88$, it delays the more severe reduction of stability by about 0.1 in C_L , *i.e.*, in this respect, it gives about half the improvement obtained with fence D
- (c) as for fence D, it becomes quite ineffective by $M = 0.94$
- (d) the drag increment, ΔC_D , is near 0.001 for all Mach numbers up to $M = 0.94$, for C_L values of 0.2 or less. The differences between the results for fences D and C are roughly as would be expected.

Fences A and B (Fig. 37), which did not extend ahead of the maximum thickness, were tested before the others in the hope that by preventing the drift of the boundary layer over the rear of the sections, some improvement might be obtained in the stability characteristics at high Mach number but as might be predicted from the results for the full fence C, no improvement was actually obtained in the tests at $R = 2 \times 10^6$. It is likely, however, that even fence A (rear upper surface only) would have been as effective as the full large fence D in eliminating the moderate reduction in stability that occurs with the plain wing at the higher test Reynolds numbers at low Mach number between $C_L = 0.5$ and 0.7 (Fig. 43).

7. *Some General Thoughts on Suitable Fence Designs.*—The discussion in sections 5 and 6 has shown that it should be possible to make a rough prediction of the effectiveness at low Mach number of any fence arrangement on such a wing as this, by estimating its effect on the spanwise and chordwise loadings, according to the methods of Refs. 12 and 13. No detailed study has been made to find what is really the optimum arrangement for this wing but it is important to give some idea whether notably better results could have been obtained with some arrangement other than those tested and what are the main factors that should be considered when assessing the effect of a variation in design. The principal features discussed here are the possible effects of changes in the shape and height of the fence and of its spanwise position on the wing and the possibilities of using more than one fence. The remarks should apply not merely to the particular wing design used in these tests but also more generally to other designs with a similar aspect ratio and thickness/chord ratio and with symmetrical wing sections and no twist.

7.1. *Effect of Shape of Fence.*—It is clear from the results of the present tests that it is not necessary to continue a fence round the lower surface aft of about $0.05c$: to extend it further merely increases the drag penalty. Other possibilities, that have been suggested in various particular examples, for reducing the size of fence (below that for fence E, Fig. 37) while maintaining the same height, are to remove the rear part of the fence aft of the wing maximum-thickness position on the upper surface or to remove the portion of the fence round the wing leading edge.

It has been suggested that the chief effect of the rear part of the fence is to prevent the spanwise drift of the boundary layer and so, in the present model tests, it is responsible for the virtual elimination of the first reduction in stability at low Mach number and the higher test Reynolds numbers above about $C_L = 0.5$. At the higher Reynolds numbers of flight, a fence may not be needed to achieve this and then the rear part of the fence might be removed with probably a further reduction in the drag penalty due to the fence. On the other hand, the rear part of the fence would certainly be essential in those applications where the separation on the outer wing sections was a turbulent separation from the rear part of the section or where the fence is effective in increasing the usable C_L -range at high subsonic Mach numbers (*see* section 5.2.2). More generally, the rear part of the fence may be needed in flight to improve the flow over the aileron or cure some buffetting trouble. The need for its retention cannot therefore be argued on the basis of merely wind-tunnel data.

The need to extend the fence around the leading edge of the wing is in a different category. It has been seen that the effectiveness of the fences tested here at Mach numbers up to near $M = 0.9$ appears to be derived principally from the decrease in the peak-suction values near the leading edge immediately outboard of the fence. It seems reasonable to suggest, therefore, that to maintain its effectiveness in this way, it is essential for the fence to extend round the leading edge in the present case. This conclusion would not necessarily be true if the fence were higher or were placed further out along the span* or in applications where the fence was being used to improve the stability characteristics at high Mach number. If it is possible, without loss of effectiveness, to remove the part of the fence round the leading edge and to increase the fence height rearwards from zero, then this should be done in order to reduce the risk of buffetting. It is probably fair to conclude that, in most cases, the fences will have to be extended round the leading edge.

The precise shape of the upper contour of the fence is unlikely to be of great significance aerodynamically.

7.2. *Effect of Spanwise Position of Fence.*—It is immediately clear from Fig. 39 that the position of the fence in these tests ($0.56 \times$ gross semi-span or $0.50 \times$ net semi-span) is a quite reasonable choice. The fence is inboard of the peak in the spanwise C_L distribution for the plain wing and so it effects a reduction (albeit small) in this peak value; the value of C_L on the inboard

* In both of these cases, the fence would have a larger effect on the local values of C_L in its vicinity and the decrease in C_L outboard of it might be sufficient in itself to delay appreciably the leading-edge separation on the section just outboard of the fence.

side of the fence is not markedly in excess of the peak value in the distribution for the plain wing and also any premature separation that may occur inboard of the fence should not result in a significant nose-up moment change about the wing mean quarter-chord point.

The decision regarding the optimum choice of spanwise position for the fence depends largely on what reduction of stability at high C_L is acceptable. The choice depends therefore on such factors as the basic value of $(-\partial C_m/\partial C_L)_M$ at low C_L for the complete aircraft with tail, referred to the correct aft c.g. position and on whether the tail effectiveness decreases at high C_L . Nevertheless, certain general trends can be deduced as below.

With the full large fence at $0.50 \times$ net semi-span; it was found that at low Mach number, the value of C_L , denoted C_{L1} , above which there is some reduction of stability, is increased by less than 0.1 by the fence but that the subsequent reduction of stability remains at about 0.12 and so possibly acceptable up to a higher value of C_L , i.e., C_{L2} , above which there is a more abrupt loss. The increase in C_{L2} , owing to the fence, is about 0.2. If the fence were moved further out but not beyond about 0.7 semi-span, a larger improvement in C_{L1} should be recorded because the fence would then have an effect on the first occurrence of a separation on the outermost sections and the part-span vortex sheet, originating from just outboard of the fence, in its new position would restrict the dead-air region outboard of it to an even greater extent than with the fence tested. If, however, the fence were moved further out (to say, beyond $0.7 \times$ semi-span), C_{L1} might be decreased by the fence because the local (C_L/α) , just inboard of the fence, would be considerably greater than for any section of the plain wing and because a premature separation there should give a nose-up contribution to the overall pitching moment.

Moving the fence further out than the position tested should, however, reduce the effectiveness of the fence on the value of C_{L2} . This is because the separation on whatever section is immediately outboard of the fence would form at a lower C_L with the fence further out and so the outer part-span vortex sheet would also disappear at a lower C_L . Also, moving the fence further in would probably give less satisfactory results. With the fence further in, the vortex sheet would be allowed to move further in before becoming 'anchored' and so the dead-air region near the tip would be larger. Hence, the reduction in stability with increasing C_L above C_{L1} would be greater than the value of 0.12, obtained with the fence tested and then, it is more likely that C_{L1} rather than C_{L2} would represent a usable limit.

It follows that if the primary concern is to postpone a severe loss in stability at low and moderate Mach numbers to as high a value of C_L as possible, i.e., to keep C_{L2} high, then the position of the fence chosen for the present tests should be close to the optimum. If, however, even a small reduction in stability (which might be accompanied by other effects such as buffeting) is unacceptable, C_{L1} should be high and probably a position near $0.7 \times$ semi-span would be preferable.

The variations in the effectiveness of the fence with Mach number up to about $M = 0.9$, as already described in section 5.2.1, are such that the case for possibly moving the fence further out along the span is even weaker at the higher Mach numbers in this range than at low Mach number*.

For Mach numbers above about $M = 0.90$, it is doubtful whether any change in the spanwise position of the fence would lead to its becoming effective. As a qualification to this general conclusion, it is just possible that a fence placed further out at 0.7 to 0.75 of the semi-span might be beneficial. With a fence in such a position, the proportion of the span over which there was a severe separation for C_L values near 0.6 at say, $M = 0.94$ might not be notably greater than for the plain wing and so at least one of the weaknesses of the design tested would be avoided.

7.3. *Effect of Height of Fence.*—It has already been seen that an increase in the height of the fence from fence C to fence D is distinctly advantageous and so it may be queried whether an

* Broadly, because at high Mach numbers, it has been seen that the gain in C_{L1} is greater and is then comparable with the gain in C_{L2} with even the fence tested.

even taller fence would lead to still better results. With fence D, the top of the fence is $0.09c$ above the wing chord, or $0.0525c$ above the upper surface of the wing at its maximum-thickness position and it is estimated¹³ that this fence gives about 50 per cent* of the full reflection effect on the chordwise loading. A taller fence would give some improvement in this respect and also would further decrease the values of (C_L/α) outboard of it but only at the expense of increasing the values of (C_L/α) inboard of the fence to the extent that the peak value would be considerably greater than the value for any section of the plain wing. Even if no adverse change in stability resulted, a premature separation of flow and increase in drag would result. Even with fence D, it was found at $R = 2.5 \times 10^6$ and low Mach number that a separation was present on the inner side of the fence by $\alpha = 10$ deg or only about 2 deg later than for the separation near the tip. Hence, with a taller fence, the separation inboard of it might occur first. A taller fence would also be undesirable structurally and would accentuate the adverse effects at high Mach number.

It seems fair to conclude that there is little advantage to be gained from an increase in fence height (compared with D or E). To a certain extent, the optimum height is a function of the spanwise position of the fence (a taller fence being required if it is placed well inboard (see below and Ref. 12)).

7.4. *Possibilities with More Than One Fence.*—From the discussion in sections 7.1 to 7.3 it appears that the results with either fence D or E are probably close to the best that could be achieved with any single fence. It can be argued, however, that better results, at least, at low Mach number, might be achieved by using more than one fence, though always at the expense of a more serious increment in drag at low C_L . With a multiple fence arrangement, one fence should be fitted near the position found to be the optimum for a single fence (see section 7.2) while the other fence(s) should be placed further inboard. The effects of a multiple fence arrangement can be seen by considering a specific example: suppose that fence D or (E) at $0.56 \times$ gross semi-span were combined with a second fence at $0.40 \times$ gross semi-span and of almost four times the height of fence D (i.e., $h/b = 0.2$). The estimated effect of this arrangement on the spanwise distribution of (C_L/α) is plotted in Fig. 39a. The principal effects, due to the addition of the second fence, are as follows:

- (a) Outboard of the outer fence, the values of (C_L/α) are further reduced, e.g., by about 3 per cent for the peak value over the outer wing and by about 5 per cent immediately beyond the outer fence. This should result in the final abrupt reduction in stability being delayed to a higher incidence.
- (b) There should also be an improvement in the flow at high incidence just inboard of the outer fence. The value of (C_L/α) is now no greater there than for this section of the plain wing and particularly at high Mach number, even the tip-reflection effect which increases the value of $(-C_p)_{\max}$ for a given C_L on the inboard side of the fence should be partly offset by the spread of the reflection effect of the opposite sign from the outer side of the inner fence. The main effect should be that for Mach numbers up to about $M = 0.90$, the rearward extent of the dead-air region on the sections just inboard of the outer fence should be limited by the part-span vortex sheet, which over a certain range of incidence, should originate from just outboard of the inner fence.
- (c) The values of (C_L/α) are increased significantly for the sections inboard of the inner fence and so more lift should have been developed by these sections by the incidence when the separation occurs further outboard. The estimated peak value of (C_L/α) on these sections is no greater than inboard of the single fence tested and so the separation should not occur at a lower incidence. Another factor is that the rearward extent of the dead-air region here should be limited by the part-span vortex sheet originating from just outboard of the wing root.

It follows that at low Mach number, this double-fence arrangement should be better than the single fence and the additional gain, for example, in the value of C_{L_2} (for the severe reduction in

* A larger proportion at zero lift.

stability) should be more than 5 per cent. It is not suggested that this particular double-fence scheme is the best possible; it has merely been introduced as an example of how an additional fence might improve the overall characteristics at high C_L . Various refinements could be suggested: for example, it could be argued that the inner fence should possibly be nearer the outer one. In this case, however, it might be necessary to add a third fence further inboard. It should be possible to derive a suitable multiple fence arrangement for the present and other similar designs by estimating the effects on the loadings over the wing by means of Refs. 12 and 13 and then interpreting these in the light of the results discussed earlier.

It is probable that, as for the single fences tested, no multiple-fence arrangement would produce a significant improvement in the value of C_L at which the reduction in stability occurs at Mach numbers above $M = 0.90$. As before, this conclusion would not necessarily apply for other wing designs which showed a marked deterioration at high Mach number in this value of C_L .

It must be emphasized that while some multiple-fence arrangements should be preferable to a single fence in delaying or eliminating the instability at high C_L at low or moderate Mach numbers, this would only be achieved at the expense of a more serious increment in drag at low C_L , particularly at high Mach numbers.

8. *Results with Leading-edge Chord Extension.*—8.1. *Stalling Behaviour at Low Mach Number.*—8.1.1. *General description of overall results.*—The first impression gained from the C_m against C_L curves for the wing with chord extension as given in Fig. 43, is that at $R = 2 \times 10^6$, the modification is apparently beneficial. No severe loss in stability at low Mach numbers occurs for C_L values below about $C_L = 0.88$ (there is a slight reduction in $(-\partial C_m / \partial C_L)_M$ of about 0.015 above about $C_L = 0.2$, followed by a moderate reduction of about 0.05 above about $C_L = 0.6$). If the usable C_L is judged merely on the basis of when a reduction in $(-\partial C_m / \partial C_L)_M$ of more than say, 0.1 occurs, then at $R = 2 \times 10^6$, the chord extension gives an improvement of about $\Delta C_L = 0.2$ and also reduces the magnitude of the subsequent reduction in stability.

The apparently favourable results at $R = 2 \times 10^6$ are not, however, fully reproduced at the higher test Reynolds numbers when it is found that the various changes in stability, etc., occur at lower values of C_L when the chord extension is fitted than for the plain wing and the only advantage remaining to the chord extension is that the reduction in stability at high C_L is less severe. For $R = 5.6 \times 10^6$, for example, the initial nose-down change in C_m and increase in $(C_D - C_L^2 / \pi A)$ with C_L (Fig. 41b) occurs above about $C_L = 0.6$ with the chord extension, compared with near $C_L = 0.7$ for the plain wing. The serious reduction in $(-\partial C_m / \partial C_L)_M$ occurs near $C_L = 0.75$ rather than $C_L = 0.8$ but amounts to about 0.17 rather than about 0.5.

The results at the higher tests Reynolds numbers are therefore disappointing but the succeeding analysis shows that the possibility of the chord extension again giving an increase in usable C_L at Reynolds numbers higher than $R = 6 \times 10^6$ is not precluded.

8.1.2. *Analysis of results at $R = 2.5 \times 10^6$.*—The first most important point to note is that a significant area of flow separation first appears on the wing with chord extension at a lower value of C_L than for the plain wing. This is shown most clearly by comparing the flow patterns observed for $\alpha = 8$ deg ($C_L = 0.5$) in Figs. 44 and 46. For the plain wing, at this incidence, the first signs of a separation are only evident outboard of $\eta = 0.85$, *i.e.*, outboard of where the chord extension was subsequently fitted. With the chord extension in place, however, the flow has evidently separated near the leading edge, outboard of about $0.6 \times$ net semi-span, *i.e.*, over about the outer two-thirds of the span of the extension. The main reason for this is undoubtedly the sharper leading edge of the extended sections which is similar to that of a 6 per cent thick, rather than a 7.5 per cent thick section (*see* section 8.1.3). Contributory reasons may be that the tip effect on the shape of the chordwise loading is more aggravated near the outer chord discontinuity than for the plain wing and the fact that, as shown in Fig. 39b, the values of (C_L / α) , over the tip region, outboard of the discontinuity, are higher than for the plain wing. Supporting evidence for this earlier separation with chord extension fitted is that the flow pattern for

$\alpha = 4$ deg, $C_L = 0.24$ (not reproduced in Fig. 46), suggests that a separation is already occurring near the leading edge near the outer chord discontinuity and also that if, as is likely, the drag-increments, due to the chord extension, are similar at $M = 0.2$ to those measured at $M = 0.5$, the values of ΔC_D increase from only about 0.001 at $C_L = 0$ to about 0.0035 by $C_L = 0.35$ (Fig. 53).

By $\alpha = 10$ deg, ($C_L = 0.62$) (Fig. 46), the flow pattern over the wing with chord extension has become very complex and possesses the following main features:

- (a) The flow has separated near the leading edge over virtually the whole of the extension and hence a part-span vortex sheet originates from just outward of the inner discontinuity.
- (b) The rearward extent of the dead-air region is greater near the outer discontinuity than either further inboard or further outboard; near this discontinuity, the separation extends back to about mid-chord.
- (c) Behind the part-span vortex sheet, there is attached flow that has evidently come from over the top of the sheet. This characteristic was not clearly observed behind the vortex sheet on the plain wing, probably because of the increased spanwise drift in the boundary layer at the higher incidences then applying but it has been noted in the flow patterns for various other swept wings (*see* also (d) below and Part I).
- (d) From the inner discontinuity itself, a vortex sheet of opposite sign to the usual part-span vortex sheet is being shed: by opposite sign is meant that it induces an inward component of velocity close to the wing surface. This sheet can be thought of being associated with the inner edge of the extension in the same way as the usual tip vortex is associated with the wing tip. It is apparently weaker than the part-span vortex sheet further out but its presence can be detected, for example, by the deflection of the flow lines in an inward direction, relative to the free stream, over the forward part of the chord (of the main wing) under the sheet. The chief practical effect of this vortex sheet is that it opposes the spanwise drift of the boundary layer and so it is effective in reducing the thickness of the boundary layer over the sections further outboard. This helps to explain why, as above, the attached flow behind the outer part-span vortex sheet can be observed in the oil-flow pattern in this case.

In several reports, it has been suggested that the presence of this vortex sheet from the inner end of the extension should be effective but the present discussion will show that actually it is only one end probably not the most important factor.

- (e) Just inboard of the inner end of the extension, there is evidently a localised separation. The white blob of titanium oxide near the leading edge probably indicates the position of the peak suction inboard of this separation.

As already mentioned, the reduction in $(-\partial C_m / \partial C_L)_M$ in the incidence range up to $\alpha = 10$ deg, so far considered here, is only about 0.01₅ and it thus appears that this result is a fortunate coincidence in that with this particular geometrical configuration the various opposing lift and moment contributions from the two major vortex sheets and from the effects of the various areas of separation happen almost to balance each other.

Between $\alpha = 10$ deg ($C_L = 0.62$) and $\alpha = 14$ deg ($C_L = 0.88$), as already noted, there is a moderate reduction in $(-\partial C_m / \partial C_L)_M$ of about 0.05. Comparing the flow patterns in Fig. 46, it appears that in this range, only changes in detail take place in the flow patterns.

At $\alpha = 14$ deg, however, the changes in flow that presumably account for the subsequent increased loss in stability are already appearing:

- (i) The dead-air region inboard of the chord extension grows considerably, both spanwise and chordwise and the part-span vortex sheet, originating from near its inner end, is further in than is the vortex sheet on the plain wing at the same incidence. This effect is analogous to that observed inboard of a fence but is less marked; it arises for the same reasons.

- (ii) There appears to be some interaction between this inner part-span vortex sheet and the vortex induced from the inner end of the chord extension. This is sufficient to reduce the effectiveness of the latter in preventing the outward drift of the boundary layer over the rear part of the chord.
- (iii) The outer part-span vortex sheet is still present and is still originating from just outboard of the inner end of the extended leading edge. Near the trailing edge, this has now less influence on the flow near the wing surface and so the spanwise drift of the boundary layer over these outer sections is again evident.

With increasing incidence above $\alpha = 14$ deg, these changes become more pronounced but it should be particularly noted that the dead-air region outboard of the outer vortex sheet covers no greater area at $\alpha = 18$ deg than at $\alpha = 10$ deg and is even possibly slightly smaller in chordwise extent near the outer end of the chord extension. This is presumably the major reason why the reduction in $(-\partial C_m/\partial C_L)_M$, between about $C_L = 0.85$ and $C_L = 1.0$, compared with the value at low C_L is only about 0.2 with the chord extension, instead of about 0.5 as for the plain wing. The reduction in $(-\partial C_m/\partial C_L)_M$ that still occurs should be caused largely by first, the re-establishment at high incidence of the spanwise drift of the boundary layer and second, the influence of the inner part-span vortex sheet which, as shown in Part I, probably gives a nose-up contribution to the overall C_m , when it originates from near the wing root.

It is probable that at some incidence beyond those tested, the flow will finally separate near the inner end of the chord extension; the outer part-span vortex sheet would then disappear and a more severe reduction in $(-\partial C_m/\partial C_L)_M$ would result, unless balanced by other effects further inboard. It is noted in section 8.2 that such an effect appears to occur in the test range at $M = 0.8$.

It is useful to summarize the main reasons why the pitching-moment results at $R = 2 \times 10^6$ are improved by the addition of the chord extensions:

- (A) Separation occurs near the leading edge of the sections near the tip at a very low incidence and extends rapidly in to near the inner end of the chord extension. Hence, a part-span vortex sheet of appreciable height never originates from far out along the span and as a result, the usual initial nose-down change in C_m does not occur. It implies also that the initial reduction in stability does not occur because on the plain wing; this results from the elimination of the initial nose-down moment change as the vortex sheet moves in. With the chord extension, the various effects remain roughly balanced in terms of overall C_m from near $C_L = 0.25$ when separation first occur to certainly $C_L = 0.6$, and to a lesser extent, $C_L = 0.88$.
- (B) A part-span vortex sheet originates from near the inner end of the chord extension over a wide range of incidence, from $\alpha = 8$ deg up to at least $\alpha = 18$ deg ($C_L = 1.0$), and this is effective in restricting the chordwise extent of the dead-air region ahead and outboard of the sheet.
- (C) Another vortex sheet is shed from the inner edge of the chord extension and is effective in preventing the spanwise drift of the boundary layer to the outer sections for values of C_L up to near $C_L = 0.88$.

It may be noted that both factors (B) and (C), which might have been expected, prior to making the tests, are dependent on the chord extension having a sharp inner end and not being faired into the basic leading edge.

A crude estimate of the values of $C_{L \text{ crit}}$ at which the flow first separates on the extended sections away from the two ends of the extension has been derived from the flow photographs for $\alpha = 8$ deg, 10 deg and the estimated¹² spanwise loading for the wing with extension (Fig. 39) and in Fig. 56 these values are correlated with the local Reynolds numbers. It appears that the sharper leading edge is responsible for a decrease in the value of $C_{L \text{ crit}}$ for a given R_l near $R_l = 2.5 \times 10^6$ of about 0.35.

8.1.3. *Effect of Reynolds number.*—It has already been seen in section 8.1.1 that at the higher Reynolds numbers, the reduction in stability occurs at a lower value of C_L when the extension is fitted than for the plain wing but the reduction is of smaller magnitude. The explanation of these results, in brief, appears to be that at the higher Reynolds numbers, factors (B) and (C) above still apply (factor (B) continuing to be the main reason for the smaller reduction in stability) but factor (A) no longer acts in a beneficial sense.

Flow photographs for the higher Reynolds numbers are not available but from the overall results, it seems likely that for $R = 5.6 \times 10^6$, the flow first separates near the leading edge of the outer end of the chord extension at an overall C_L of about 0.6, compared with $C_L \approx 0.25$ at $R = 2 \times 10^6$ and that this separation extends to near the inner end of the extension by about $C_L = 0.8$, compared with $C_L = 0.5$ at $R = 2 \times 10^6$. Hence, the part-span vortex sheet when it lies across the outermost wing sections should be at least twice as high at $R = 5.6 \times 10^6$ as at $R = 2 \times 10^6$ and as a result, the sequence of changes in C_m with increasing C_L is similar qualitatively to that for the plain wing, *i.e.*, a nose-down change in C_m near $C_L = 0.6$, followed by a reduction in $(-\partial C_m / \partial C_L)_M$, compared with its value at low C_L , above about $C_L = 0.75$. The fortunate coincidence whereby the various effects of the vortex sheets and areas of separation tended to balance out at $R = 2 \times 10^6$ does not apply at the higher Reynolds numbers. Once this favourable balance ceases to exist, the reduction in stability occurs at a lower value of C_L for the wing with chord extension as a result of the lower values of $C_{L \text{ crit}}$ on the extended sections with their small leading-edge radius. From the overall results, it can be estimated that for $R = 5.6 \times 10^6$, the values of $C_{L \text{ crit}}$ for the extended sections away from the two ends of the extension are about 0.2 less than for the original 7.5 per cent thick, RAE 101 section, *i.e.*, $C_{L \text{ crit}} \approx 0.85$. A further improvement in these values of $C_{L \text{ crit}}$ might result from a further increase in Reynolds number although the results of two-dimensional tests suggest that even at high Reynolds numbers, the values of $C_{L \text{ crit}}$ (and local $C_{L \text{ max}}$) for sections with leading-edge radii appropriate to a 6 per cent thick section would not be as high as for a 7.5 per cent thick section.

The discussion above suggests that the results obtained at $R = 2 \times 10^6$ are quite misleading and that even though the results for the plain wing obtained at $R = 6 \times 10^6$ are likely to apply at higher Reynolds number, this cannot be definitely asserted for the wing with chord extension. In view of this doubt, it is not possible to draw a definite conclusion whether the chord extension would or would not improve the value of C_L for the serious reduction in stability in flight: it is likely to have little effect either way. On the other hand, it seems certain that the chord extension would greatly reduce the magnitude of this reduction in stability, whatever the Reynolds number.

8.2. *Effect of Mach Number on Stalling Behaviour.*—For Mach numbers up to about 0.85, the chord extension improves the pitching-moment characteristics at $R = 2 \times 10^6$ in similar way to that at low Mach numbers at this Reynolds number. This is shown in Fig. 54a by the results for $M = 0.5$ and $M = 0.8$. The value of C_L , above which there is an appreciable reduction in stability, is delayed by the chord extension by an amount varying from $\Delta C_L = 0.2$ to $\Delta C_L = 0.25$. For all Mach numbers up to $M = 0.88$, for the wing with chord extension, this reduction in stability does not occur until beyond $C_L = 0.8$. The question immediately arises as to whether these apparently favourable results are also likely to be partly invalidated, as at low Mach number, by changes with Reynolds number. It is of interest to discuss this question briefly because it can again be suggested that the overall results in themselves are somewhat misleading in this respect.

The results for $M = 0.5$ are similar qualitatively to those at low Mach number, already discussed but the overall results for $M = 0.8$ suggest at first sight that the chord extension is then merely delaying to a higher value of C_L , the various changes in flow that occur for the plain wing. For example, it is not only the final loss in stability which occurs at a higher C_L but also an initial nose-down change in C_m occurs near $C_L = 0.65$ for the wing with chord extension, compared with near $C_L = 0.45$ for the plain wing. Also, Fig. 53 shows that the chord extension is more effective at $M = 0.8$ than at lower Mach numbers in reducing the drag at high C_L , *e.g.*,

it is only over a very limited range of C_L near $C_L = 0.3$ that the chord extension gives an appreciable increase (about 0.0035) in C_D . Despite these favourable indications, however, examination of the photographs of the behaviour of surface tufts at $M = 0.8$ (Fig. 57) shows that, qualitatively, the basic reasons for the improvement due to the chord extension are still the same as at low Mach number, at this Reynolds number, *e.g.*, it appears that:

- (a) a separation has occurred over almost the whole of the leading edge of the chord extension by $\alpha = 6$ deg, $C_L = 0.42$ with a part-span vortex sheet originating from its inner end
- (b) the area affected by this separation hardly increases between $C_L = 0.42$ and $C_L = 0.85$
- (c) the severe reduction in stability which occurs above about $C_L = 0.82$ corresponds to the flow becoming more disturbed over the rear part of the chord of the outer sections (as at low Mach number when the vortex sheets cease to prevent the spanwise drift of the boundary layer) and when the separation has extended completely in to the inner end of the chord extension, thus leading ultimately to the probable disappearance of the outer part-span vortex sheet. This spread of the separation* to the inner end of the extension can be seen by noting particularly the behaviour of the innermost tuft near the leading edge of the extension. This tuft is not disturbed for $C_L = 0.78$ but is so for $C_L = 0.85$.

The overall results obtained at $R = 2 \times 10^6$ in this range up to $M = 0.85$ are therefore suspect as at low Mach number and the only certain feature is that at higher Reynolds numbers, the reduction in stability at high C_L should continue to be less severe with the extension fitted.

For Mach numbers of $M = 0.88$ and above, the effects of the chord extension on the flow characteristics are not the same as at low Mach number and there is less risk that the results may be invalidated by an increase in Reynolds number. Figs. 54a and 54b show that the addition of the chord extension increases the value of C_L above which there is a reduction in stability by about 0.1 to 0.15 at $M = 0.88$ but that this gain decreases with Mach number until at $M = 0.94$, there is no significant difference between the results with and without the chord extension. It appears that, for these high Mach numbers, any apparent advantage of the chord extension is associated with the separation over the outer sections occurring at a lower C_L with the chord extension than for the plain wing. This earlier separation is shown by the lift and drag results, *e.g.*, the chord extension gives a considerable increase in C_D at $M = 0.94$ for all values of C_L between $C_L = 0.2$ and at least 0.7. It is also confirmed by the behaviour of the tufts. The photographs at the foot of Fig. 57 show that at $M = 0.915$, a separation from close to the leading edge is already evident near the outer end of the extension at $C_L = 0.47$ and that this extends progressively to cover almost the whole of the outer wing by $C_L = 0.73$ whereas for the plain wing, this separation occurs near $C_L = 0.55$ to 0.6 but over almost all the outer half of the wing at about the same value of C_L . It is easy to see that this relative behaviour of the wing with and without the chord extension should lead to the observed pitching-moment characteristic, *e.g.*, in particular, the chord extension gives a positive increment to C_m at moderate values of C_L but delays the serious reduction in stability, for those Mach numbers when it has any significant effect.

This analysis of the results at high Mach number suggests that it would be unwise to conclude that any gain in the usable C_L range near $M = 0.9$ can be achieved in practice with the chord extension tested. No device that effects an improvement in the overall stability characteristics partly by inducing an earlier separation of flow near the tips can be considered fully satisfactory.

8.3. General Assessment of Basic Idea.—Despite the somewhat disappointing results obtained with the chord extension tested, the detailed analysis above has shown that the basic concept of a leading-edge chord extension somewhere on the outer wing possesses various important potential advantages. These include the following:

- (a) The obvious advantage that the local values of (C_L/α) are reduced over the part of the span where the chord is extended

* This effect would probably also occur at low Mach number at an incidence higher than those tested, giving a more severe reduction in stability at low Mach number at some value of C_L above $C_L = 1.05$.

- (b) The chordwise loading near the leading edge at the inner end of the extended leading edge is modified in the same way as at the root of a swept-back wing. The flow does not, therefore, separate there until a high incidence is reached and a part-span vortex sheet continues to originate from just outboard of the inner end of the extension and is effective in limiting the dead-air region on the sections further outboard
- (c) A vortex sheet of opposite sign to the usual part-span vortex sheet is shed from the inner edge of the extension and this acts as a barrier, preventing the spanwise drift of the boundary layer over the rear part of the sections and so reducing the thickness of the boundary layer over the sections further outboard.

In all these respects, the action of a chord extension is similar to that of a fence sited at the same spanwise position as the inner end of the extension but in all these respects, the chord extension should be more effective than a fence, *e.g.*:

- (i) The effect on (C_L/α) remains roughly constant over the span of the extension whereas, with the fence, it decays with distance spanwise from the fence
- (ii) The effect on the chordwise loading only applies near the leading edge where it is required to delay separation and not further aft where it would merely serve to increase the drag, particularly at high Mach number
- (iii) The arresting of the spanwise drift of the boundary layer is accomplished with less disturbance of the flow over the rest of the wing
- (iv) It is also important to note that with an appreciable forward extension, a vortex sheet originating from a given point along the span crosses the wing trailing edge further out than with no extension and so is more effective in limiting the rearward extent of the dead-air region.

With the chord extension tested, these advantages were off-set at low and moderate Mach numbers by the fact that the separation occurred at a smaller local C_L on the extended section than on the original section. This was partly because the extended section had a sharper leading edge and partly because the outer end of the extension was placed near where the flow over the plain wing tended to separate first. It follows that to achieve satisfactory results at low or moderate Mach numbers (*i.e.*, in the 'subcritical' Mach-number range in which as the incidence is increased, the separation over a given section occurs first from a point close to the leading-edge), the section should not be just stretched forward but should either be no thinner close to the nose than the original section or if it is allowed to be sharper, some droop should be incorporated as well. More precisely, the peak suction and the adverse pressure gradients near the nose should not be greater than for the original section. Further, the chord extension should either be continued right out to the tip or its outer end should be much further in than with the design tested.

It also appeared that with the chord extension tested, the shock-induced separation occurring at Mach numbers between 0.88 and 0.94 appeared at a lower C_L on the sections near the outer end of the extension than for these sections on the plain wing. It should not, however, be concluded from this that the effects of a sharpened leading edge are necessarily detrimental at high Mach numbers. Indeed, it has now been found in several cases that a leading-edge extension with a sharpened leading edge may give a positive improvement at high subsonic Mach numbers. If the degree of sharpening is not very marked, it is possible that any beneficial effects due to it may only be obtained at relatively high Mach numbers, *e.g.*, with the chord extension considered in this report, some improvement might have been found for Mach numbers greater than the highest of the tests, *i.e.*, greater than $M = 0.94$.

Tests have since been made with a model having a wing with 8 per cent thick sections, a sweepback of 45 deg on the quarter-chord line and with a leading-edge chord extension extending from $0.45 \times$ semi-span out to the tip but with a nose sharper than that of the extension considered in the present report. In this case, the leading-edge radius of the extended section was made equal to that of a 5.5 per cent thick section of the same family as the original section. The test results for this model without chord extension are very similar to those for the basic wing

in the present report. With the chord extension (at $R = 1.0 \times 10^6$), a gain of between 0.05 and 0.1 in the value of C_L above which there is a marked pitch-up has been found even for Mach numbers near $M = 0.9$ and the C_m against C_L curve shows even more striking improvements at the highest Mach numbers reached in the tests ($M = 0.95$).

The precise mechanism by which these gains, with a sharpened leading edge at high subsonic speeds, are achieved is not at present clearly understood and further experiments are planned to investigate this.

To sum up, it would appear that a leading-edge chord extension with a sharpened leading edge may be an attractive proposition in certain applications. The sharpened leading edge may give an improvement at high Mach numbers and if it is also drooped and if it is designed correctly in plan-form, *e.g.*, with the extension extended right out to the tip, it may be successful in preventing the deterioration in low-speed stalling characteristics that would occur if sharpening were employed alone.

The correct choice of the amount of the forward extension and of the positions of the inner and outer ends of the extension depend on more than the spanwise and chordwise loadings over the wing in potential flow. For example, the choice of the inner end and of the amount of the extension determine the relative position of the outer part-span vortex sheet and the outer wing sections. Again, it depends on the nature of the stalling characteristics of the original plain wing. For example, if the wing were of higher aspect ratio or were thicker than the one tested here, the action of the extension in opposing the spanwise drift of boundary layer would become more important and a different choice of extension might be made. Care should be taken not to be misled by the results of experimental investigations made at too low a Reynolds number.

For the present example, the position chosen for the inner end of the extension and the amount of the extension can both be considered satisfactory but as regards its spanwise extent, two alternatives could be variously proposed:

- (A) An extension of very small length spanwise. This has the advantage that the part-span vortex sheet originating on it would be even more effective in limiting the dead-air region further outboard. Against this 'geometrical' advantage must be set the disadvantage that the values of (C_L/α) near the tip (and probably including the peak value on the wing) would no longer be reduced by extension.
- (B) Maintaining the extension right out to the tip. This sacrifices some of the 'confining' powers of the part-span vortex sheet but compensates for this by reducing the values of (C_L/α) close to the tip and by avoiding the introduction of an aggravated 'tip' effect on the chordwise loading near the outer discontinuity.

It is thought that (B) is likely to be the more satisfactory and certainly should be the only alternative that may possibly lead to an improvement at high Mach numbers.

Other tests with this basic design of wing have shown that incorporation of a drooped and thickened leading edge over the outer half of the wing can give an improvement of about 0.2 in the value of C_L for the serious reduction in stability at low Mach number and up to near $M = 0.9$ and even about 0.1 at higher Mach numbers. From the present discussion, it appears that even better results should be possible by combining these two ideas of a drooped, thickened leading edge and a leading-edge chord extension (provided the latter entails no reduction in the amount of leading-edge droop and thickening used). It is also possible that further improvements may be obtained from a modification of the leading-edge shape inboard of the extension in order to delay the separation there for it has been seen that the inner part-span vortex sheet, associated with this separation is eventually responsible for the elimination of the favourable effect of the vortex sheet from the inner edge of the extended leading edge. Further experiments will be made to investigate these suggestions for a 'hybrid' leading-edge modification.

9. *Conclusions.*—9.1.—The conclusions regarding the characteristics of the plain wing are given in Part I and are not repeated here.

9.2.—The addition of the full large fence gives the following results at low Mach number:

- (a) The reduction in stability at the higher test Reynolds numbers between $C_L = 0.5$ and 0.7 is almost completely eliminated by the action of the fence in preventing the spanwise drift of the boundary layer from the inner to the outer wing
- (b) The value of C_L at which the initial nose-down moment change occurs is little affected by the fence but the value of C_L above which there is some reduction of $(-C_m/\partial C_L)_M$ is increased by about 0.07 at $R = 6 \times 10^6$ and the reduction in $(-\partial C_m/\partial C_L)_M$ remains less than 0.12 and probably acceptable to near $C_L = 1.05$, compared with $C_L = 0.85$ for the plain wing. The fence also reduces C_D at high C_L (by 0.0035 for $C_L = 1.05$).

The gain in usable C_L , owing to the fence, at low Mach number may be as great as 0.2 . The effectiveness of the fence stems chiefly from its effect on the chordwise loading over the wing immediately outboard which discourages the boundary layer from separating near the leading edge. As a result, a part-span vortex sheet originates from just outboard of the fence up to at least $C_L = 1.05$ at $R = 6 \times 10^6$ and this vortex sheet restricts the rearward extent of the dead-air region over the outer sections. While this effect persists, no severe reduction in stability occurs.

9.3.—With increasing Mach number up to near $M = 0.88$, the improvement due to the fence is maintained and, even in some respects, increased. At higher Mach numbers, however, the effectiveness of the fence dies out until at $M = 0.94$, the reduction in $(-\partial C_m/\partial C_L)_M$ occurs at a lower C_L with the fence than for the plain wing. The ineffectiveness of the fence at high Mach numbers when the separation over the outer wing sections is shock-induced is a result principally, of the absence of strong part-span vortex sheets in the flow and of the effect of the fence in increasing rather than decreasing the spanwise extent of the separation.

9.4.—The penalty in drag, owing to the fitting of the full large fence amounts to about $\Delta C_D = 0.002$ at low C_L for all Mach numbers up to $M = 0.94$ but this increment may be halved, with no loss in effectiveness by removing the portion of the fence round the lower surface aft of $0.05c$.

9.5.—Guidance is given in section 7 regarding the probable effect of changes in fence design. No marked improvement is likely from any change in height or spanwise position of a single fence, compared with that tested but it may be possible, in the case of the present wing, that the fence will be fully effective at flight Reynolds numbers when the rear part over the upper surface is removed. A multiple fence arrangement with additional fence(s) further inboard might give better results at low Mach number and up to $M = 0.9$, at the expense of a more severe penalty in drag.

9.6.—The chord extension tested gives an improvement of 0.2 to 0.25 in the value of C_L at which the serious reduction in stability occurs at Mach numbers up to near $M = 0.9$ at $R = 2 \times 10^6$. This improvement is not reproduced at $R = 5.6 \times 10^6$ at low Mach number when the chord extension actually decreases the value of C_L at which the reduction in stability occurs and only gives the advantage that the magnitude of the reduction is much smaller. As with the fences, the effectiveness of the chord extension at even $R = 2 \times 10^6$ decreases above about $M = 0.88$ and at $M = 0.94$, it is quite ineffective.

9.7.—Despite these disappointing results with the chord extension tested, the basic concept has various important points in its favour. The most noteworthy of these are first that the chordwise loading near the inner end of the extension is modified near the leading edge so that the flow does not separate here and a part-span vortex sheet originates from near here and restricts

the rearward extent of the dead-air regions on the sections further outboard over a wide range of incidence and second, that a vortex sheet shed from the inner edge of the extension acts as a barrier to the spanwise drift of the boundary layer. To realize these potential advantages, without incurring a premature separation near the extended leading edge, the nose shape of the extension (and probably of the sections just inboard of the extension) should be modified, *e.g.*, with droop and the chord extension should either, for preference, be continued right out to the tip or should be of relatively small spanwise extent. For the present wing, the choice of $\eta = 0.56$ for the inner end is probably reasonable.

REFERENCES

- | <i>No.</i> | <i>Author</i> | <i>Title, etc.</i> |
|------------|---|--|
| 1 | L. N. Holmes and A. B. Haines .. | High-speed wind-tunnel tests on six wings of 40-deg sweepback, with various section shapes. R. & M. 2930. January, 1952. |
| 2 | A. B. Haines and L. N. Holmes .. | A comparison of the results of tests in the R.A.E. 10-ft \times 7-ft High-Speed Tunnel on three 40-deg swept wings with different thickness/chord ratios. R.A.E. Report. (To be issued.) |
| 3 | J. Black | A note on the vortex patterns in the boundary-layer flow of a swept-back wing. <i>J. R. Ae. Soc.</i> April, 1952. |
| 4 | J. Y. G. Evans | Corrections to velocity for wall constraint in any 10-ft \times 7-ft rectangular subsonic tunnel. R. & M. 2662. April, 1949. |
| 5 | D. Küchemann | Types of flow on swept wings with special reference to free boundaries and vortex sheets. A.R.C. 15,756. March, 1953. (<i>See also J. R. Ae. Soc.</i> November, 1953). |
| 6 | A. B. Haines and C. W. Rhodes .. | Tests in the R.A.E. 10-ft \times 7-ft High-Speed Tunnel on a 7.5 per cent swept wing fitted with stall fences and a leading-edge chord extension (Part II of this R. & M.). |
| 7 | E. W. E. Rogers, C. J. Berry and R. F. Cash | Tests at high subsonic speeds on a 10 per cent thick pressure-plotting aerofoil of RAE 104 section. Part II. Pressure distributions and flow photographs. R. & M. 2863. February, 1951. |
| 8 | H. H. Pearcey and M. E. Faber .. | Detailed observations made at high incidence and at high subsonic Mach numbers on Goldstein 1442/1547 aerofoil. R. & M. 2849. November, 1955. |
| 9 | D. Küchemann | A simple method of calculating the span and chordwise loadings on straight and swept wings of any given aspect ratio at subsonic speeds. R. & M. 2935. August, 1952. |
| 10 | A. B. Haines and C. W. Rhodes .. | Tests in the R.A.E. 10-ft \times 7-ft High-Speed Tunnel on three wings with 50-deg sweepback and 7.5 per cent thick sections (Part I of this R. & M.). |
| 11 | A. B. Haines | A comparison of the stalling characteristics at low Mach number of various swept-back wings tested in the R.A.E. 10-ft \times 7-ft High-Speed Tunnel. R.A.E. Tech. Note. (To be issued.) |
| 12 | J. Weber | Theoretical load distributions on a wing with vertical plates. R. & M. 2960. March, 1954. |
| 13 | J. Weber and J. A. Lawford .. | The reflection effect of fences at low speeds. R. & M. 2977. May, 1954. |
-

TABLE 1
Leading Dimensions of Models

	A*	B	C*
<i>Half wings</i>			
Gross area of wing (<i>i.e.</i> , from chord to tip chord)	3.395	3.504	2.97 sq ft
Net area of wing (<i>i.e.</i> , from root chord to tip chord)	2.804	2.913	2.44 sq ft
Gross mean chord	17.78	18	16.61 in.
Net mean chord	16.77	16.9	15.64 in.
Centre-line chord	26.08	26.08	24.10 ₅ in.
Root chord	24.02	24.02	22.20 in.
Tip chord (theoretical, by extending leading and trailing edge)	9.44	8.02	9.12 in.
Span	27.5	29.84	25.75 ₅ in.
Gross aspect ratio	3.10	3.53	3.10
Taper ratio (based on theoretical tip chord)	0.362	0.308	0.378
Sweepback of quarter-chord line	50°	50°	48° 49'
Thickness/chord ratio	0.075	0.075	0.075
Section maximum-thickness position	0.31 _c	0.31 _c	0.38 _c
Distance of net mean quarter-chord point aft of leading-edge centre-line chord	22.86	23.36	20.75
Distance of gross mean quarter-chord point aft of leading-edge centre-line chord	—	—	18.42
Dihedral	0°	0°	— 1°
Wing-body angle	0°	0°	1.5°
<i>Half bodies</i>			
Maximum height (<i>i.e.</i> , in spanwise direction)	3.4	3.4	3.28 in.
Maximum width (<i>i.e.</i> , in plane of symmetry)	2.0	2.0	3.28 in.

* Area, mean chord, aspect ratio, etc., for wings A and C are based on a square tip with the 'theoretical' tip chord, tip chord, rather than the true curved tip.

TABLE 2
Section Ordinates

Wing x/c	A. and B y/c	C y/c
0.005	0.0065	0.0071
0.01	0.0092	0.0097
0.0125	0.0103	—
0.02	0.0129	0.0130
0.025	0.0144	—
0.05	0.0200	0.0193
0.075		0.0229
0.10	0.0271	0.0259
0.15	0.0317	0.0302
0.20	0.0347	0.0332
0.25	0.0366	0.0353
0.30	0.0375	0.0368
0.35	0.0371	0.0374
0.40	0.0360	0.0375
0.45	0.0343	—
0.50	0.0320	0.0357
0.55	0.0294	—
0.60	0.0265	0.0313
0.65	0.0234	—
0.70	0.0201	0.0248
0.75	0.0168	—
0.80	0.0134	0.0167
0.85	0.0101	—
0.90	0.0067	0.0084
0.95	0.0034	—
1.00	0	0
L.E. radius	0.0043	—*
T.E. angle	7.67°	9.6°
Section	RAE 101	—
	7.5 per cent thick	

* The radius of curvature is changing so rapidly very close to the nose that to quote any value would be misleading.

TABLE 3

Leading Dimensions

Half wing (area, etc., based on 'theoretical' tip chord (*see below*))

Gross area of wing (<i>i.e.</i> , from centre-line chord to tip chord)	3.395 sq ft
Net area of wing (<i>i.e.</i> , from root chord to tip chord)	2.804 sq ft
Gross mean chord	17.78 in.
Net mean chord	16.97 in.
Centre-line chord	26.08 in.
Root chord	24.02 in.
Tip chord ('theoretical', by extending straight leading and trailing edges)	9.44 in.
Span	27.5 in.
Gross aspect ratio	3.1
Taper ratio (based on 'theoretical' tip chord)	0.362
Sweepback of 0.25 chord-line	50 deg
Thickness/chord ratio	0.075 in.
Section maximum-thickness position	0.31c
Distance of net mean quarter-chord point aft of leading-edge centre-line chord	22.86 in.

Half body

Maximum height (<i>i.e.</i> , in spanwise direction)	3.4 in.
Maximum width (in place of aircraft centre-line)	2.0 in.

Fences

Placed at 0.56 of gross semi-span, *i.e.*, at 15.40 in. from aircraft centre-line.

Local chord at fence position	17.92 in.
-------------------------------	---------	-----------

Total height of fences (*see Fig. 37*):

	<i>Small fence</i>	<i>Large fence</i>
In terms of local wing thickness 1.2t	2.4t
In terms of local wing chord 0.09c	0.18c
In absolute dimensions 1.61 in.	3.22 in.
In terms of total wing span (<i>i.e.</i> , 2 × half-model span) 0.029	0.058 ₅

Extension of fences ahead of leading-edge local chord	0.1c or 1.79 in.
Extension of fences behind trailing-edge local chord	0.02c or 0.36 in.

Leading-edge chord extension

Distance from aircraft centre-line of inboard end of extension	15.40 in.
Distance from aircraft centre-line of outboard end of extension	(0.56 × gross semi-span) 24.36 in.
		(0.89 × gross semi-span)

Amount of extension = 0.10c
(*i.e.*, varying from 1.79 in. at inboard end to 1.31 in. at outboard end)

The section shape is basically an ellipse with origin at the maximum thickness position of the original section but is blended into the original shape at about 0.2c back from the original leading edge (*See Table 4 for ordinates*).

TABLE 4
Ordinates of Wing Sections

All ordinates in table given in terms of c , the original section chord and relative to the original leading edge.

x	z (semi-thickness)	
	Original section	Extended section
$\bar{0}\cdot095$	—	0·0055
$\bar{0}\cdot090$	—	0·0078
$\bar{0}\cdot080$	—	0·0109
$\bar{0}\cdot070$	—	0·0133
$\bar{0}\cdot060$	—	0·0153
$\bar{0}\cdot050$	—	0·0169 ₅
$\bar{0}\cdot040$	—	0·0184
$\bar{0}\cdot020$	—	0·0210
$\bar{0}$	—	0·0231 ₅
0·0215	0·0103	—
0·02	0·0129	0·0250
0·025	0·0144	—
0·05	0·0199	0·0273
0·10	0·0270	0·0303
0·15	0·0316	0·0327
0·20	0·0346	0·0347
0·25	0·0366	
0·30	0·0375	
0·35	0·0371	
0·40	0·0360	
0·45	0·0342	
0·50	0·0320	
0·55	0·0293	
0·60	0·0264	
0·65	0·0233	
0·70	0·0200	
0·75	0·0167	
0·80	0·0134	
0·85	0·0100	
0·90	0·0067	
0·95	0·0033	
1·00	0.	
Leading Edge Radius	0·0043	0·0031

In terms of true local chord,

Leading-edge radius of original section = 0·0043

Leading edge radius of extended section = 0·0028

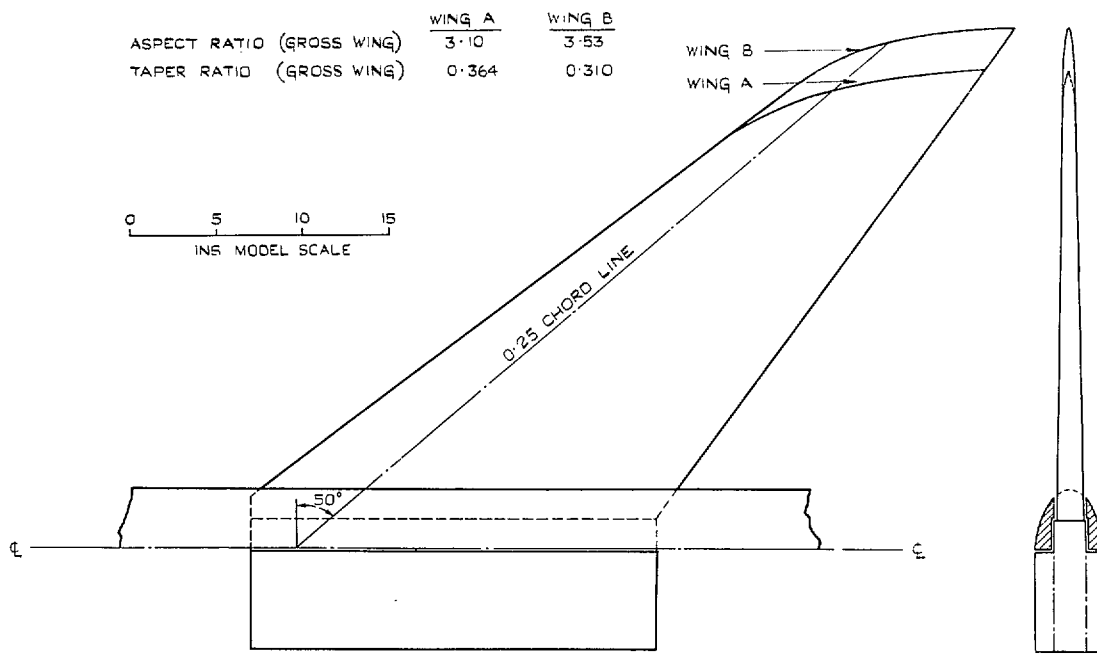


FIG. 1. General arrangement of wings A and B.

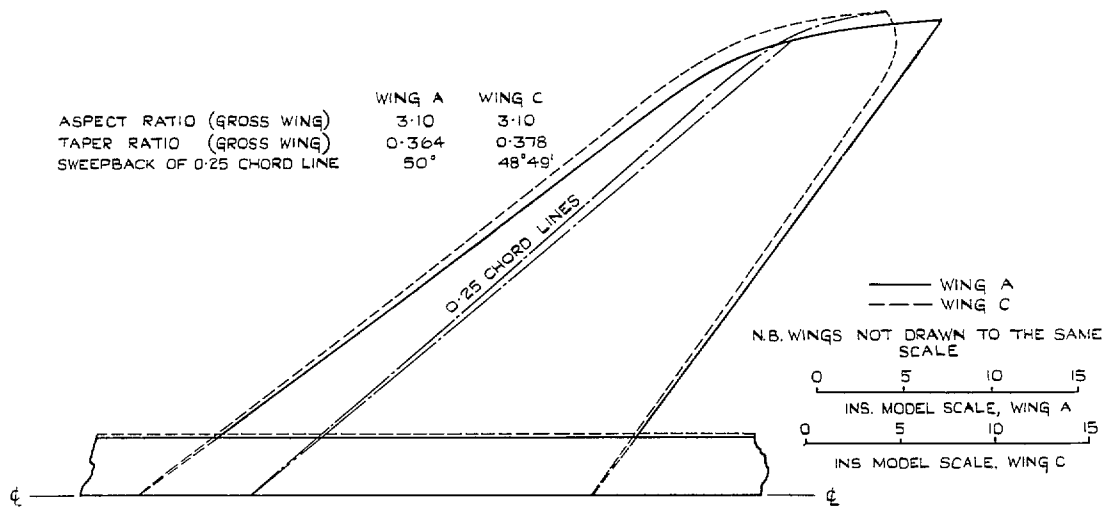
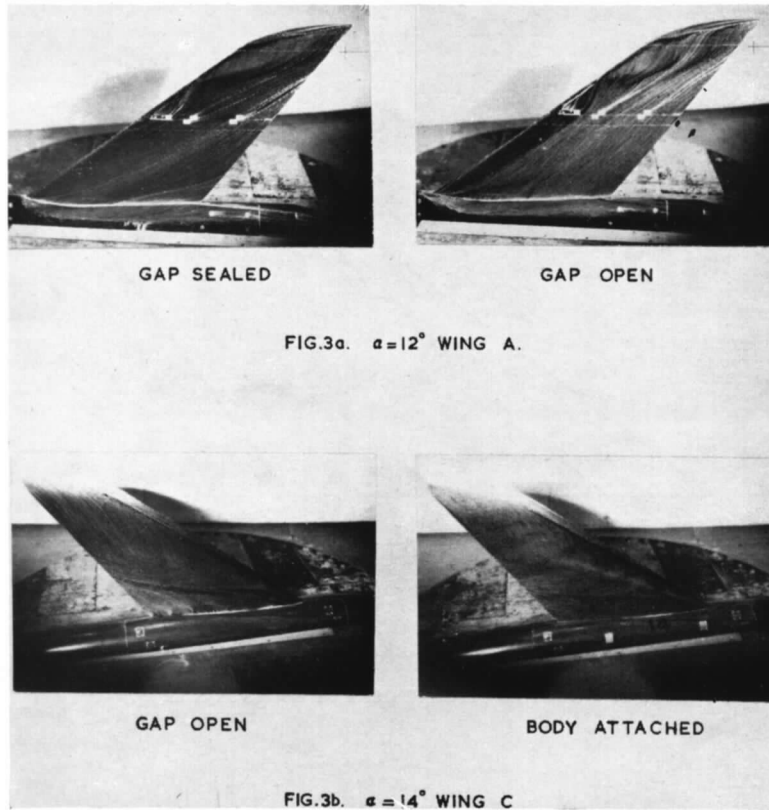


FIG. 2. Comparison of plan-forms of wings A and C.



FIGS. 3a and 3b. Effect of flow through gap in wing-body junction on flow patterns.

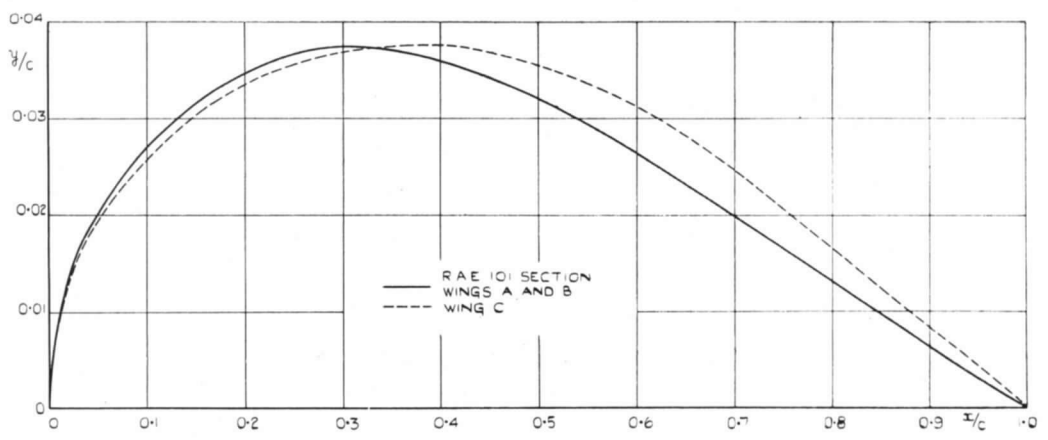


FIG. 4. Comparison of wing sections.

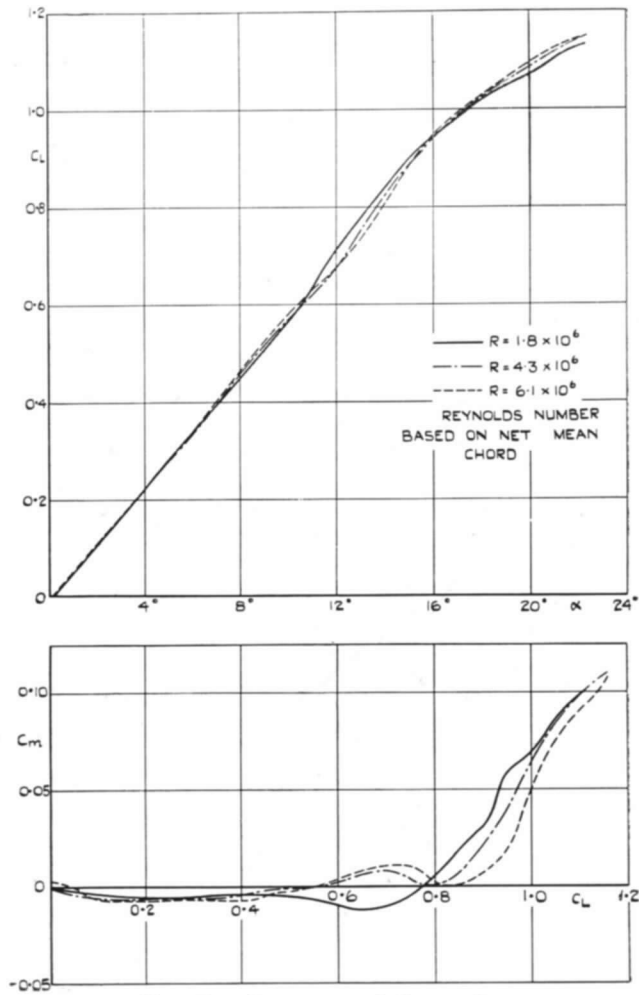


FIG. 5. C_L vs. α and C_m vs. C_L .
Effect of Reynolds number at $M = 0.18$ wing A.

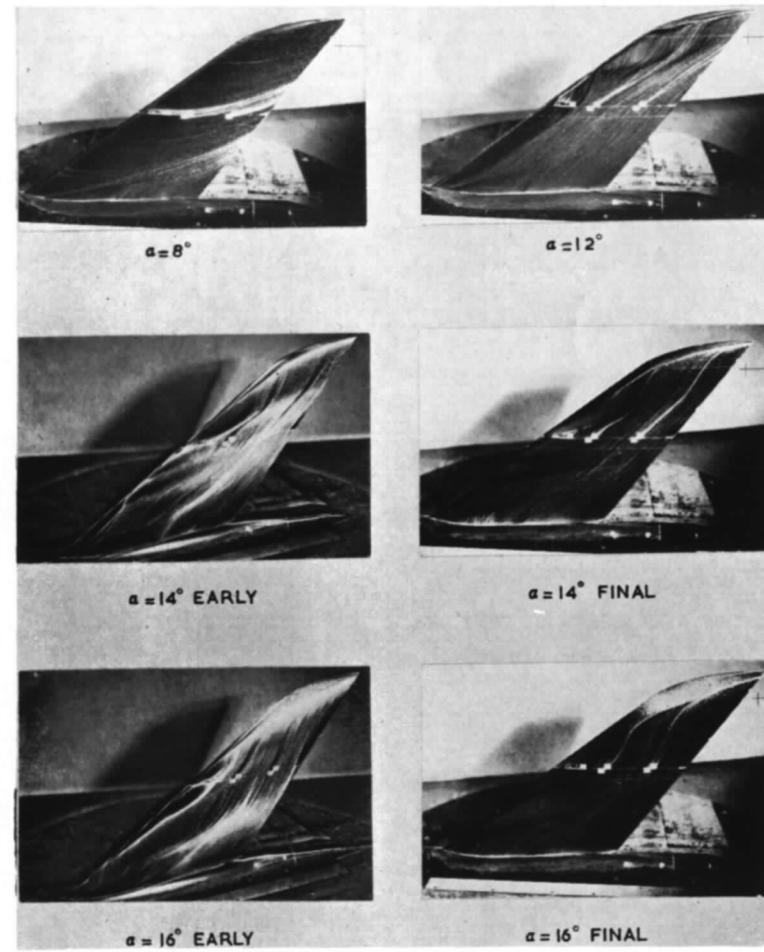
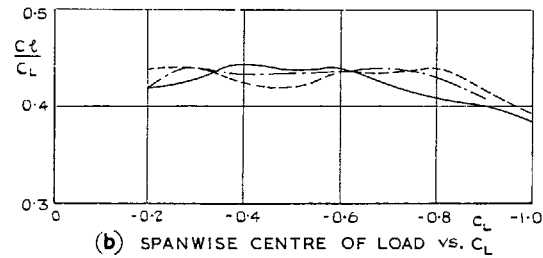
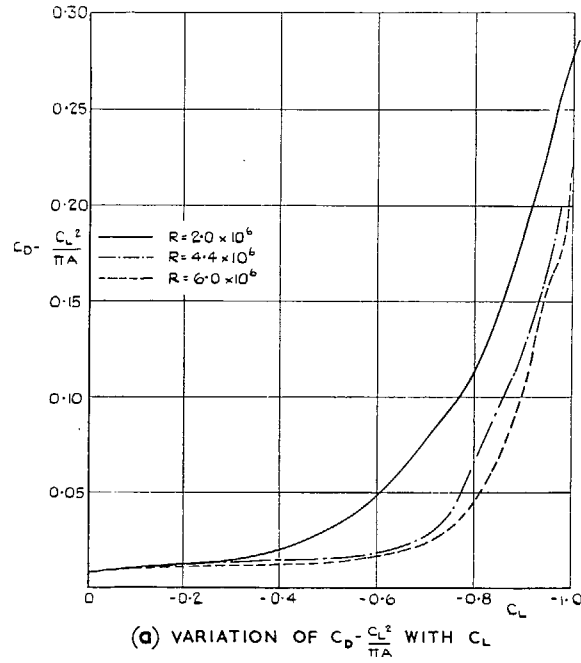


FIG. 6. Flow patterns. Wing A. $R = 2.5 \times 10^6$.



FIGS. 7a and 7b. Effect of Reynolds number on the variation of $C_D - (C_L^2/\pi A)$ and spanwise centre of load with C_L . Wing A.

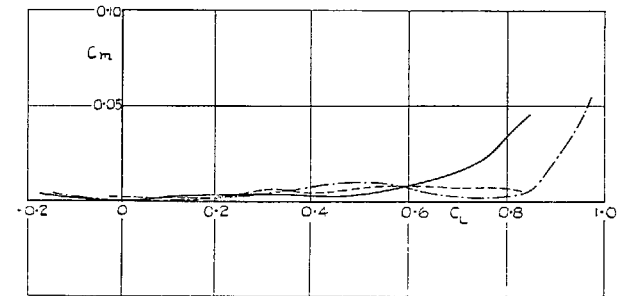
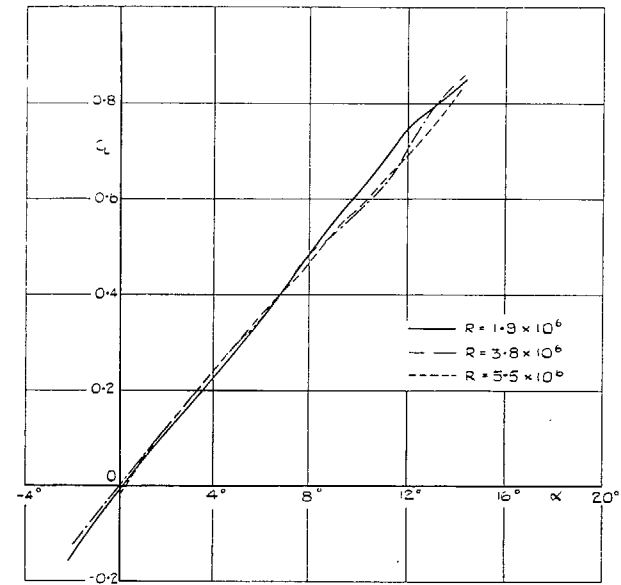


FIG. 8. C_L vs. α and C_m vs. C_L . Effect of Reynolds number at $M = 0.18$. Wing C. Positive incidences.

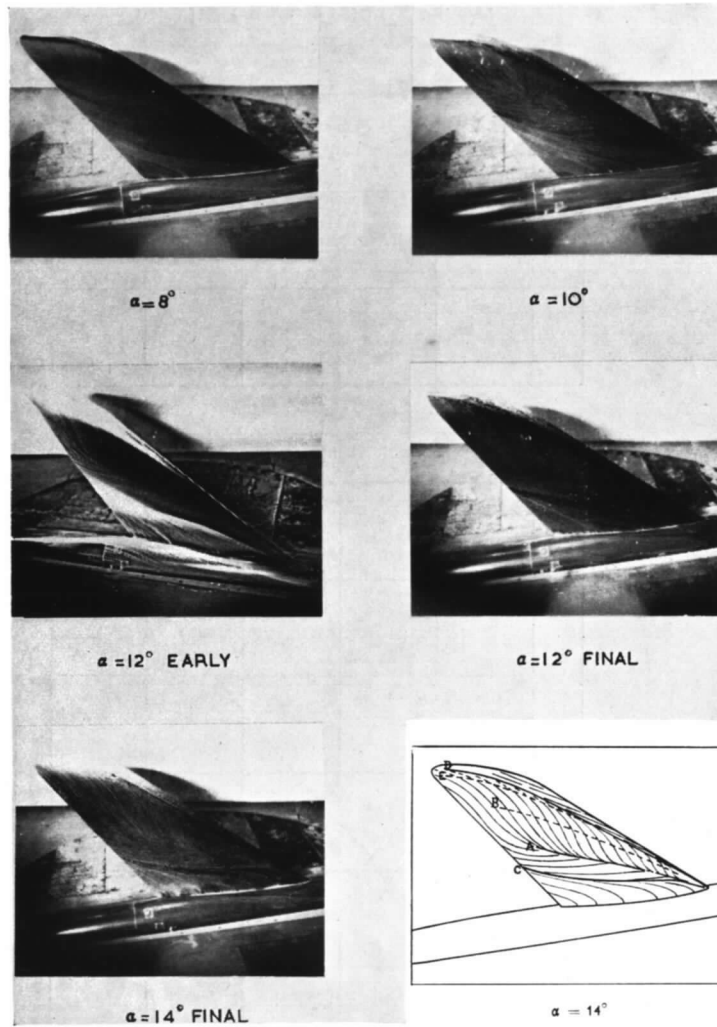
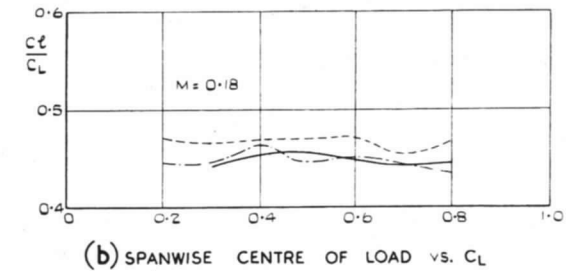
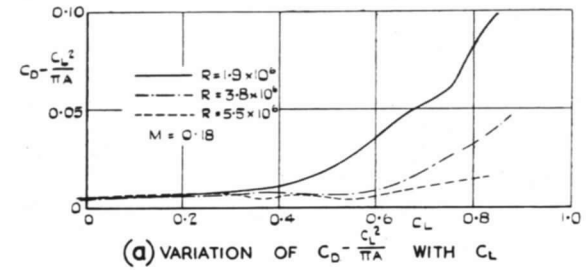


FIG. 9. Flow patterns. Wing C. $R = 2.5 \times 10^6$.



FIGS. 10a and 10b. Effect of Reynolds number on the variation of $C_D - (C_L^2/\pi A)$ and spanwise centre of load with C_L . Wing C. Positive incidences.

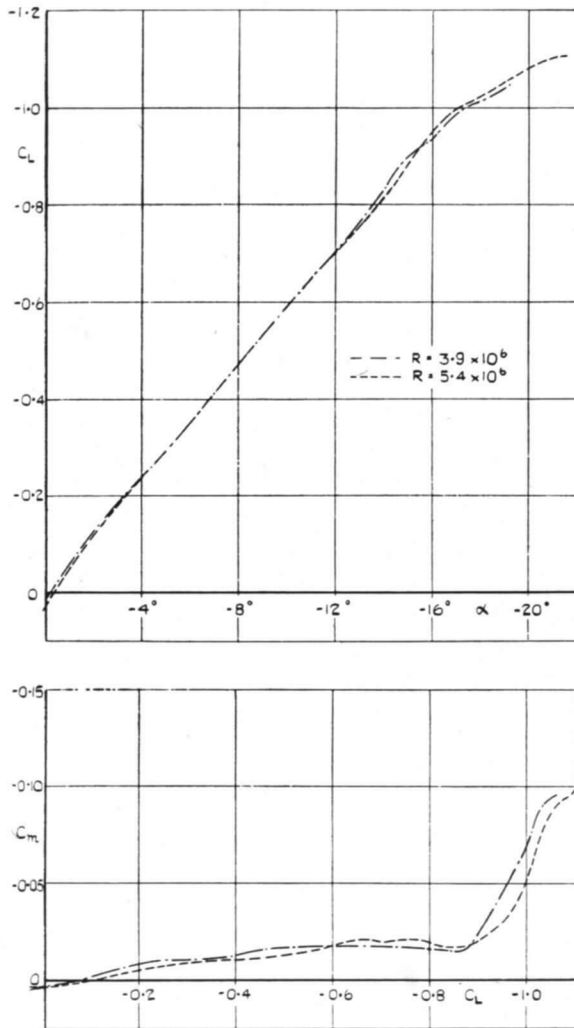


FIG. 11. C_L vs. α and C_m vs. C_L .
Effect of Reynolds number at $M = 0.18$.
Wing C. Negative incidences.

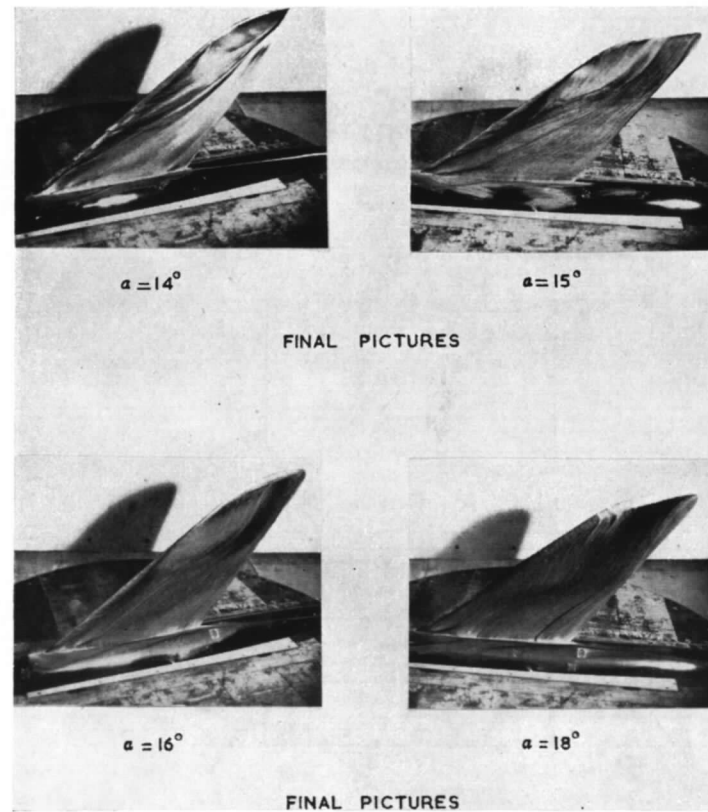
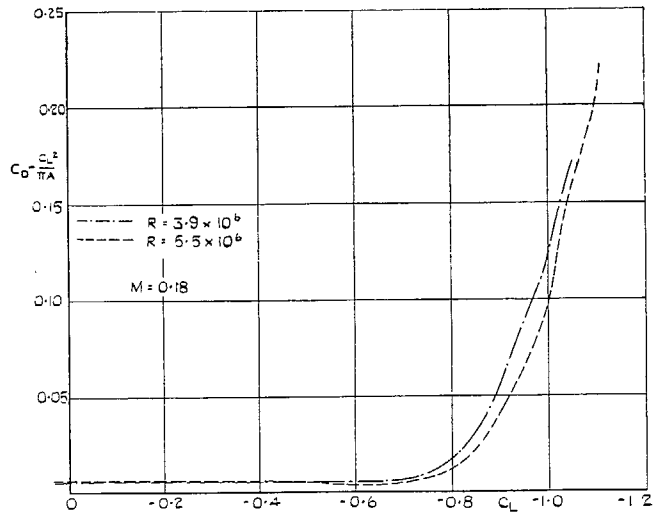
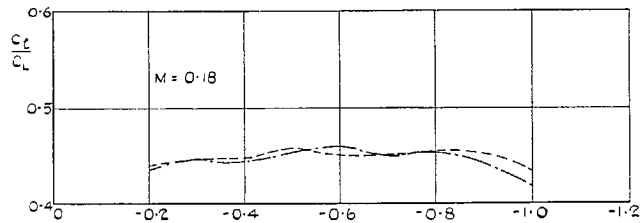


FIG. 12. Flow patterns. Wing C. $R = 6 \times 10^6$.



(a) VARIATION OF $C_D - \frac{C_L^2}{\pi A}$ WITH C_L



(b) SPANWISE CENTRE OF LOAD VS. C_L

FIGS. 13a and 13b. Effect of Reynolds number on the variation of $C_D - (C_L^2/\pi A)$ and spanwise centre of load with C_L . Wing C. Negative incidences.

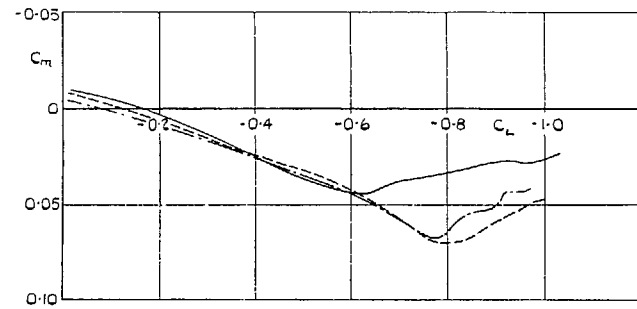
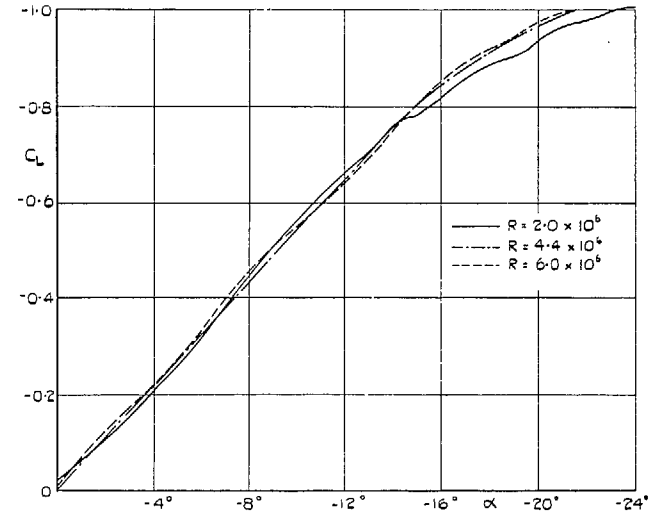
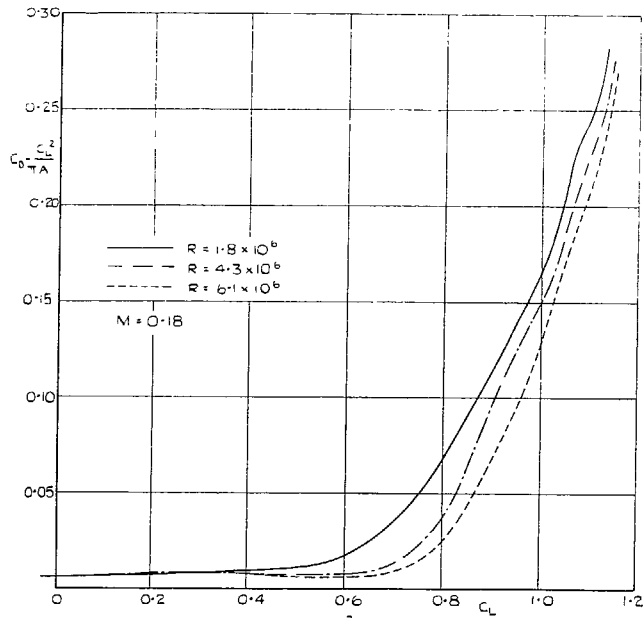
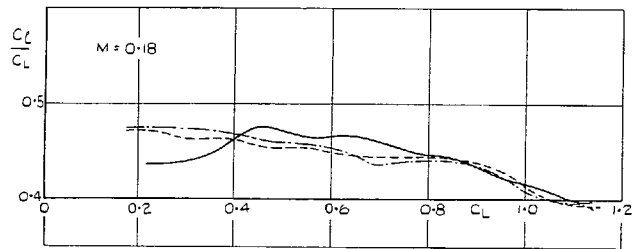


FIG. 14. C_L vs. α and C_m vs. C_L . Effect of Reynolds number at $M = 0.18$. Wing C with body attached.



(a) VARIATION OF $C_D - \frac{C_L^2}{\pi A}$ WITH C_L



(b) SPANWISE CENTRE OF LOAD vs C_L

FIGS. 15a and 15b. Effect of Reynolds number on the variation of $C_D - \frac{C_L^2}{\pi A}$ and spanwise centre of load with C_L . Wing C with body attached.

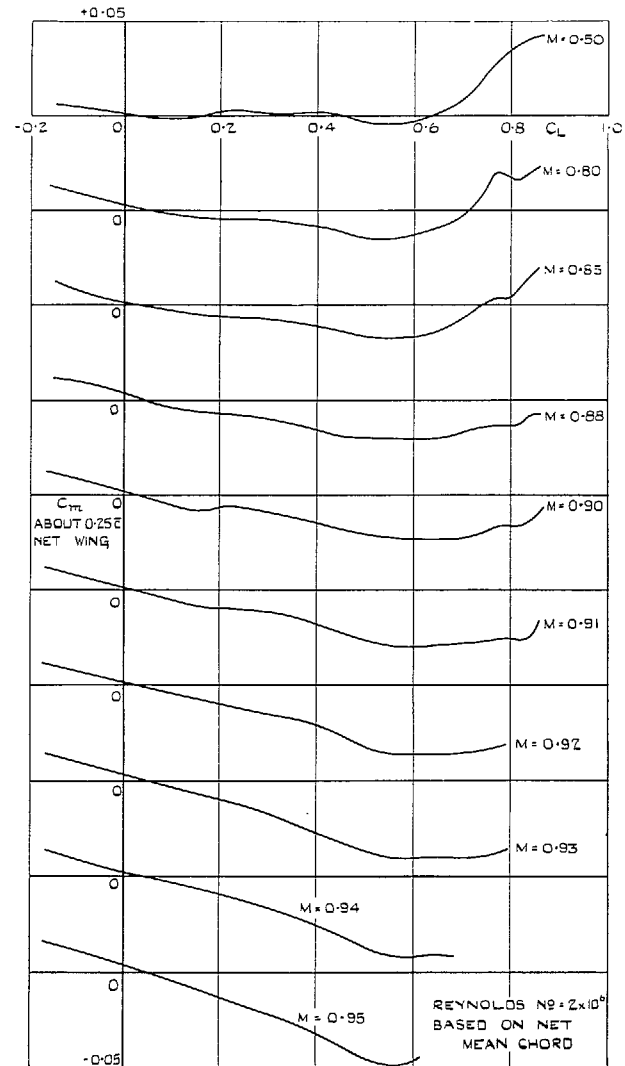


FIG. 16. $C_m \sim C_L$ for wing A.

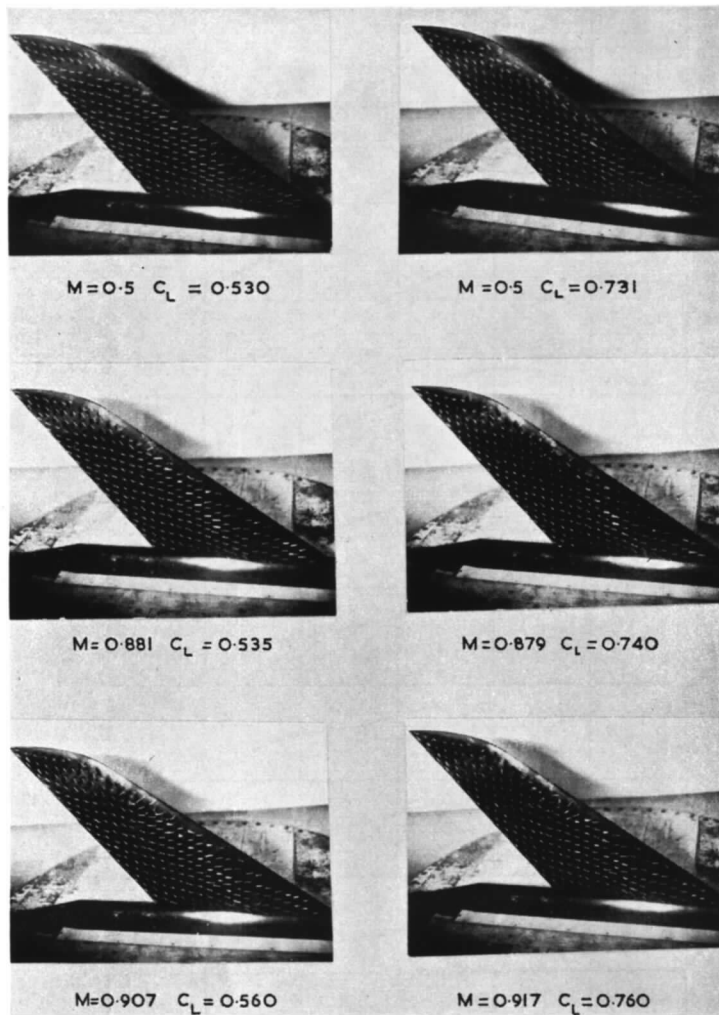


FIG. 17a. Tuft photographs for wing A. $R = 2 \times 10^6$.

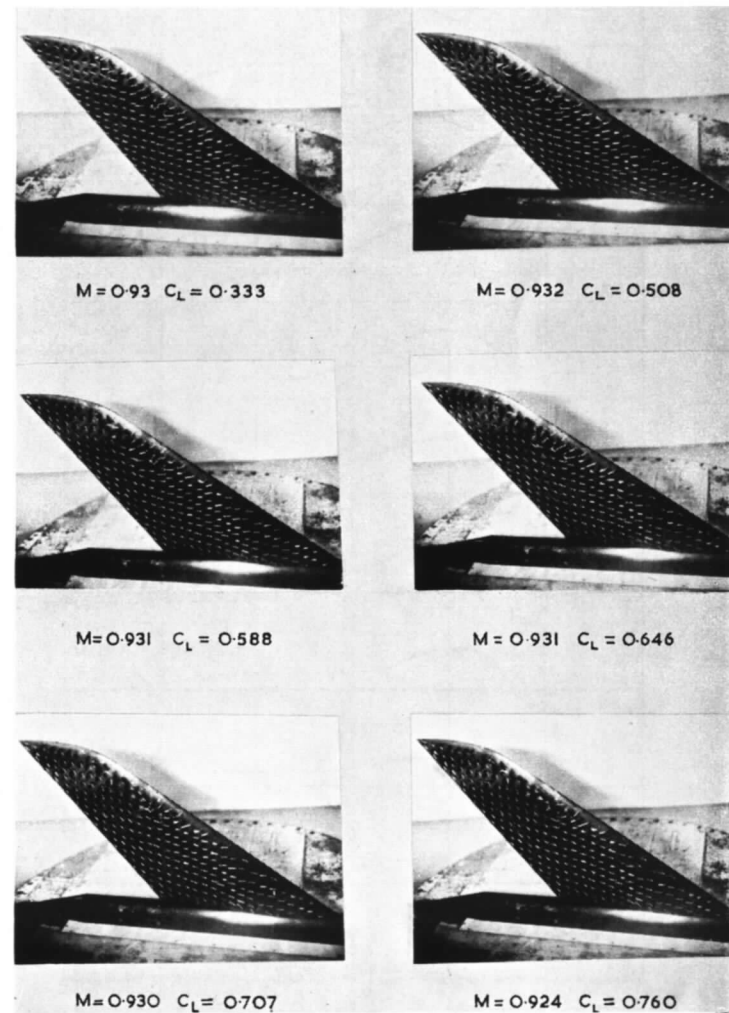


FIG. 17b. Tuft photographs for wing A—*continued*. $R = 2 \times 10^6$.

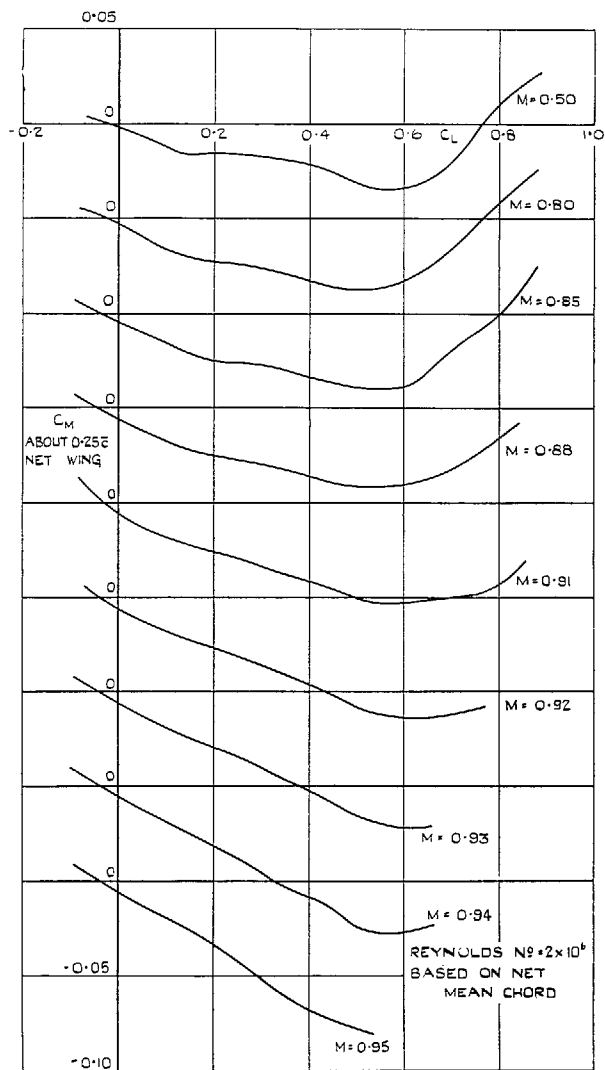


FIG. 18. C_M vs. C_L for wing B.

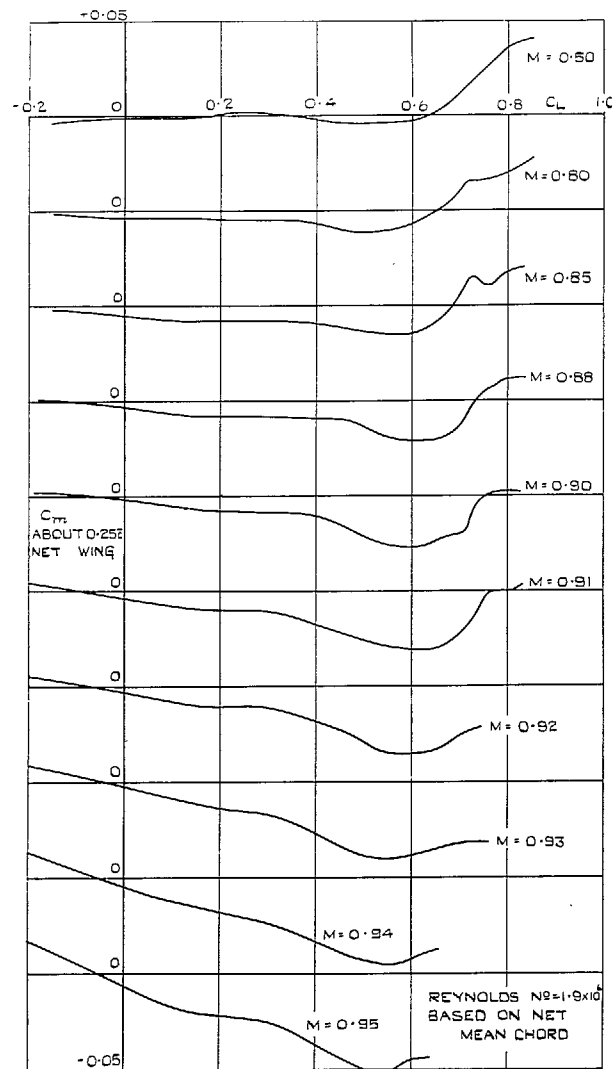


FIG. 19. C_m vs. C_L for wing C.

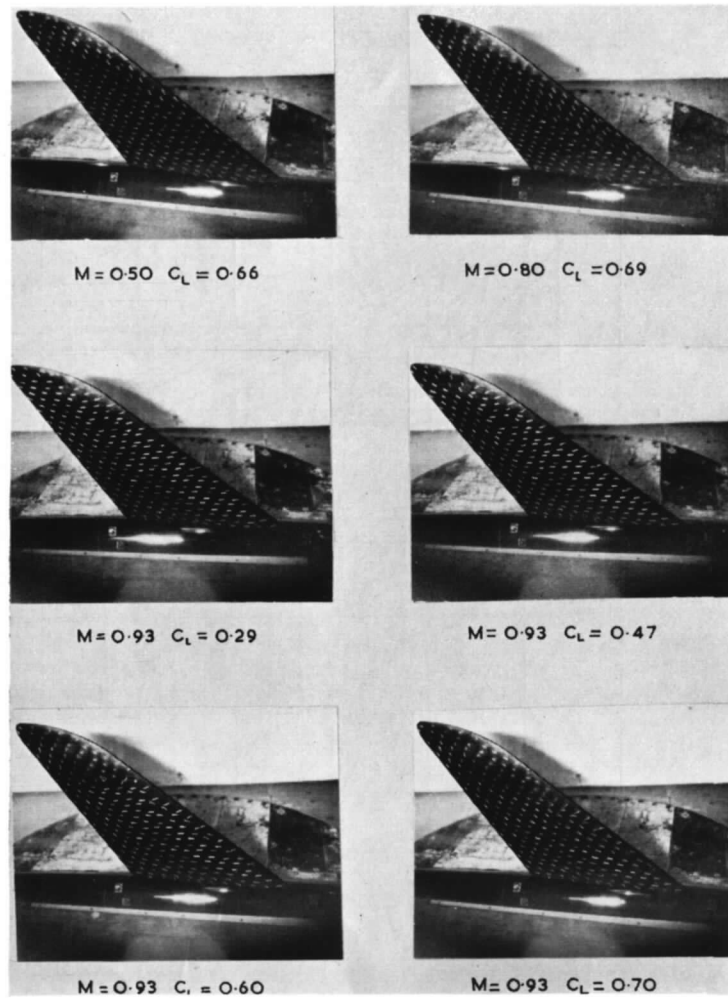


FIG. 20. Tuft photographs for wing C. $R = 2 \times 10^6$.

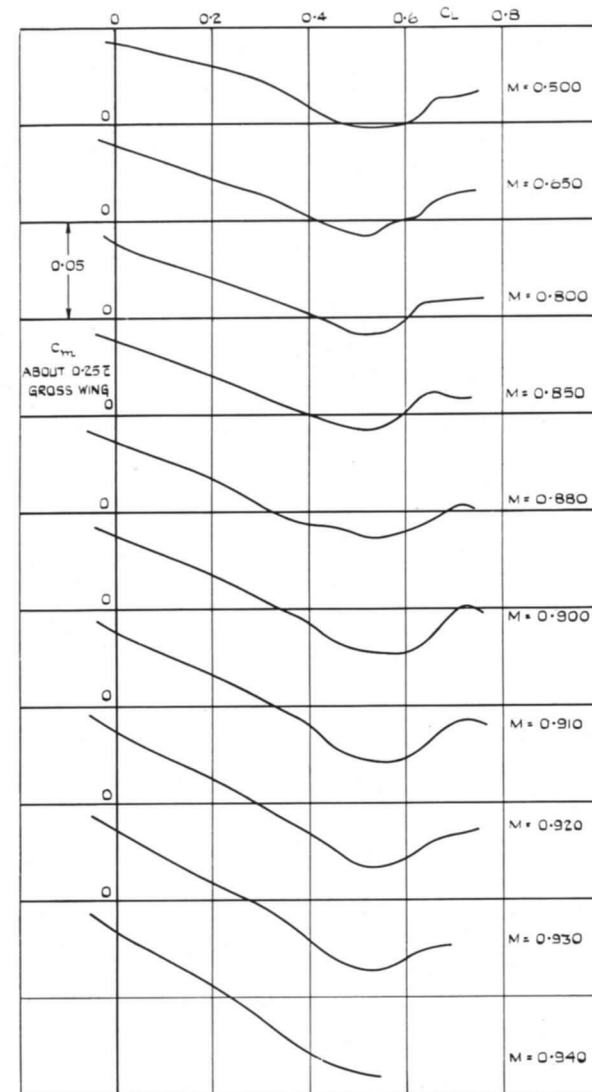


FIG. 21. C_m vs. C_L for wing C with body attached.

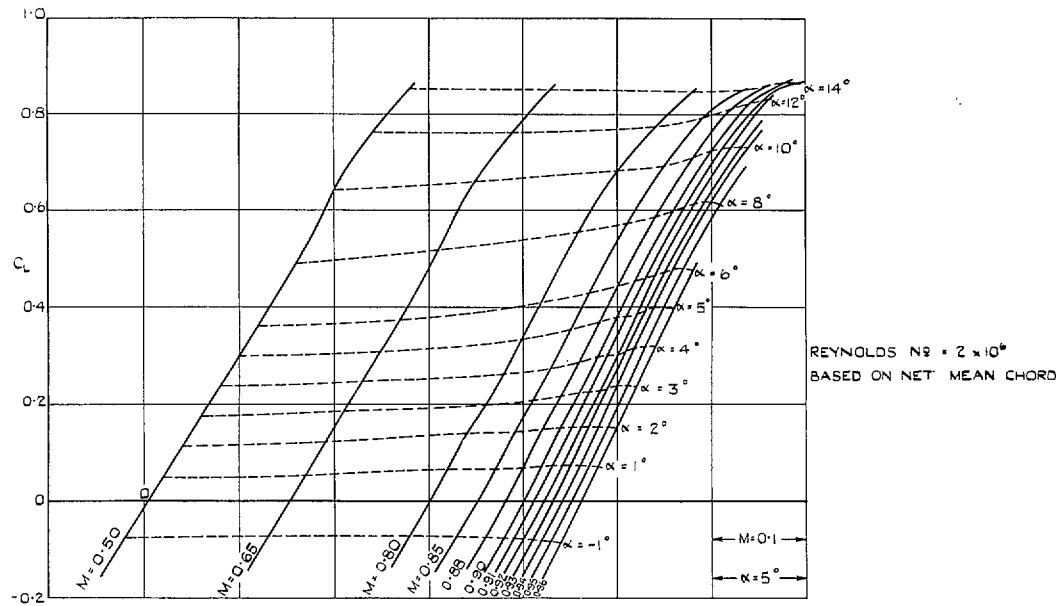


FIG. 22. Lift carpet for wing A.

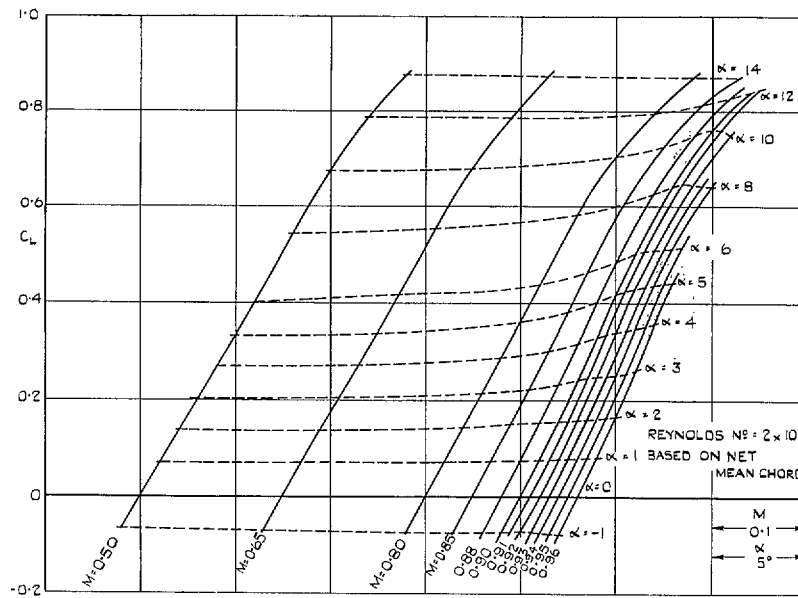


FIG. 23. Lift carpet for wing B.

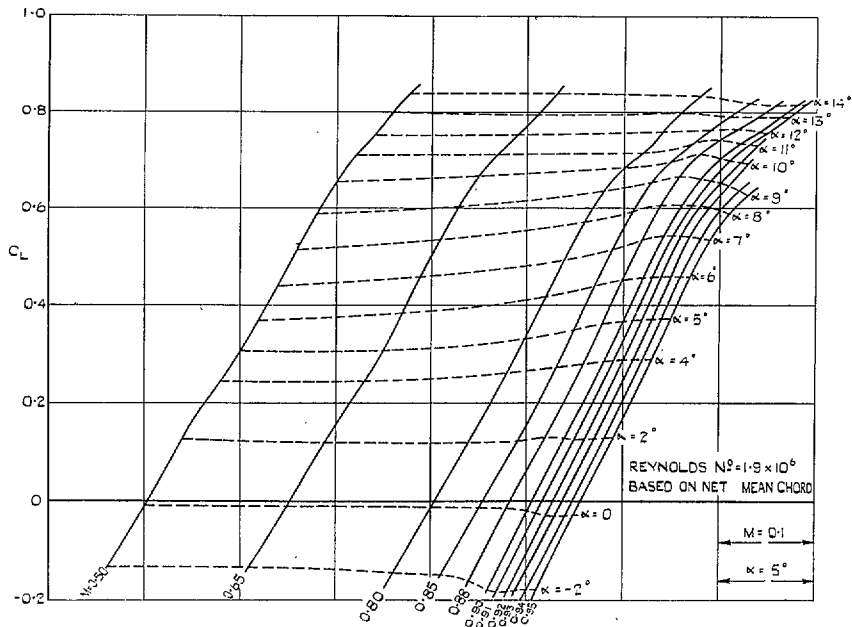


FIG. 24. Lift carpet for wing C.

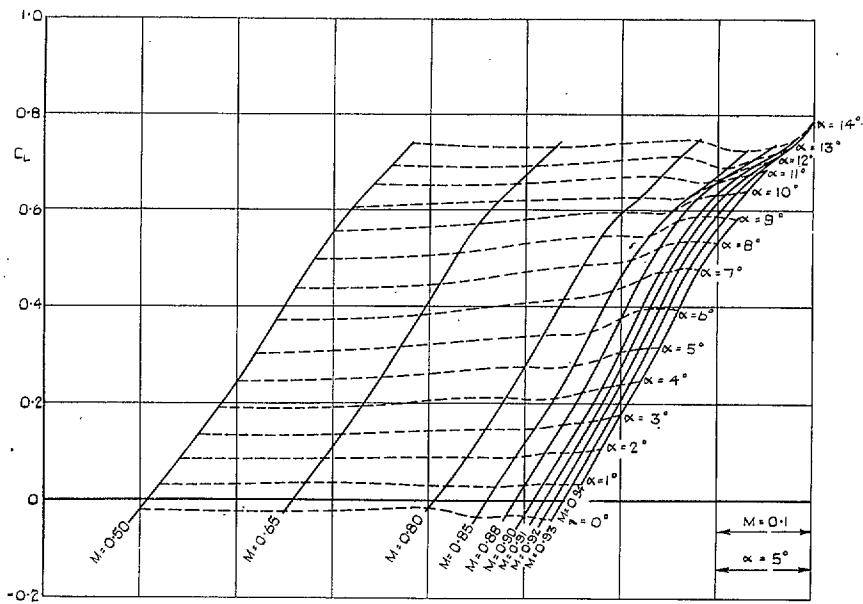


FIG. 25. Lift carpet for wing C with body attached.

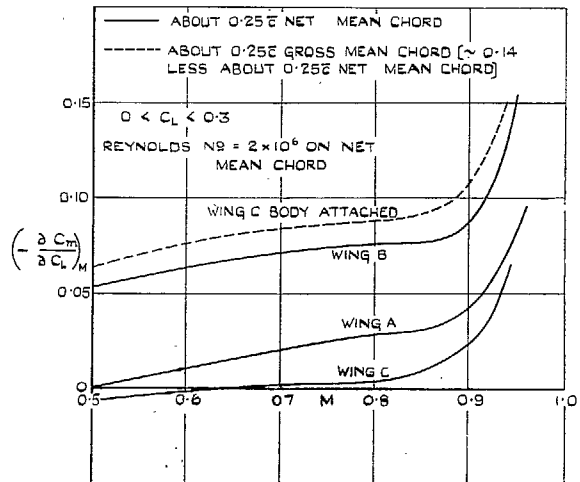
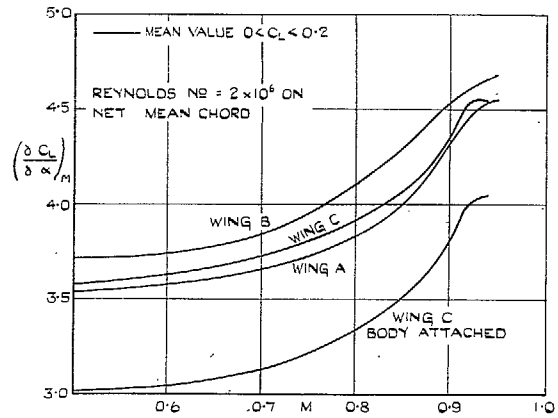


FIG. 26. Variation of $(\partial C_L / \partial \alpha)_M$ and $(-\partial C_m / \partial C_L)_M$ with Mach number wings A, B, and C.

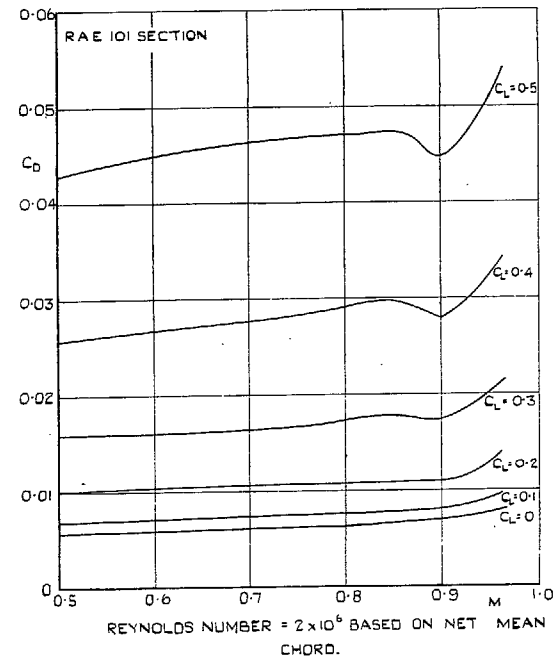


FIG. 27. Variation of C_D with M at constant C_L for wing A.

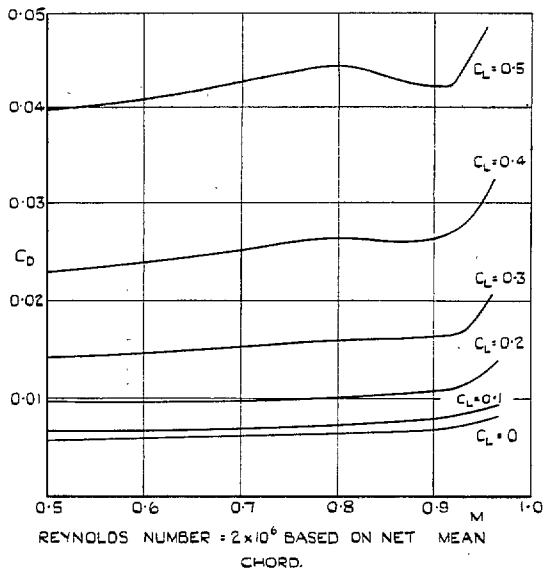


FIG. 28. Variation of C_D with M at constant C_L for wing B.

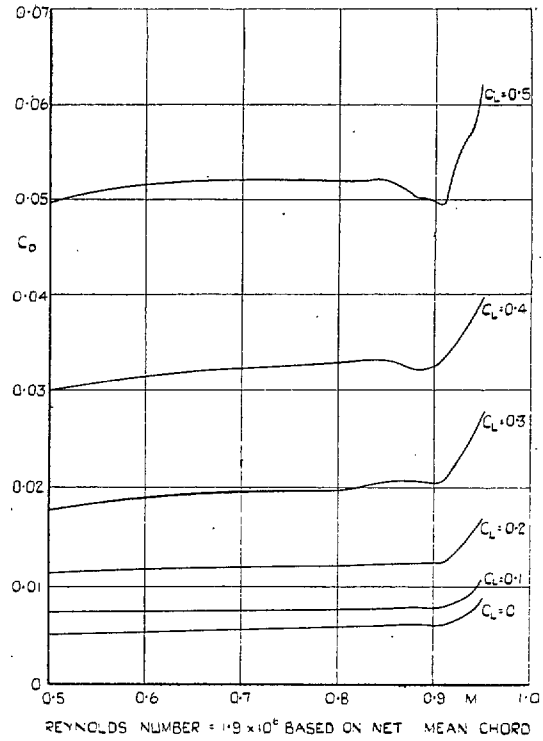


FIG. 29. Variation of C_D with M at constant C_L for wing C.

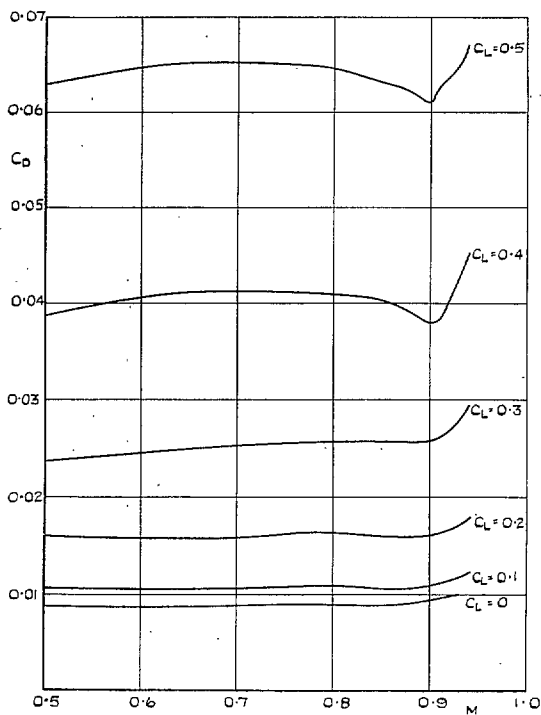


FIG. 30. Variation of C_D with M at constant C_L . Wing C with body attached.

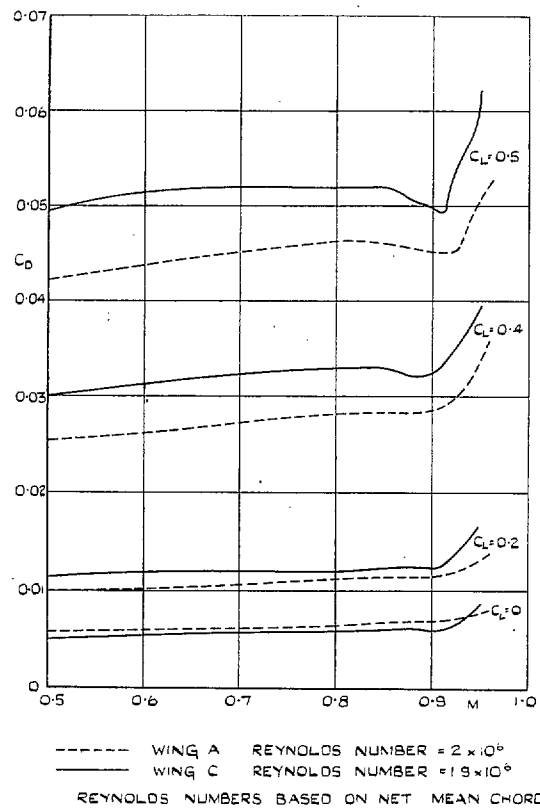
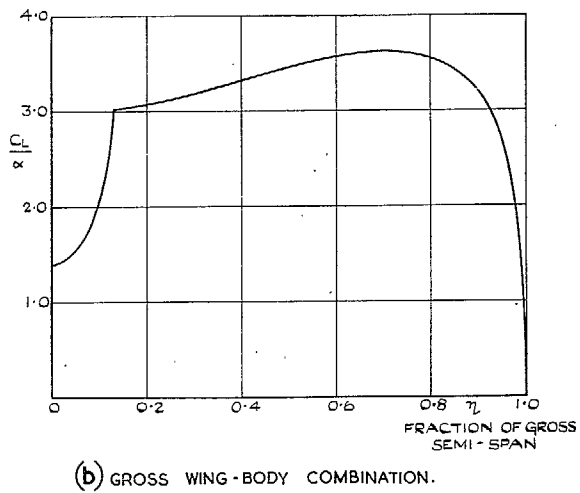
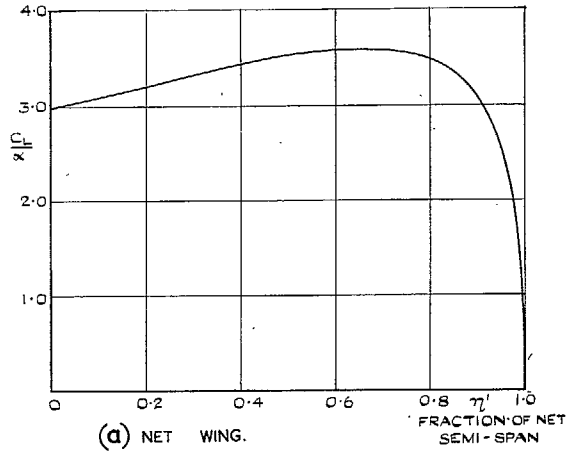


FIG. 31. Comparison of C_D for wings A and C at several values of C_L .



FIGS. 32a and 32b.
Estimated span loading for $M = 0$. Wing C.

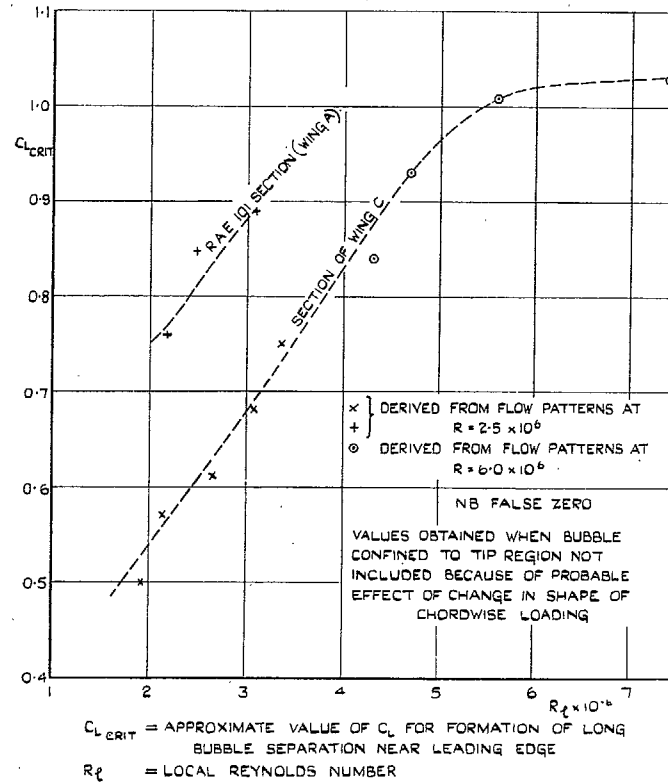


FIG. 33.
Effect of Reynolds number on formation of long bubble.

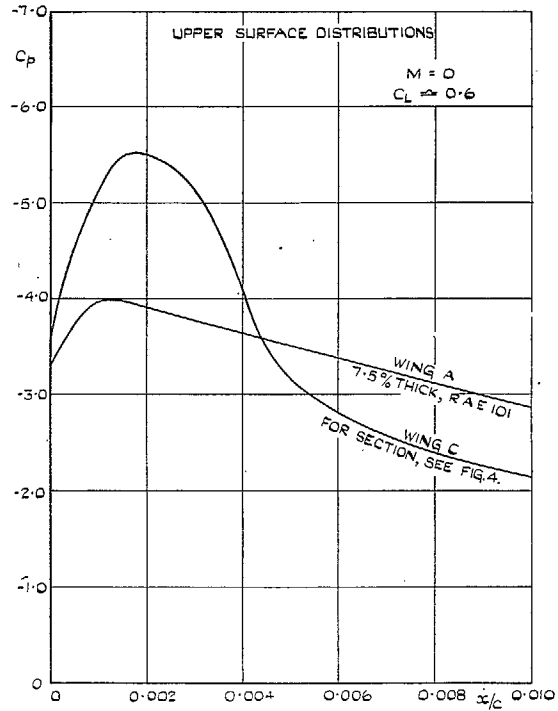


FIG. 34. Comparison of pressure distributions near leading edge for two shapes.

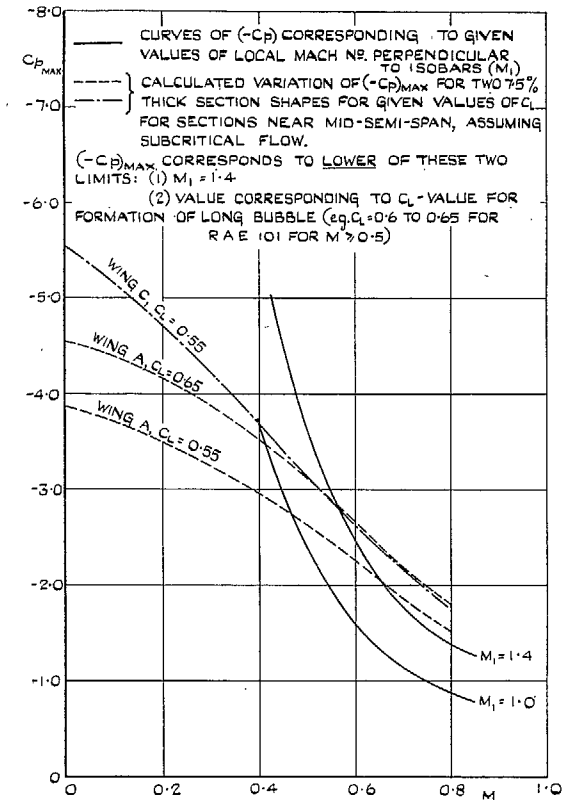


FIG. 35. Diagram illustrating values of $(-C_p)_{max}$ attainable near leading edge.

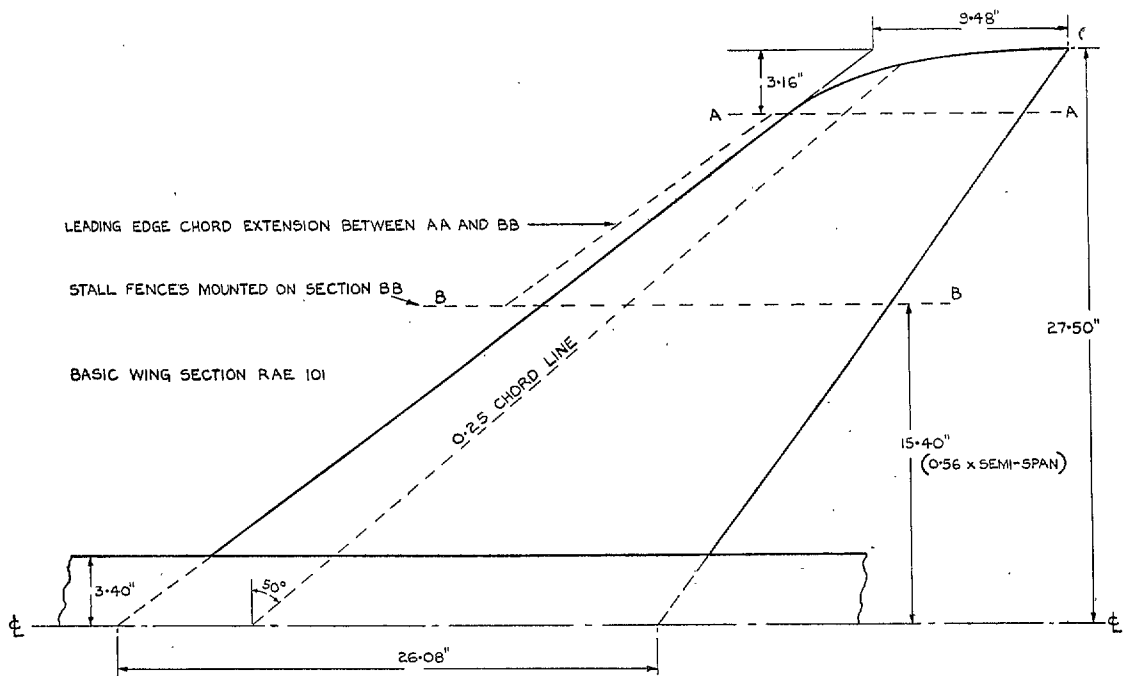


FIG. 36. Plan-form of wing showing position of stall fences and of extended leading edge.

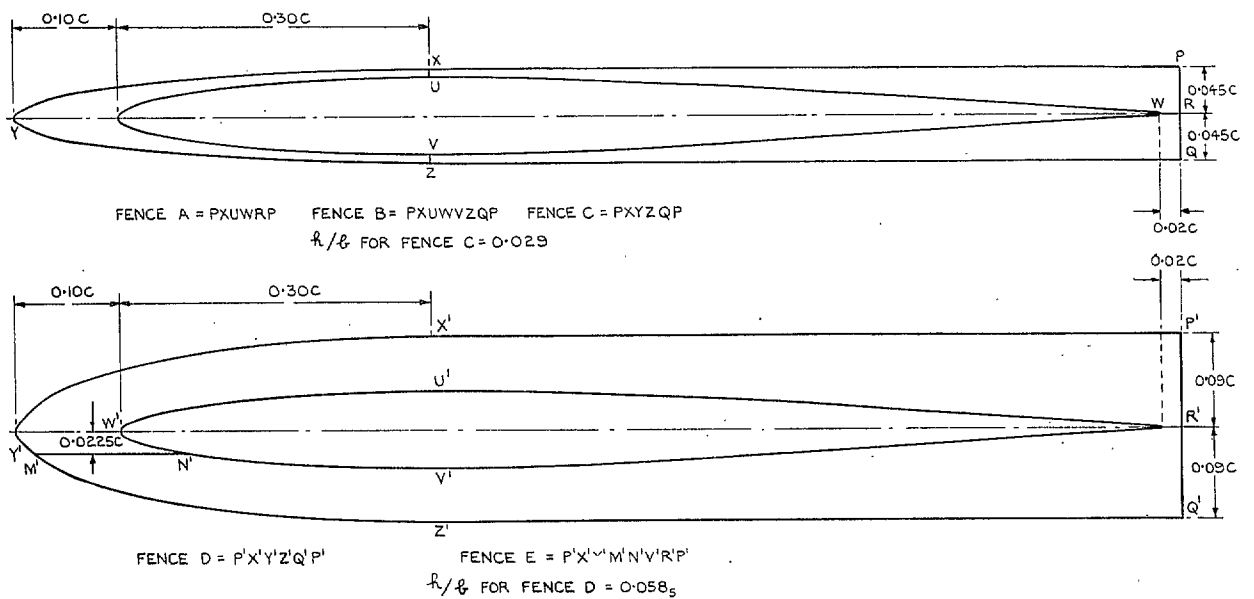
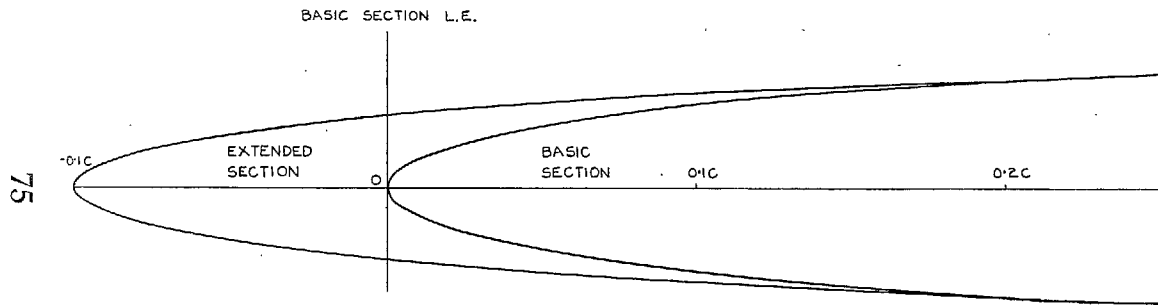
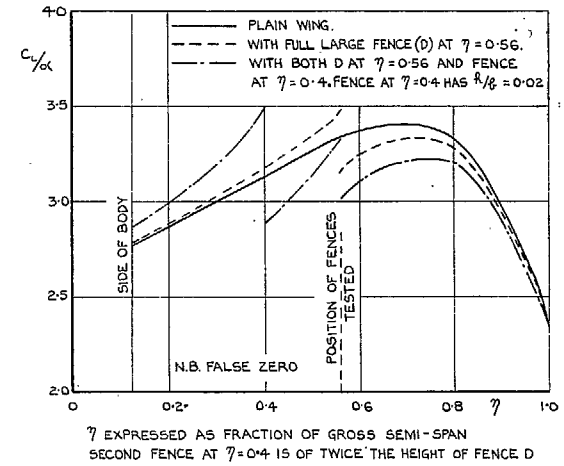


FIG. 37. Stall fences fitted on wing at 0.56 semi-span.

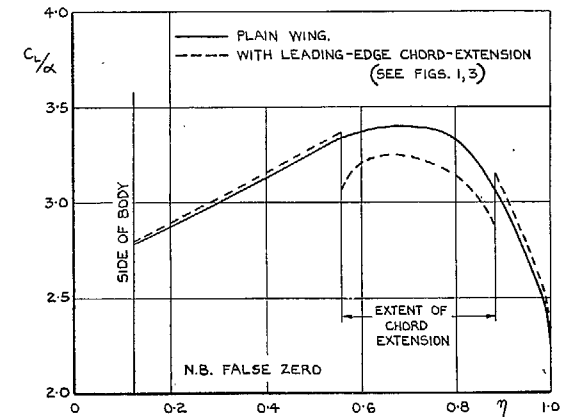


0.1c EXTENSION OF CHORD . BASIC SECTION UNALTERED AFT OF 0.20c
 L.E. RADIUS OF EXTENDED SECTION = 0.0028 x NEW WING CHORD OR 0.0031 x ORIGINAL CHORD

FIG. 38. Leading-edge chord extension
 (Applied between sections AA and BB (see Fig. 36)).



(a) ESTIMATED EFFECT OF FENCES.



(b) EFFECT OF LEADING-EDGE CHORD EXTENSION.

Figs. 39a and 39b.
 Spanwise lift distribution at low Mach number.

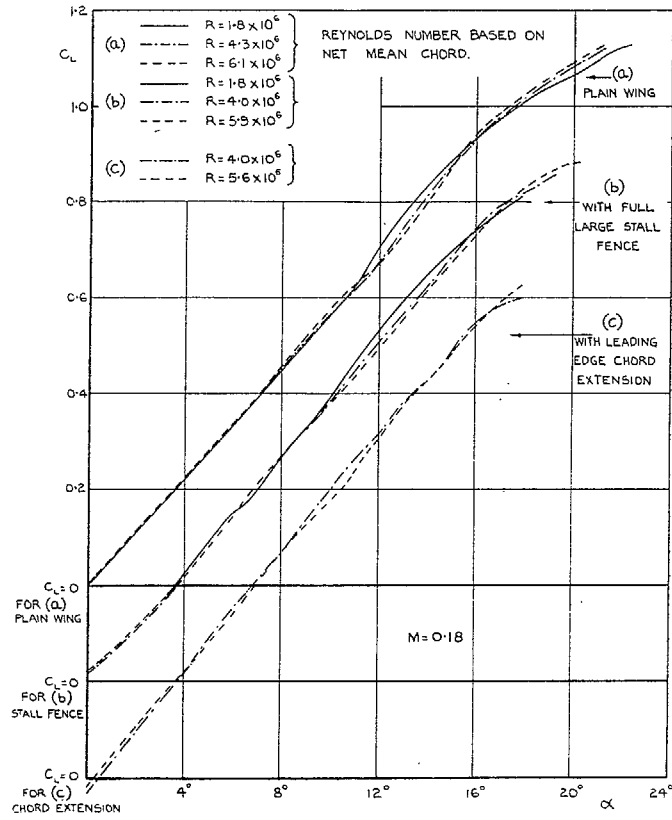


FIG. 40. C_L vs. α at low Mach number. Effect of Reynolds number.

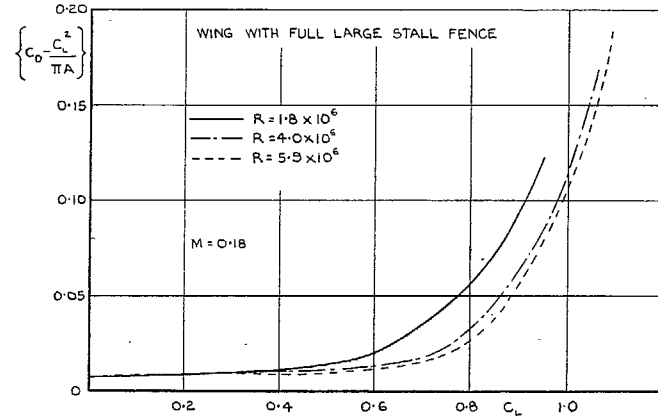
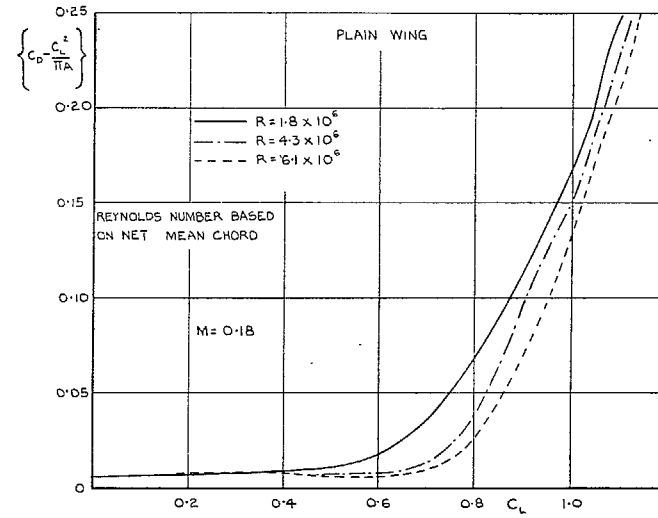


FIG. 41a. $\{C_D - (C_L^2/\pi A)\}$ vs. C_L at low Mach number. Effect of Reynolds number.

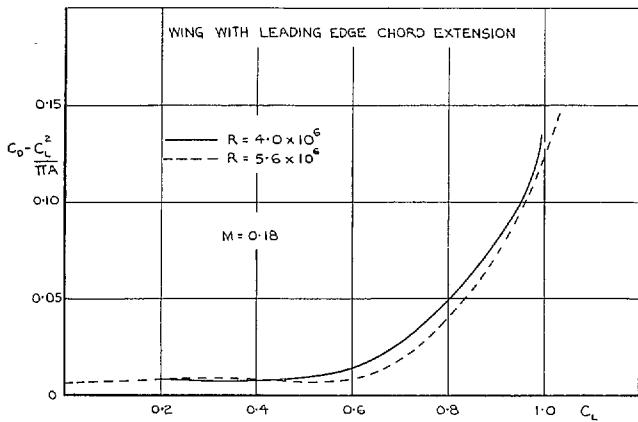


FIG. 41b. $\{C_D - (C_L^2/\pi A)\}$ vs. C_L at low Mach number. Effect of Reynolds number.

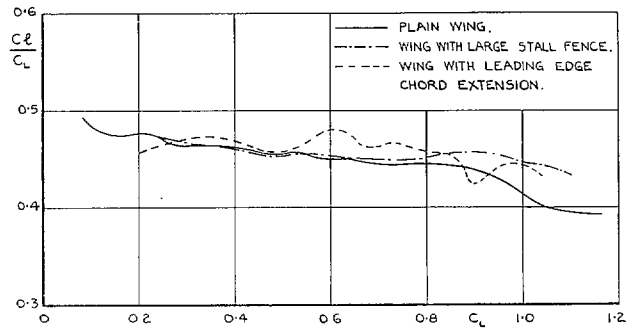


FIG. 42. Spanwise centre of load at $M = 0.18$, $R \approx 6 \times 10^6$. Effect of various devices.

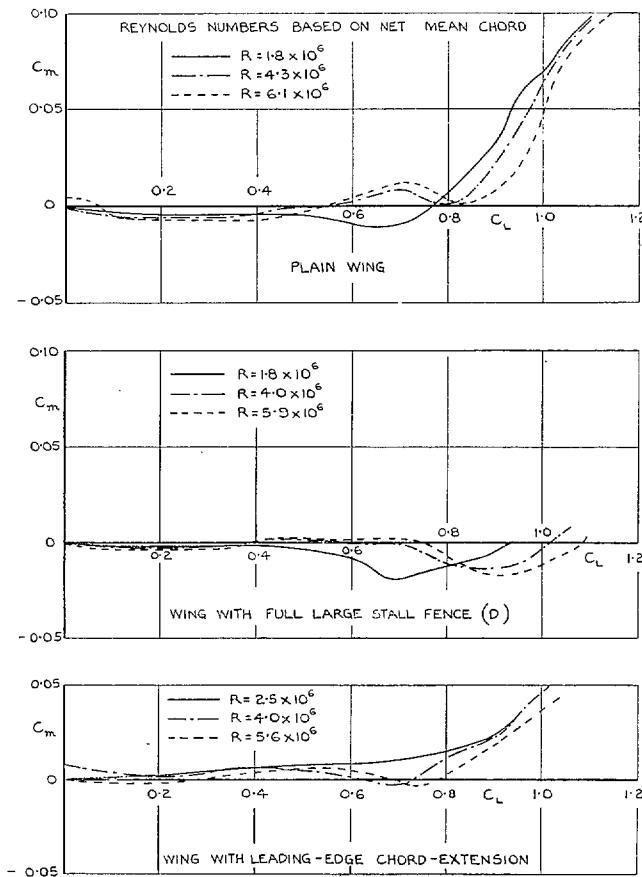


FIG. 43. C_m vs. C_L at $M = 0.18$. Effect of fence and chord extension.

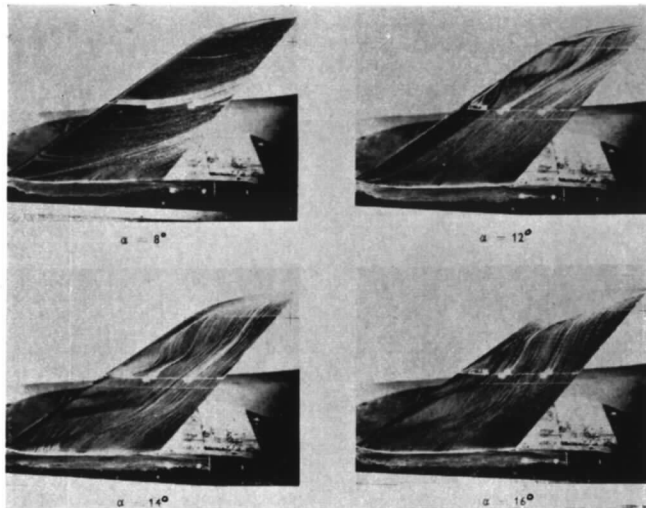


FIG. 44. Flow patterns for plain wing.
 $R = 2.5 \times 10^6$, $M = 0.2$.

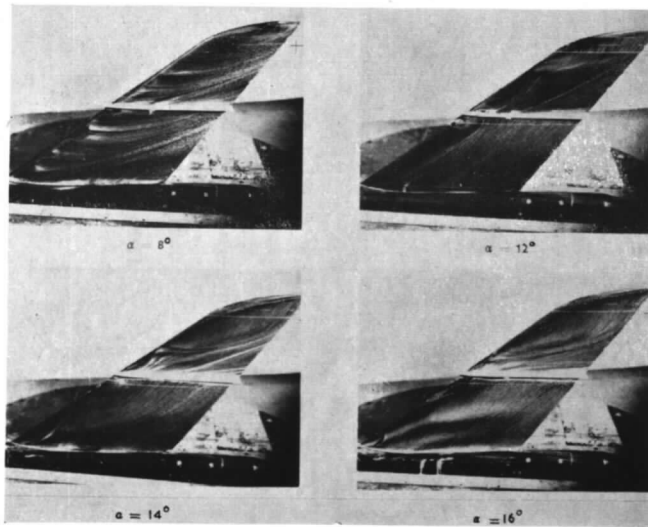


FIG. 45. Flow patterns for wing with stall fences.
 $R = 2.5 \times 10^6$, $M = 0.2$.

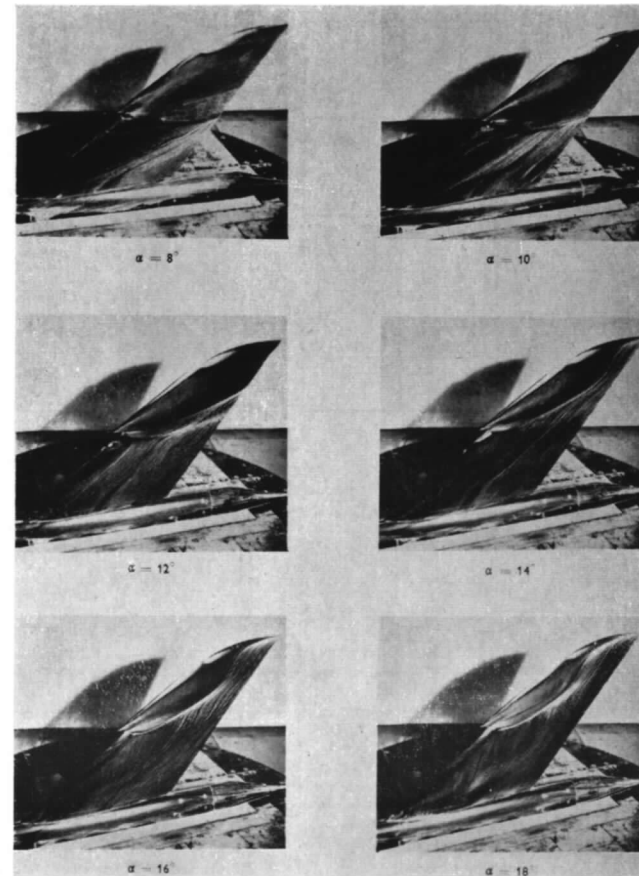


FIG. 46. Flow patterns for wing with leading-edge chord extension.
 $R = 2.5 \times 10^6$, $M = 0.2$.

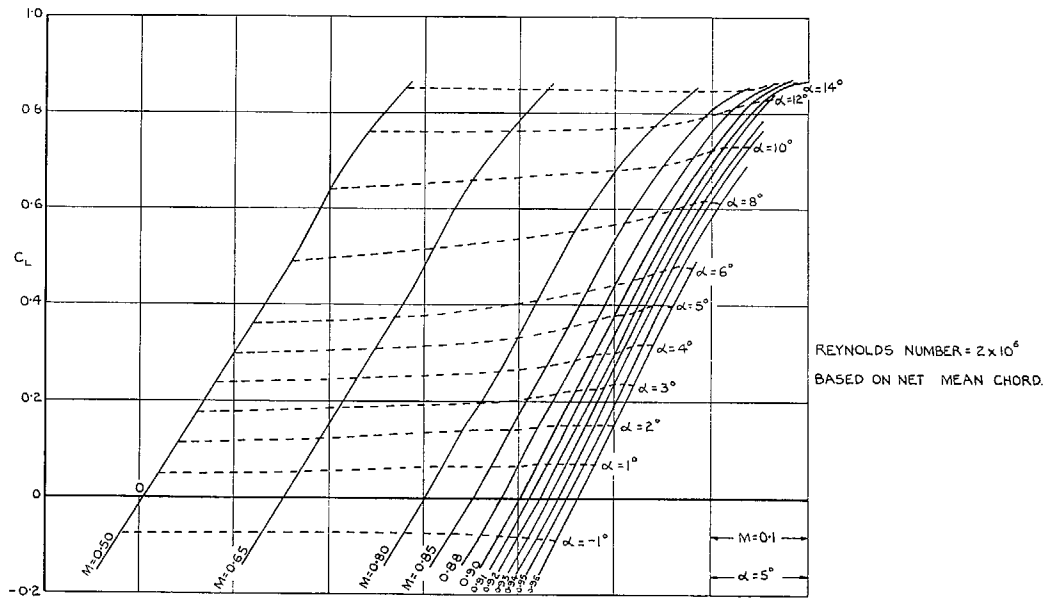


FIG. 47. Lift carpet for plain wing.

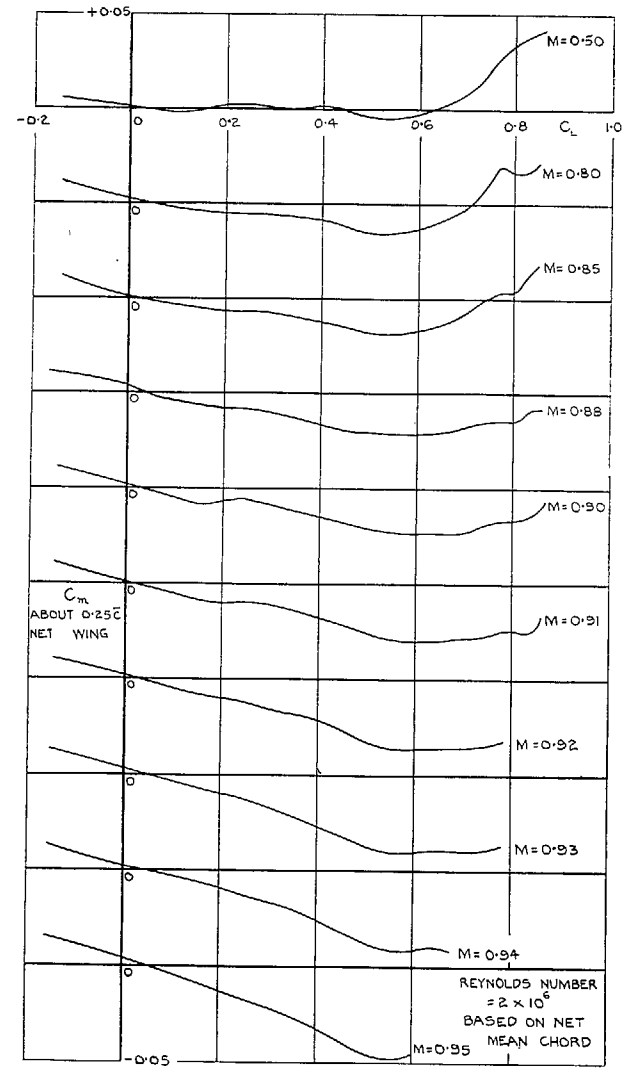


FIG. 48. C_m vs. C_L for plain wing.

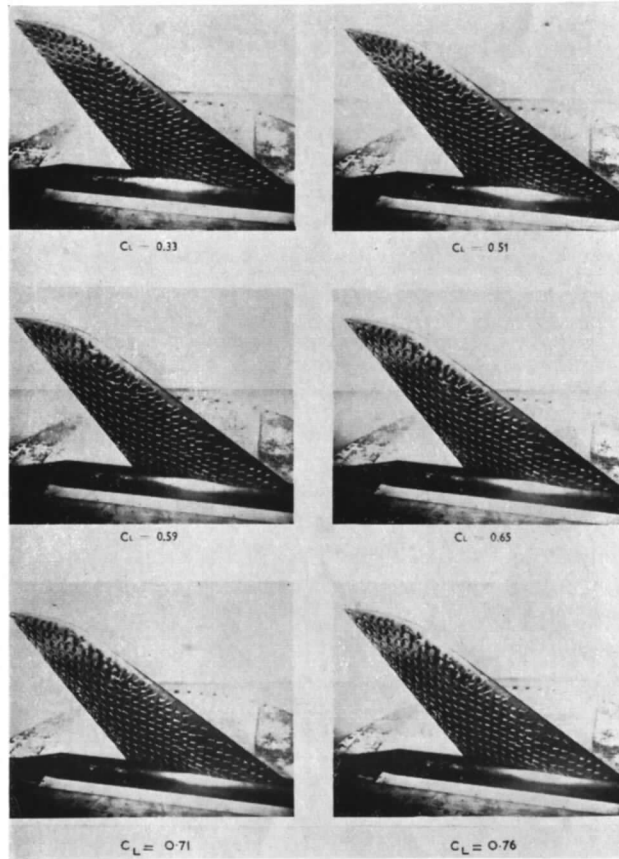


FIG. 49. Tuft photographs for plain wing. $M = 0.93$.

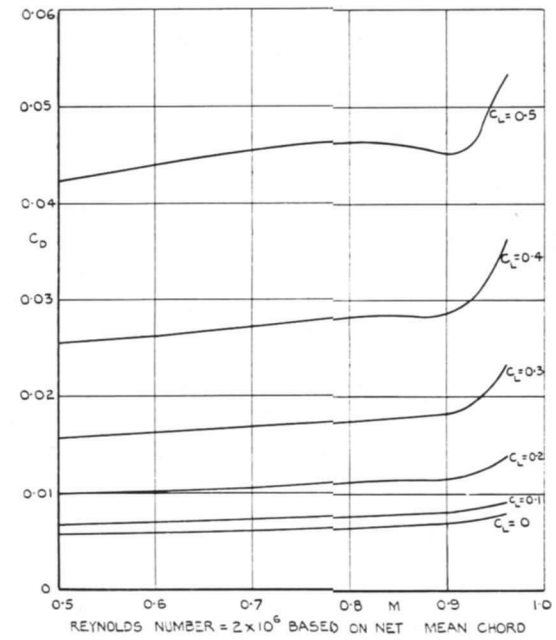


FIG. 50. Variation of C_D with M at constant C_L for plain wing.

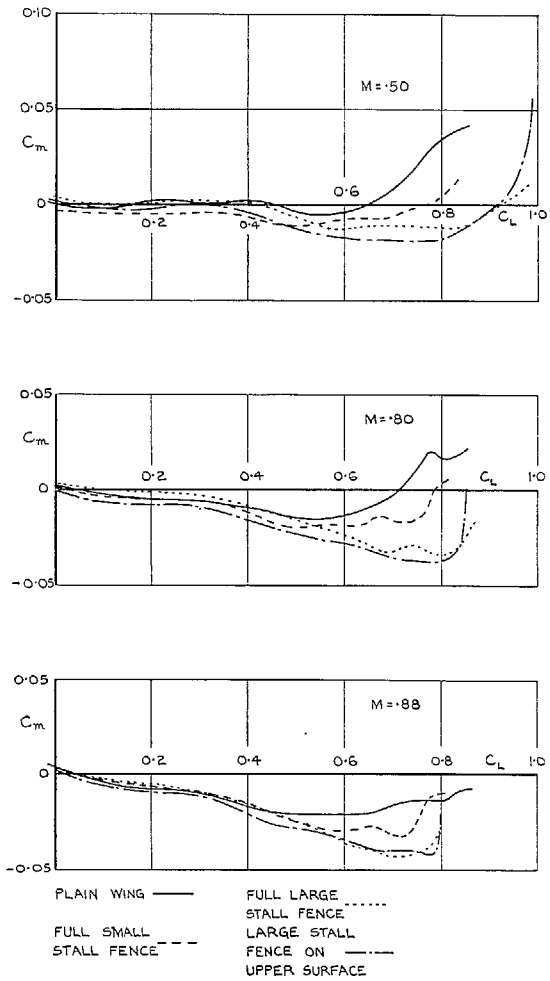


FIG. 51a. C_m vs. C_L at various Mach numbers. Effect of stall fences.

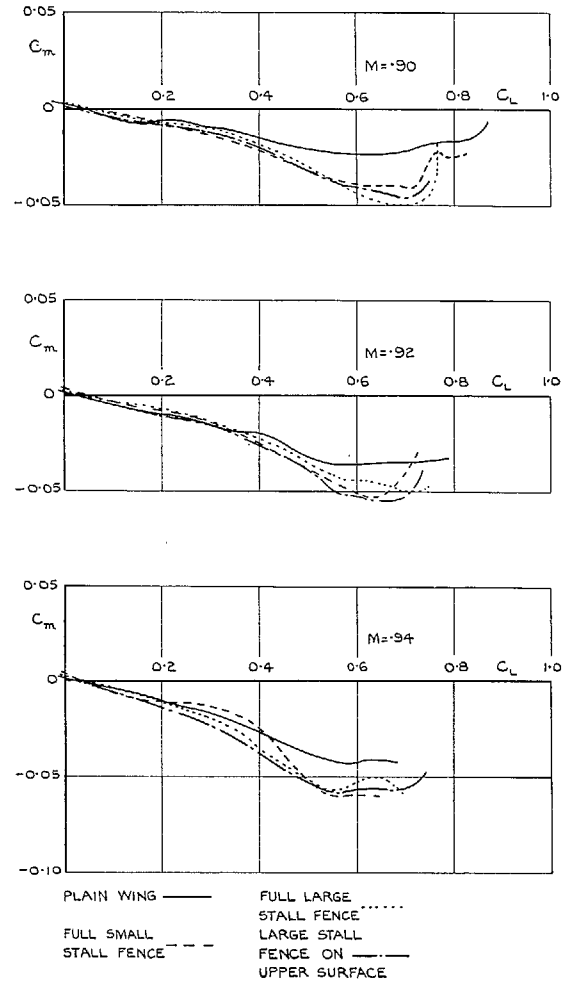


FIG. 51b. C_m vs. C_L at various Mach numbers. Effect of stall fences.

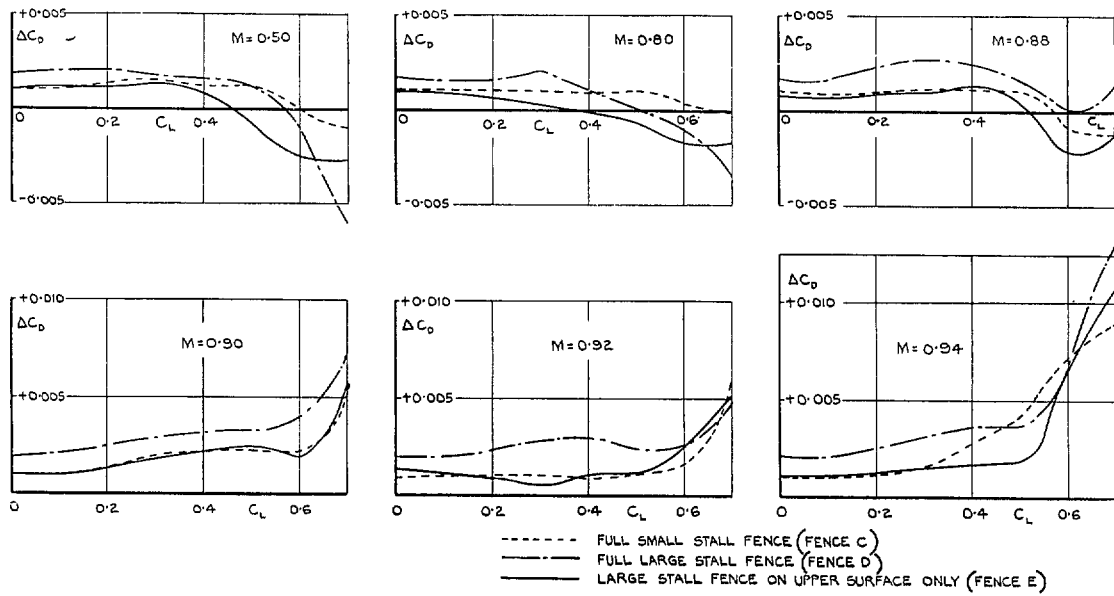
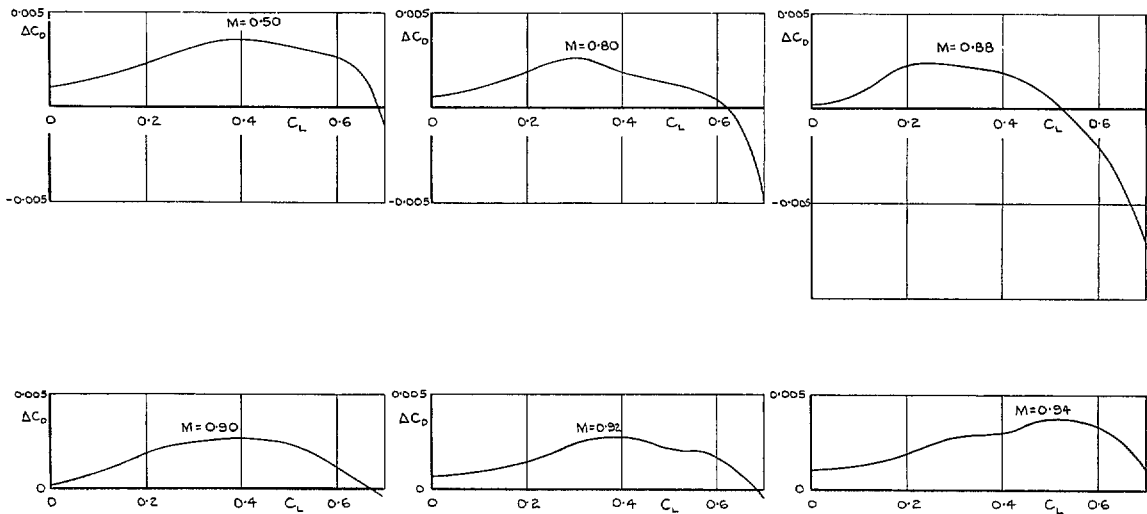
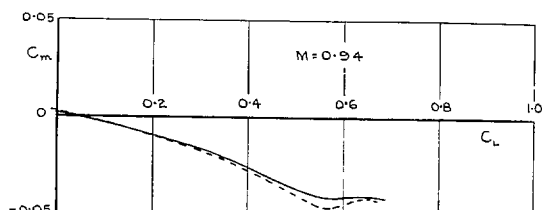
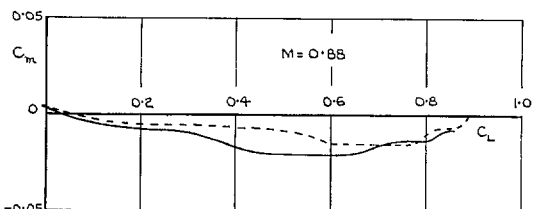
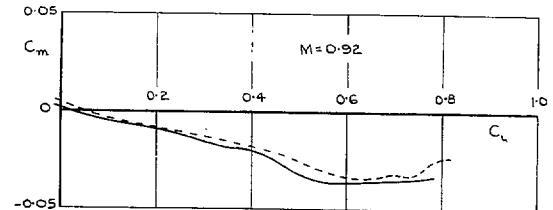
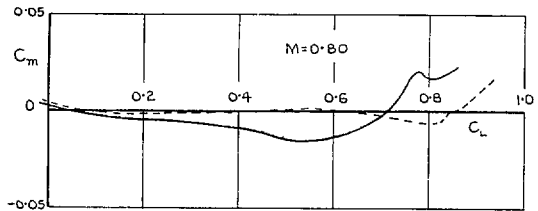
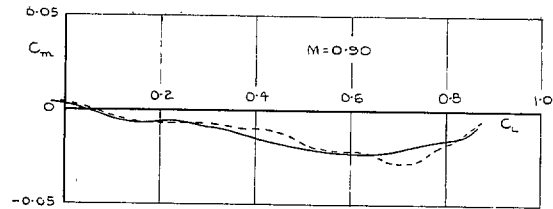
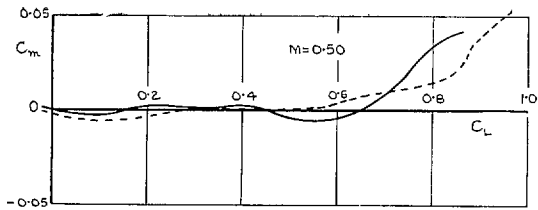


FIG. 52. Increments in C_D due to various stall fences. Variation with C_L at several Mach numbers.



N.B. C_D FOR WING WITH CHORD EXTENSION BASED ON AREA OF ORIGINAL WING.

FIG. 53. Increments in C_D due to leading-edge chord extension. Variation with C_L at several Mach numbers.

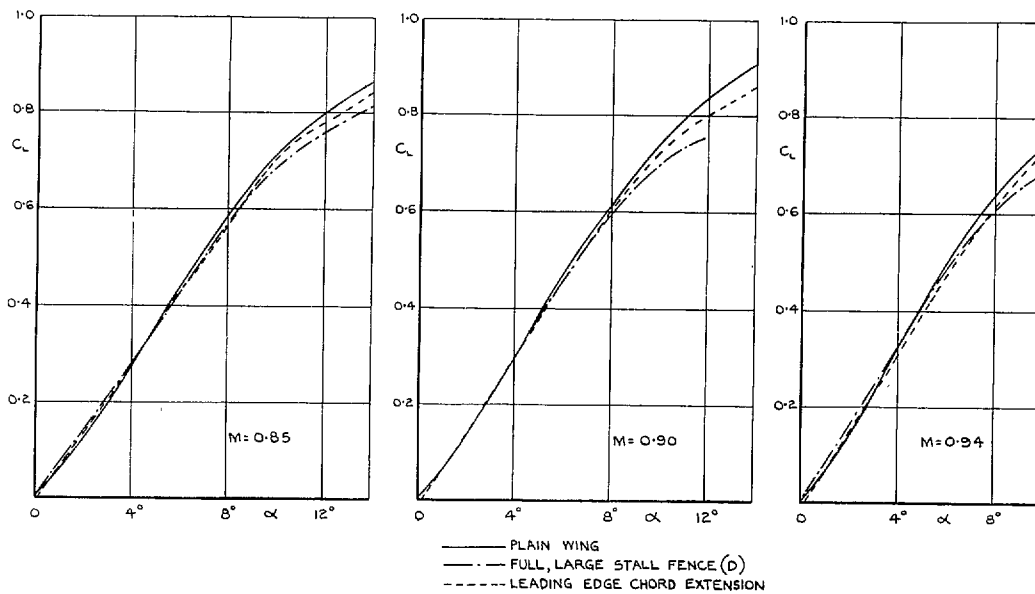


— PLAIN WING
- - - WING WITH CHORD EXTENSION

— PLAIN WING
- - - WING WITH CHORD EXTENSION

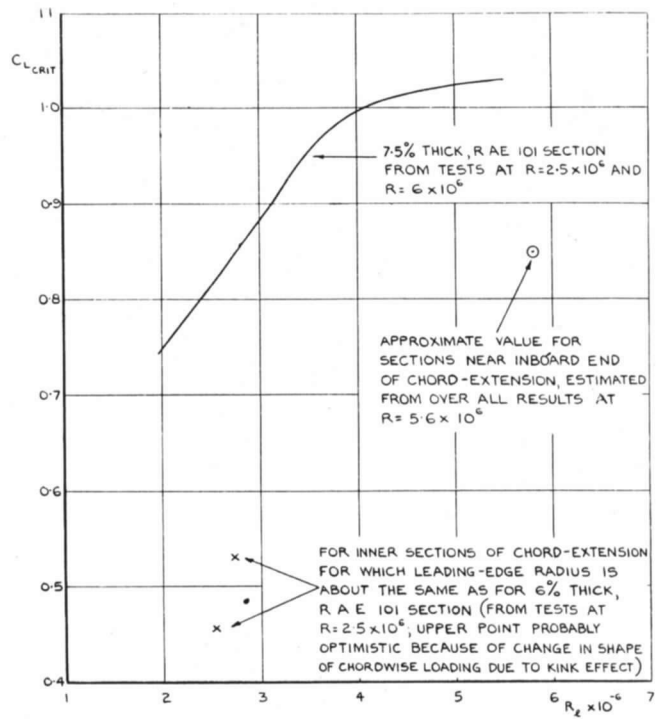
FIG. 54a. C_m vs. C_L at various Mach numbers. Effect of leading-edge chord extensions.

FIG. 54b. C_m vs. C_L at various Mach numbers. Effect of leading-edge chord extension.



— PLAIN WING
- - - FULL, LARGE STALL FENCE (D)
· · · LEADING EDGE CHORD EXTENSION

FIG. 55. Effect of stall fence and chord extension on C_L vs. α at high Mach number.



$C_{L,crit}$ = APPROXIMATE VALUE OF C_L AT WHICH A LONG SEPARATION-BUBBLE FIRST FORMS NEAR LEADING EDGE.
 R_x = LOCAL REYNOLDS NUMBER.

FIG. 56. Effect of Reynolds number on formation of 'long' separation bubble.

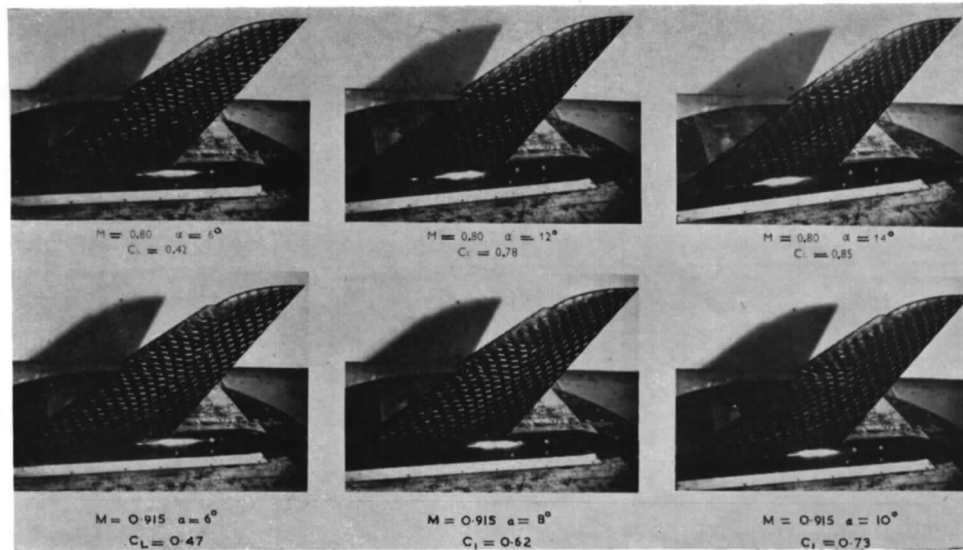


FIG. 57. Photographs of tufts on wing with leading-edge chord extension.

Publication of the Aeronautical Research Council

ANNUAL TECHNICAL REPORTS OF THE AERONAUTICAL RESEARCH COUNCIL (BOUND VOLUMES)

- 1939 Vol. I. Aerodynamics General, Performance, Airscrews, Engines. 50s. (51s. 9d.).
Vol. II. Stability and Control, Flutter and Vibration, Instruments, Structures, Sea-planes, etc. 63s. (64s. 9d.)
- 1940 Aero and Hydrodynamics, Aerofoils, Airscrews, Engines, Flutter, Icing, Stability and Control Structures, and a miscellaneous section. 50s. (51s. 9d.)
- 1941 Aero and Hydrodynamics, Aerofoils, Airscrews, Engines, Flutter, Stability and Control Structures. 63s. (64s. 9d.)
- 1942 Vol. I. Aero and Hydrodynamics, Aerofoils, Airscrews, Engines. 75s. (76s. 9d.)
Vol. II. Noise, Parachutes, Stability and Control, Structures, Vibration, Wind Tunnels. 47s. 6d. (49s. 3d.)
- 1943 Vol. I. Aerodynamics, Aerofoils, Airscrews. 80s. (81s. 9d.)
Vol. II. Engines, Flutter, Materials, Parachutes, Performance, Stability and Control, Structures. 90s. (92s. 6d.)
- 1944 Vol. I. Aero and Hydrodynamics, Aerofoils, Aircraft, Airscrews, Controls. 84s. (86s. 3d.)
Vol. II. Flutter and Vibration, Materials, Miscellaneous, Navigation, Parachutes, Performance, Plates and Panels, Stability, Structures, Test Equipment, Wind Tunnels. 84s. (86s. 3d.)
- 1945 Vol. I. Aero and Hydrodynamics, Aerofoils. 130s. (132s. 6d.)
Vol. II. Aircraft, Airscrews, Controls. 130s. (132s. 6d.)
Vol. III. Flutter and Vibration, Instruments, Miscellaneous, Parachutes, Plates and Panels, Propulsion. 130s. (132s. 3d.)
Vol. IV. Stability, Structures, Wind Tunnels, Wind Tunnel Technique. 130s. (132s. 3d.)

Annual Reports of the Aeronautical Research Council—

1937 2s. (2s. 2d.) 1938 1s. 6d. (1s. 8d.) 1939-48 3s. (3s. 3d.)

Index to all Reports and Memoranda published in the Annual Technical Reports, and separately—

April, 1950 - - - - - R. & M. 2600 2s. 6d. (2s. 8d.)

Author Index to all Reports and Memoranda of the Aeronautical Research Council—

1909—January, 1954 R. & M. No. 2570 15s. (15s. 6d.)

Indexes to the Technical Reports of the Aeronautical Research Council—

December 1, 1936—June 30, 1939	R. & M. No. 1850	1s. 3d. (1s. 5d.)
July 1, 1939—June 30, 1945	R. & M. No. 1950	1s. (1s. 2d.)
July 1, 1945—June 30, 1946	R. & M. No. 2050	1s. (1s. 2d.)
July 1, 1946—December 31, 1946	R. & M. No. 2150	1s. 3d. (1s. 5d.)
January 1, 1947—June 30, 1947	R. & M. No. 2250	1s. 3d. (1s. 5d.)

Published Reports and Memoranda of the Aeronautical Research Council—

Between Nos. 2251-2349	R. & M. No. 2350	1s. 9d. (1s. 11d.)
Between Nos. 2351-2449	R. & M. No. 2450	2s. (2s. 2d.)
Between Nos. 2451-2549	R. & M. No. 2550	2s. 6d. (2s. 8d.)
Between Nos. 2551-2649	R. & M. No. 2650	2s. 6d. (2s. 8d.)

Prices in brackets include postage

HER MAJESTY'S STATIONERY OFFICE

York House, Kingsway, London W.C.2; 423 Oxford Street, London W.1 (Post Orders: P.O. Box 569, London S.E.1); 13a Castle Street, Edinburgh 2; 39 King Street, Manchester 2; 2 Edmund Street, Birmingham 3; 109 St. Mary Street, Cardiff; Tower Lane, Bristol, 1; 80 Chichester Street, Belfast,
or through any bookseller.